Effects of Piston Cavity Impingement and Split Injection on Mixture Formation and Combustion Processes of Diesel Spray

（ディーゼル噴霧のピストンキャビティ衝突と分割噴射が混合気形成及び燃焼過程に及ぼす影響）

By

楊　康（Kang YANG）

Dissertation

Submitted to the Graduate School of Engineering

Hiroshima University

in Partial Fulfillment of the requirements

For the Degree of

Doctor of Engineering

Hiroshima University

September, 2018

ABSTRACT

The objective of this work is to obtain an enhanced understanding of the effect of split injection on mixture formation and combustion processes of diesel spray and 2-D cavity impinging spray. Three kinds of injection amounts (0.27 mg, 0.89 mg, 2.97 mg) were adopted to investigate the effect of small injection amount on the mixture formation and combustion processes of free spray. For the split injection, the injection process comprised a pre-injection followed by the main injection. The main injection was carried out either as a single injection of injection pressure 100 MPa (Pre + S100), 160 MPa (Pre + S160) or split injection of injection pressure 160 MPa itself was either of two types defined by mass fraction ratios 50 : 50 and 75 : 25 (Pre + D160_50-50, Pre + D160_75-25). S100 and D160_75-25 strategies were also compared with Pre + S100 and Pre + D160_75-25 to check the effect of pre-injection on the combustion process under 2-D cavity impinging spray. Low oxygen concentration (15% O2) was investigated in the 2-D cavity under split injection.

Mie scattering method and laser absorption-scattering (LAS) technique were employed to qualitatively and quantitatively characterize the spray development. Tracer LAS fuel with 97.5 vol% of n-tridecane and 2.5 vol% of 1-methylnaphthalene (α-MN) was employed. The characteristics of the combustion process of Diesel spray were investigated by adopting a color camera which directly perceived the flame natural luminosity, OH* chemiluminescence recording system, and two-color perometry techniques.

The experimental results revealed that the vapor distribution of split injection was significantly more homogeneous than that of single injection. Pre-injection could improve the main injection combustion. The split injection can reduce the soot emissions under free spray flame. Increase the split injection interval should be a positive way to reduce the soot emissions in the 2-D impinging spray flame.

TABLE OF CONTENTS

ABSTRACT i

TABLE OF CONTENTS ii

NOMENCLATURES v

CHAPTER 1 INTRODUCTION 1

1.1 BACKGROUND AND MOTIVATIONS 1

1.2 OBJECTIVES AND APPROACHES 6

1.3 OUTLINES 6

1.4 REVIEW OF PREVIOUS WORKS 8

1.4.1 Characterization of Diesel Spray 8

1.4.2 Impinging spray 10

1.4.3 Multiple Injection 11

1.4.4 Optical Diagnostic Technique for Diesel Spray and Process 13

CHAPTER 2 EXPERIMENTAL APPERATUS AND MEASURING METHODS 22

2.1 MIE SCATTERING METHOD FOR NON-EVAPORATION CONDITION 22

2.2 TRACER LAS TECHNIQUE FOR EVAPORATION OBSERVATION 23

2.2.1 Principles of tracer LAS Technique 23

2.2.2 Experiment Setup 28

2.2.3 Fuel for LAS Technique 31

2.2.4 Molar Absorption Coefficient of Tracer Fuel 34

2.3 TWO-COLOR PYROMETRY FOR COMBUSTION 38

2.3.1 Principle of Two-color Pyrometry 38

2.3.2 Calibration Method 39

2.4 OH* CHEMILUMINESCENCE METHOD 42

CHAPTER 3 MIXTURE AND COMBUSTION CHARACTERISTICS OF SMALL INJECTION AMOUNT FUEL SPRAY 44

3.1 INTRODUCTION 44

3.2 EXPERIMENTAL CONDITIONS 44
3.3 SPRAY MIXTURE CONCENTRATION DISTRIBUTIONS 45
3.3.1 Effect of Injection Amount 45
3.3.2 Effect of Injection Pressure 53
3.4 COMBUSTION PROCESS 58
3.5 SUMMARY 63
CHAPTER 4 CHARACTERISTICS OF FREE SPRAY DEVELOPMENT, MIXTURE FORMATION AND COMBUSTION UNDER HIGH-PRESSURE SPLIT INJECTION 65
4.1 INTRODUCTION 65
4.2 EXPERIMENTAL CONDITIONS 65
4.3 INJECTION RATE 66
4.4 NON-EVAPORATION CHARACTERISTICS 67
4.5 EVAPORATION CHARACTERISTICS 71
4.6 COMBUSTION CHARACTERISTICS 76
4.7 SUMMARY 82
CHAPTER 5 CHARACTERISTICS OF FUEL EVAPORATION, MIXTURE FORMATION AND COMBUSTION OF 2-D CAVITY IMPINGING SPRAY UNDER HIGH-PRESSURE SPLIT INJECTION 84
5.1 INTRODUCTION 84
5.2 EXPERIMENTAL CONDITIONS 84
5.3 INJECTION RATE 85
5.4 EVAPORATION CHARACTERISTICS 86
5.5 COMBUSTION CHARACTERISTICS 91
5.6 SUMMARY 102
CHAPTER 6 COMPARISON OF FREE SPRAY AND 2-D CAVITY IMPINGING SPRAY EVAPORATION AND COMBUSTION CHARACTERISTICS 104
6.1 INTRODUCTION 104

6.2 EXPERIMENTAL CONDITIONS 104
6.3 COMPARISON OF EVAPORATION CHARACTERISTICS OF FREE SPRAY AND 2-D CAVITY IMPINGING SPRAY 105
6.4 COMPARISON OF COMBUSTION CHARACTERISTICS OF FREE SPRAY AND 2-D CAVITY IMPINGING SPRAY 110
6.5 SUMMARY 119
CHAPTER 7 EFFECTS OF PRE-INJECTION AND LOW OXYGEN CONCENTRATION ON THE DIESEL EVAPORATION AND COMBUSTION CHARACTERISTICS 121
7.1 INTRODUCTION 121
7.2 EXPERIMENTAL CONDITIONS 122
7.3 COMBUSTION CHARACTERISTICS (21% O_2 WITHOUT PRE-INJECTION) 123
7.4 COMBUSTION CHARACTERISTICS (15% O_2 WITH PRE-INJECTION) 127
7.5 COMBUSTION CHARACTERISTICS (15% O_2 WITHOUT PRE-INJECTION) 131
7.6 IGNITION DELAY 135
7.7 SUMMARY 136
CHAPTER 8 CONCLUSIONS 138
8.1 MAIN FINDINGS OF THIS STUDY 138
8.2 RECOMMENDATIONS FOR FUTURE WORKS 141
REFERENCE 143
ACKNOWLEDGEMENTS 159

NOMENCLATURES

ASOI	After Start of Injection
AEOI	After End of Injection
AMIG	After Main Ignition
Atpeak	After tpeak
Atpeak1	After tpeak1
Atpeak2	After tpeak2
α-MN	α-methylnaphthalene
BMEP	Brake Mean Effective Pressure
C_d	Mass concentration of droplets, kg/m^3
C_v	Mass concentration of vapor, kg/m^3
CDC	Conventional Diesel Combustion
CFD	Computational Fluid Dynamics
CI	Compression Ignition
D.I.	Direct Injection
D_{32}	Sauter mean diameter of droplets, μm
DOC	Diesel Oxidation Catalyst
DPF	Diesel Particulate Filter
DMN	Dimethylnaphthalene
ε	Molar Absorption Coefficient
EPA	Environmental Protection Agency
EOI	End of Injection
EGR	Exhaust Gas Recirculation
Φ_{all}	The mass frequency to total fuel and equivalence ratio to total fuel
HCCI	Homogeneous Charge Compression Ignition
HCPC	Homogenous Charge Progressive Combustion
HD	Heavy Duty

HRR	Heat Release Rate
HSDI	High-Speed Direct Injection
LAS	Laser Absorption-Scattering
LES	Large Eddy Simulation
LDA	Laser Doppler Anemometer
LIEF	Laser Induced Exciplex Fluorescence
LIF	Laser Induced Fluorescence
LRS	Laser Rayleigh Scattering
LTC	Low Temperature Combustion
MIG	Main Ignition
PLIF	Planar Laser-Induced Fluorescence
PCCI	Premixed Charge Compression Ignition
PDA	Phase Doppler Anemometry
PDPA	Phase Doppler Particle Analysis
PM	Particle Matters
PIA	Particle Image Analysis
PIV	Particle Image Velocimetry
Pinj	Injection Pressure
RANS	Reynolds-averaged Navier–Stokes
RCCI	Reactivity Controlled Compression Ignition
SCR	Selective Catalytic Reduction
SMD	Sauter Mean Diameter
SOMI	Strat of Main Injection
SO1MI	Start of First Main Injection
SO2MI	Start of Second Main Injection
SRS	Spontaneous Raman Scattering
tpeak	The Integrated KL Peak Timing
tpeak1	tpeak for the First Main Injection Flame

tpeak2	tpeak for the Second Main Injection Flame
tvalley	The Valley for the Integrated KL
UV	Ultraviolet
Vis	Visible
VGT	Variable Geometry Turbo

CHAPTER 1 INTRODUCTION

1.1 BACKGROUND AND MOTIVATIONS

The diesel engine (also known as a compression-ignition or CI engine), named after Rudolf Diesel in 1892. Diesel engines were popular in larger cars earlier, as the weight and cost penalties were less noticeable [1]. Diesel engines tend to be more economical at regular driving speeds and are much better at city speeds. However, the reduction of oil reserves and the more and more stringent exhaust diesel emission regulations are the challenges.

The oil is the nonrenewable resources, while the oil demand had been expanding rapidly with the global developing of industrialization. Figure 1.1 shows the Primary energy consumption by fuel from past to future [2], it reveals that the global oil consumption is increasing until 2040. For the oil part, the traditional vehicle is one of the most common consumption sources, is facing the situation of little fuel useable in the future. Therefore, as the most widely used commercial vehicle, diesel engine should enhance fuel economy performance, which can effectively relieve the pressure caused by the shortage of the resources.

Nowadays, more and more attentions are paid to environmental protection, emission regulations gradually become stringent. Figure 1.2 shows the EPA and EU on-road technology pathways for HD diesel vehicles [3]. Thanks to the new techniques such as high pressure and high flexibility injection system, multiple injections, VGT (Variable Geometry Turbo), advanced combustion, engine calibration, sub-system integration, cooled EGR (Exhaust Gas Recirculation), DOC (Diesel Oxidation Catalyst) + DPF (Diesel Particulate Filter) and SCR (Selective Catalytic Reduction) et al., the modern diesel engine can satisfy the present stringent emission laws. But diesel engine still has high NOx and soot emissions compared with gasoline engine. Therefore, the

clean diesel engine is pursued persistently by engine researchers.

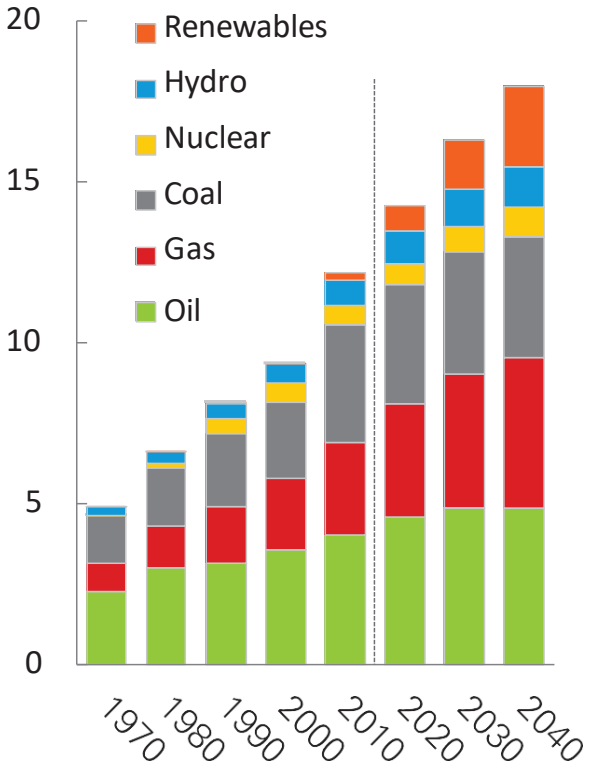

Figure 1.1 Primary energy consumption by fuel

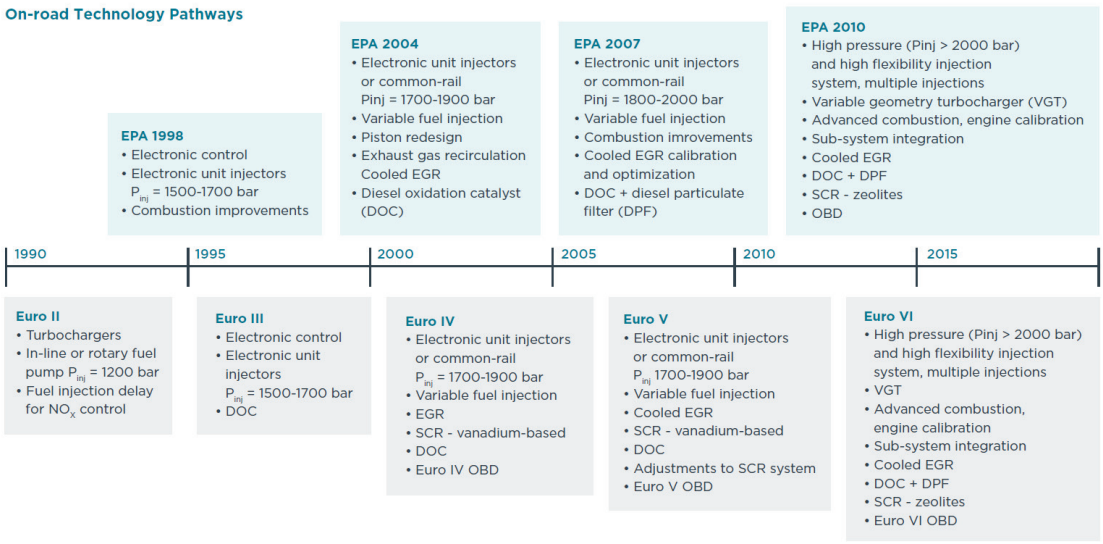

Figure 1.2 EPA and EU on-road technology pathways for HD diesel vehicles

In order to realize the clean diesel engine, the advanced combustion concepts which are thought possible to reduce NOx and PM emission simultaneously are proposed such as HCCI (Homogeneous Charge Compression Ignition), RCCI (Reactivity Controlled

Compression Ignition), PCCI (Premixed Charge Compression Ignition), HCPC (Homogenous Charge Progressive Combustion), LTC (Low Temperature Combustion) et al. These advanced combustion concepts can achieve satisfied performance, reduce NOx and PM emission and control the engine cost same time.

HCCI (Homogeneous Charge Compression Ignition) using diesel fumigation in the intake port was first described in 1958 [4]. HCCI is an internal combustion that well-mixed fuel and oxidizer (typically air) are compressed to the point of auto-ignition. It has the advantages of high efficiencies, clean combustion and low emissions.

RCCI (Reactivity Controlled Compression Ignition) is a dual fuel engine combustion technology that was developed at the University of Wisconsin-Madison Engine Research Center laboratories [5]. RCCI is a variant of Homogeneous Charge Compression Ignition (HCCI) that provides more control over the combustion process and has the potential to dramatically lower fuel use and emissions. This concept combustion has the advantage of lower NOx and PM emissions, reduce heat transfer losses, increase fuel efficiency and eliminates need for costly after-treatment systems

PCCI (Premixed Charge Compression Ignition) is a compromise offering the control of CIDI combustion with the reduced exhaust gas emissions of HCCI, specifically lower soot [6]. The heat release rate is controlled by preparing the combustible mixture in such a way that combustion occurs over a longer time duration making it less prone to knocking.

HCPC (Homogenous Charge Progressive Combustion) is based on a split cycle concept, with the intake and compression phases performed outside the cylinder [7]. Highest efficiency can be obtained for a given maximum admissible pressure, as well as noiseless and smooth engine operation mechanical efficiency is improved due both to the absence of pressure peaks and to the consequent reduction of reciprocating masses.

LTC (Low Temperature Combustion) is designed to reduce or eliminate the two most problematic pollutants, particulate matter (PM) and nitrogen oxides (NOx) which are emitted by diesel engines. PM is composed of black soot particles, which are often

soaked with unburned or partially burned fuel components. NOx emissions are toxic and combine with other pollutants in the atmosphere to create ground-level ozone, or smog [8].

Figure 1.3 shows the ϕ–T map for the formation of NOx and soot emissions [9]. The typical combustion regions of conventional diesel combustion (CDC), HCCI, and PCCI were marked on the diagram [10, 11]. The ultimate goal is to avoid the combustion region falling on the soot and NOx contours, thereby reducing these two emissions simultaneously.

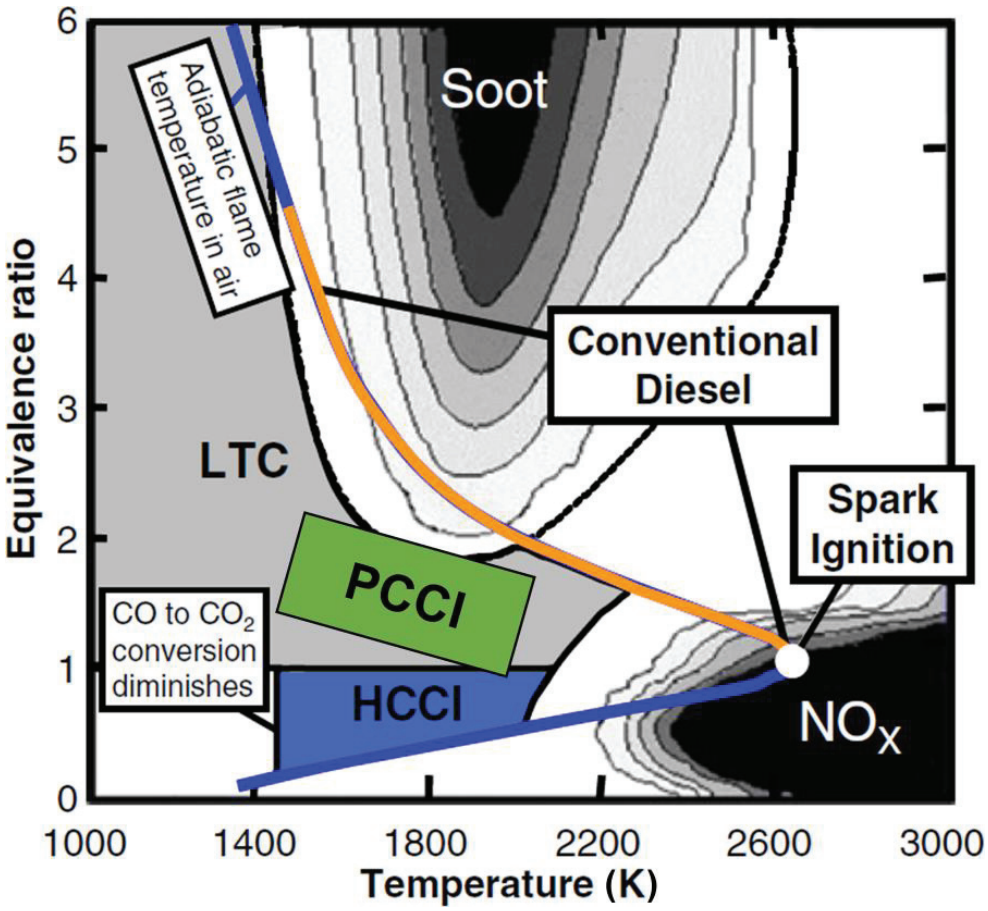

Figure 1.3 Illustration on the regions of CDC, HCCI, and PCCI on a ϕ–T map with soot–NOx contour

One of the effective way to satisfy the performance is to improve the mixture formation, which can realize clean diesel combustion. Numerous investigations which focused on the diesel spray mixture formation, such as increase the injection pressure [1,

[12, 13, 14] or adopt small nozzle diameter [15, 16], can improve the mixture formation process. The small-bore diesel engine is widely used in the passenger car, as for this, the spray/wall interaction cannot be avoided. The spray/wall impingement has a significant influence on mixture formation [17-19], combustion and emissions in engines [20-24]. The flat wall was always selected to form impinging spray for simplicity during the past decades by plenty of researchers. However, the structure of impinging wall in a practical engine is complicated, wherein the impinging spray is formed on the piston crown. The mixture formation and combustion process are dissimilar to that of flat wall impinging spray. Therefore, it is worthwhile to investigate the spray mixture formation and combustion process by employing a 2-D piston cavity. Moreover, small injection amount is also one important factor to investigate the mixture formation as the small-bore diesel engine is widely used. What's more, multiple injection strategy incorporating pre-injection or pilot injection of a marginal quantity of fuel to reduce combustion noise and NOx emissions and post injection of another marginal fuel mass to enhance soot oxidation rate has been widely employed [25]. In addition, multiple injection strategy decreases each stage injection amount, which is also an effective way to investigate the small injection amount condition.

To realize homogeneous combustion, decreasing compression ratio is thought as one effective way for diesel engine. By decreasing compression ratio, it can improve combustion efficiency and make the combustion clean, then excellent emission performance without using expensive NOx aftertreatment device can be achieved. It means the diesel-powered cars can be offered at an affordable price range. A low compression ratio can also reduce the weight of parts, which enables the engine to lightly rev up to high rev range. In the Mazda Skyactiv-D engine, the focus was on reduction of NOx [26, 27]; an "egg-shaped" engine was designed. According to this Skyactiv-D engine, the world lowest compression ratio can be obtained.

1.2 OBJECTIVES AND APPROACHES

The target of this study is to investigate the D. I. Diesel spray mixture formation and the combustion characteristics in a high pressure high temperature constant volume test rig, the specific objectives of this research are shown as follows:

1. Investigating the effect of small injection amount on the free spray and flame characteristics.
2. Analyzing the effect of split injection on mixture formation and combustion processes of diesel free spray.
3. Analyzing the effect of split injection on mixture formation and combustion processes of 2-D cavity impingement diesel spray.
4. Comparing the mixture formation and combustion characteristics of free spray and 2-D cavity under split injection.
5. Observing the effects of pre-injection on the combustion processes.
6. Clarifying the influence of low oxygen concentration on the diesel combustion characteristics.

In this study, the Mie Scattering technique was applied to obtain the qualitative information of Diesel spray. And the Laser Absorption-Scattering (LAS) technique was adopted to qualitatively and quantitatively analyze the mixture formation process of Diesel spray. The flame features which were estimated from natural luminosity and OH* chemiluminescence were concentrated on by employing a high-speed video color camera and a high-speed black/white video camera coupled with an image intensifier system respectively. In addition, Two-Color Pyrometry was used to quantitatively measure the soot concentration and flame temperature.

1.3 OUTLINES

To present this work, the dissertation is organized as follows: a review of previous

work such as the small injection amount, multiple injection strategy, impinging spray on the mixture formation characteristics and combustion concepts of D. I. Diesel spray. The optical diagnostic techniques for spray and combustion is given in Chapter 1. Chapter 2 describes the experimental apparatus such as fuel injection system and constant volume vessel, and the observation techniques adopted in this work such as Mie scattering method, Laser Absorption Scattering technique, Natural luminosity recording system, Two-Color method and OH* chemiluminescence technique. The KL factor and temperature images, which are calculated by applying the two-color method, are shown in black background. In the OH* images, the background is colored blue, and the OH* chemiluminescence was displayed in the default jet colormap from Matlab. Chapter 3 illuminates the effect of small injection amount on Diesel spray mixture formation and combustion characteristics. Chapter 4 analyzes the effect of split injection on mixture formation and combustion processes of diesel free spray. Chapter 5 analyzes the effect of split injection on mixture formation and combustion processes of 2-D cavity impingement diesel spray. Chapter 6 compares the free spray and 2-D cavity impinging spray under same split injection strategies. Chapter 7 clarifies the influence of low oxygen concentration on the diesel combustion characteristics and investigates the effects of pre-injection on the combustion processes. Finally, general conclusions on mixture formation and combustion processes of diesel free spray and 2-D cavity impinging spray with split injection are summarized in Chapter 8. In this paper, the integrated KL factor and OH* chemiluminescence was calculated by integrating the pixel values over the two images. The average temperature is defined as the result that the sum of the temperatures inside the valid pixels divides the valid pixels number. These results were averaged over three different runs at the same experiment condition.

1.4 REVIEW OF PREVIOUS WORKS

1.4.1 Characterization of Diesel Spray

Characteristics of fuel has been identified that has significant influence on the combustion. The characteristics such as spatial and temporal fuel distributions have been investigated by numerous researchers [28-34]. The empirical equations for break-up length, spray angle, spray tip penetration and drop size distribution of the diesel sprays are introduced to discuss the internal structure of the spray. Injection characteristics such as injection rate, injection timing and injection duration play the most important role in determining engine performance, especially in pollutant emissions. Raeie et al. [35] investigate the effects of injection timing on the propulsion and power in a diesel engine. It has been concluded that the use of early injection provides lower soot and higher NOx emissions than the late injection. Sayin et al. [36] also investigate the effects of injections no the engine performance and exhaust emissions of a dual-fuel diesel engine. With the advanced injection timings, decreasing HC and CO emissions diminished. Borz et al. [37] studied the effects of injection timing and duration on jet penetration and mixing in multiple-injection schedules. It was found that the jet spreading angles between the first and second injections differed, with the first injection having a higher average angle during the quasi-steady portion of the injection. Vaporizing characteristics such as the temperature distribution, liquid fuel concentration and vapor fuel concentration have also been investigated to check the fuel-air mixing which is an important phenomenon on the ignition. Diwakar et al. [38] shows the experimental and computational study on the liquid and vapor fuel distributions. The results reveal that highly stratified fuel-air distributions with steep vapor-concentration gradients are found for injection and ignition timings typical of light-load operation of a direct-injection two-stroke-cycle engine. Suzuki et al. [39] adopted a new technique which can get the simultaneous concentration measurement of vapor and liquid in an evaporating diesel spray. And from the ignition to combustion,

the partially pre-mixed combustion and partially diffusion combustion have been focused by many researchers. The earliest systematic description of the D.I. Diesel engine combustion concept was summarized by Dec [40] and Flynn et al. [41], which is shown in Figure 1.4. They observed the auto-ignition by Planar Laser-Induced Fluorescence (PLIF) technique, and used the Laser Induced Incandescence (LII) method soot concentration. The results reveal that a sheath of fuel vapor and hot air is formed around the spray and also at the leading edge of the spray after the fuel injected into the chamber; auto-ignition is occurring at multi points nearly simultaneously at the downstream region, the premixed burn mainly occurs volumetrically throughout the cross section of the leading portion of the jet. The injected fuel is heated to 825 K by mixing with entrained hot gas during the mixing-controlled combustion. A thin diffusion flame is formed surrounding the burning plume and the rich combustion products (CO, UHC and particles) are completely burnt in this region, the high temperature and high oxygen concentrations at the diffusion flame interface provide an ideal environment for NOx formation reactions [42]. It is impossible to reduce the soot and NOx at the same time, this phenomenon is called as soot -NOx trade off [43]. The rate of heat release is also calculated during the combustion process. Marc [44] provides a comprehensive set of equations and guidelines to determine the rate of heat release in full-scale fire tests based on the O2 consumption principle. Miguel et al. [45] focused on the study of heat release rate (HRR) and in-cylinder pressure on the homogeneous charge compression ignition (HCCI) process in a modified diesel engine. The HCCI combustion mode shows a HRR clearly different from the HRR correspondent to conventional diesel combustion as it is approached in Wiebe's function of two modes.

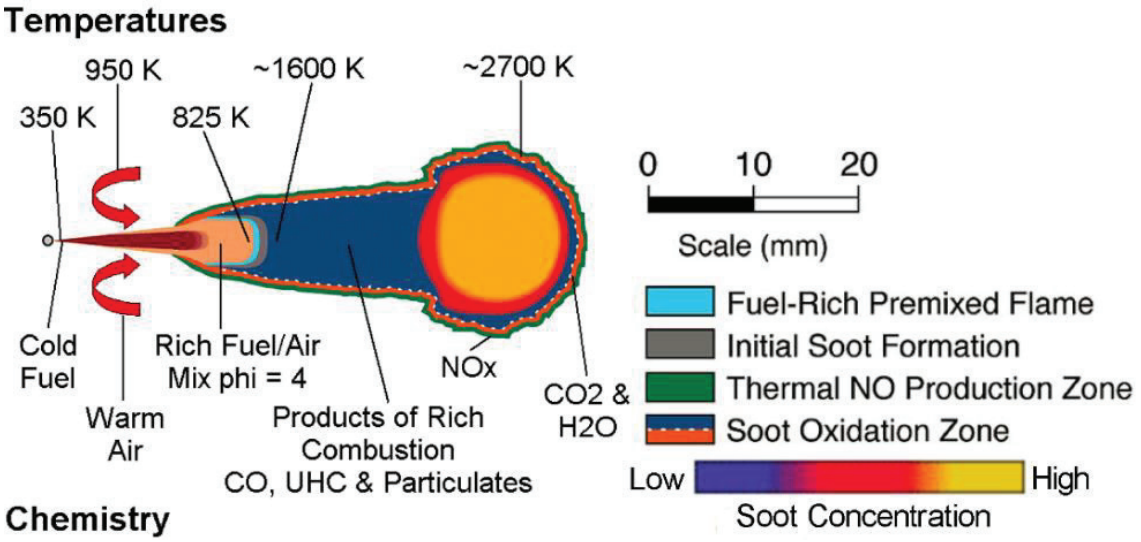

Figure 1.4 Schematic of conceptual model of Diesel spray combustion described by Dec [106] and Flynn et al. [107].

1.4.2 Impinging spray

Bruneaux [46] investigated the wall impingement mixing process using Laser Induced Exciplex Fluorescence (LIEF) and compared it with free jet. It is determined that wall impingement has a more significant effect on the mixing rate compared to free jet. Zhang et al. [47] studied the effect of impingement on mixture formation by applying LAS technique. The study demonstrated that the spray tip penetration length decreases with flat wall impingement; however, it has a marginal influence on gas entrainment. Bruneaux et al. [48] studied the air entrainment of an impinging spray and determined that spray–wall interaction also plays a role in air entrainment before impingent occurs. Mohammadi et al. [49] investigated ambient air entrained processes in detail by applying Laser Sheet Imaging method. It is concluded that higher injection pressure, larger orifice diameter or shorter impinging distance can enhance gas entrainment under impinging condition. Li et al. [50] studied the effect of impinging distance on diesel spray and combustion behaviors. It was determined that the combustion process of impinging spray was highly complicated. López and Pickett [51] investigated the effect of spray–wall interaction on soot formation processes and demonstrated that soot emissions of

impingement flame were lower compared to that of free jet. Pickett and López [52] investigated OH* chemiluminescence and soot emissions of impinging flame, and also determined that combustion was enhanced and soot emission was reduced. However, a fuel film was formed after impingement, which caused inadequate combustion and undesirable emissions. Wang et al. [53] determined that flat wall impingement increases soot formation significantly. Dec and Tree [54] also concluded that that spray–wall interaction is likely to increase particulate matter and unburned hydrocarbon emissions and reduce thermal efficiency. Moreover, the structure of the impinging wall in a practical engine is complicated, wherein the impinging spray is formed on the piston crown. Therefore, it is worthwhile to investigate the spray mixture formation and combustion process by employing a 2-D piston cavity.

1.4.3 Multiple Injection

Recently, multiple injection strategy incorporating pre-injection or pilot injection of a marginal quantity of fuel to reduce combustion noise and NOx emissions and post injection of another marginal fuel mass to enhance soot oxidation rate has been widely employed [55]. Cheng et al. [56] studied the effect of multiple injection strategies on diesel fuel combustion process. With the advancement of pilot injection timing, NOx and soot emissions are reduced; however, HC and CO emissions are increased. By retarding the post injection timing, the NOx emission reduced, whereas soot emission first increased and then decreased. The pre-injection strategy is considered to be one of the most important methods to improve diesel engine performance, emission, and combustion [57]. Farrell et al. [58] determined that diesel spray with pre-injection is effective to enhance fuel/gas mixing and decrease the Sauter mean diameter (SMD). However, it is common recognition that pre-injection deteriorates soot emission because of the shorter ignition delay of main injection. Ricaud and Lavoisier [55] indicated that the effect of pre-injection depends on the pre-injected mass fraction, injection interval and pre-injection frequency.

The term split injection is occasionally used to refer to multiple injection strategies where the main injection is split into two smaller injections of approximately equal size or into a smaller pre-injection followed by a main injection [59]. Bianchi et al. [60] investigated the effect of split injection in reducing NOx and soot emissions of HSDI Diesel engines by CFD code KIVA-III. The results indicate that split injection is highly effective in reducing NOx, while soot reduction is related to a more effective use of the oxygen available in the combustion chamber. With split injection, nitrogen oxide emissions and smoke emissions were reduced because of the moderated combustion speed and enhanced local homogeneity [61]. Skeen et al. [62] investigated the mixing, penetration, and ignition characteristics of high-pressure n-dodecane sprays with a split injection schedule. These studies significantly increased the amount of data available on split injections and improve understanding of split injections. Blomberg et al. [63] investigated n-dodecane split injections of "Spray A" from the ECN using two different turbulence treatments (RANS and LES). It demonstrates that the simulations did not predict the generation of soot at the lower temperature, which is in agreement with experimental observations. Cha et al. [64] investigated the high-pressure and split injection strategies in a single cylinder DI diesel engine. The experimental data demonstrates the enhancement of fuel consumption of the split main injection events, remarkable at around 100 MPa of fuel pressure. It also reveals the complex effect of the fuel pressure and split main injection events on gaseous emissions. Nehmer and Reitz [65] investigated the effect of split injection ratio (double injections) on particulate and NOx emissions of diesel engine and determined that split injection tends to reduce NOx without increasing particulate emissions rapidly. Tow et al. [66] also determined that double and triple injections can reduce particulate and NOx emissions in the same engine. On the other hand, Nishida et al. [67] observed that the spray tip of the second injection pulse catches up and also passes the first one when the fuel quantity injected in the second pulse is significantly high and the dwell between the two injection pulses is highly marginal. Seo et al. [68] that a split injection can increase thermal efficiency and fuel consumption rate; however, without

optimization, it can result in poor combustion characteristics such as knocking, incomplete combustion and soot emissions. Nishioka et al. [69] compared the effect of single injection and split injection on a free spray and 2-D impinging spray of diesel. It is determined that the soot emission with split injection is lower than that with single injection of free spray. However, soot emission with 2-D impinging spray has a trend opposite to that with free spray. Therefore, it is necessary to investigate the spray mixture formation and combustion process by adopting split injection in a 2-D piston cavity.

1.4.4 Optical Diagnostic Technique for Diesel Spray and Process

Zhao and Ladommatos [70] have summarized the optical diagnostic techniques in Table 1.1 which are widely applied to investigate the diesel sprays characteristics. Here, those optical diagnostic techniques will be briefly introduced.

Mie scattering is applied to measure the liquid fuel distribution such as liquid phase penetration [71] and the spray structure [72]. However, the results of the droplet diameter and droplets concentration analyzed from Mie scattering intensity are not very accurate especially compared with other recently developed optical diagnostic techniques. Mie scattering has no upper size limitation and converges to the limit of geometric optics for large particles [73].

As Mie scattering is applied to non-evaporating diesel spray, much fewer measurements of evaporating diesel sprays were reported due to the complexity of the vapor diagnostics in diesel engines. The vapor diagnostics in diesel sprays include schlieren photography, holography, laser induced fluorescence (LIF), laser induced exciplex fluorescence (LIEF), laser Rayleigh scattering (LRS), spontaneous Raman scattering (SRS), laser absorption scattering (LAS).

Schlieren and shadowgraphy can simultaneously observe the spray vapor phase and liquid phase, but mainly used to measure the structure of spray as the limitation of quantitative analysis, which is same as the Mie scattering. However, the advantage of

Schlieren and shadowgraphy compare with Mie scattering is that they can not only detect liquid phase but also observe vapor phase. Schlieren photography was applied to assess the vapor amount generated within a diesel spray in the earlier of last decade [Huber, 1971. However, vapor concentration could not be obtained by this method. Optical arrangement, principle of operation, and data analysis are discussed detail by Panigrahi and Muralidhar [74]. Figure 1.5 and Figure 1.6 show the schematic diagram of a Z-type laser schlieren setup and Schematic drawing of the shadowgraph technique, respectively [74].

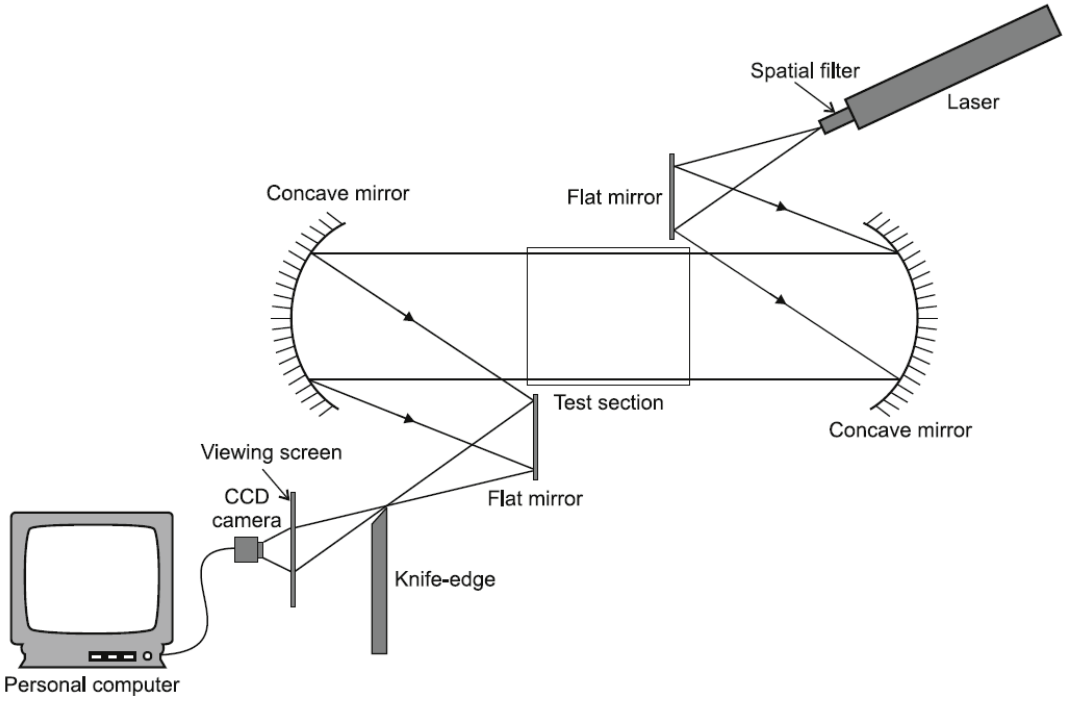

Figure 1.5 Schematic diagram of a Z-type laser schlieren setup

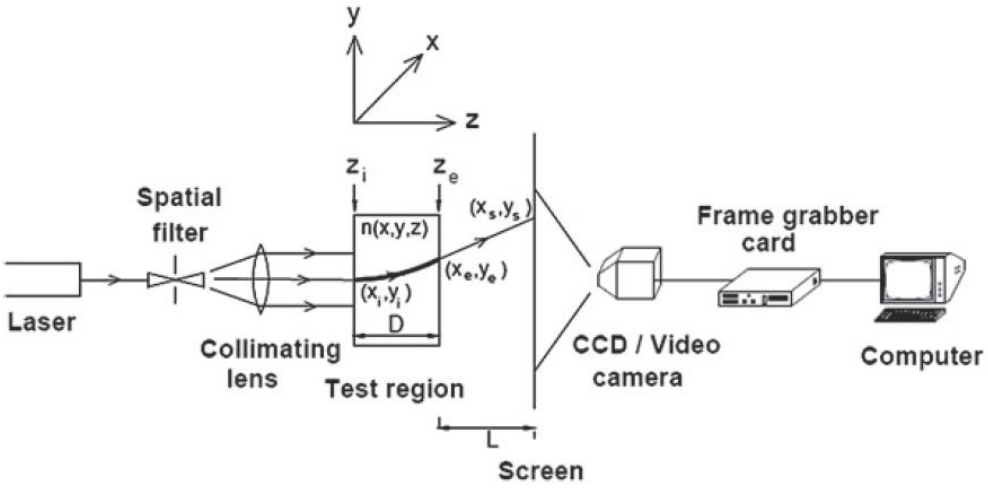

Figure 1.6 Schematic drawing of the shadowgraph technique

Holography is applied to the vapor probe in diesel sprays by utilizing the interference of laser light to record spray information. Nishida et al. [75] used the pulsed laser holography technique to observe a diesel spray injected into a high-pressure bomb. The fuel droplets and vapor around the spray could be observed by single-pulsed laser holography. Schnars et al. [76] shows the hologram recording and hologram reconstruction detail in Figure 1.7 and Figure 1.8. An observer sees a virtual image, which is optically indistinguishable from the original object. The reconstructed image exhibits all effects of perspective, parallax and depth-of-field.

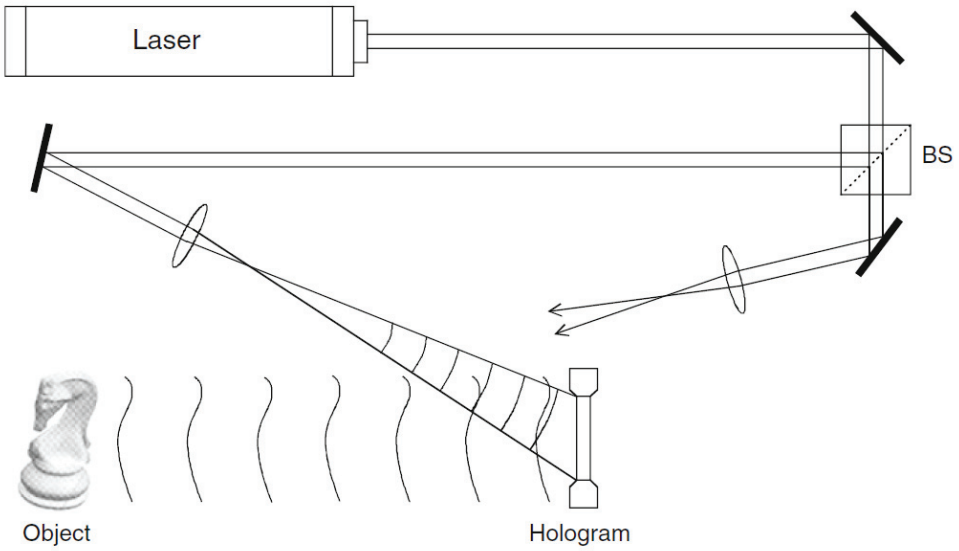

Figure 1.7 Hologram recording

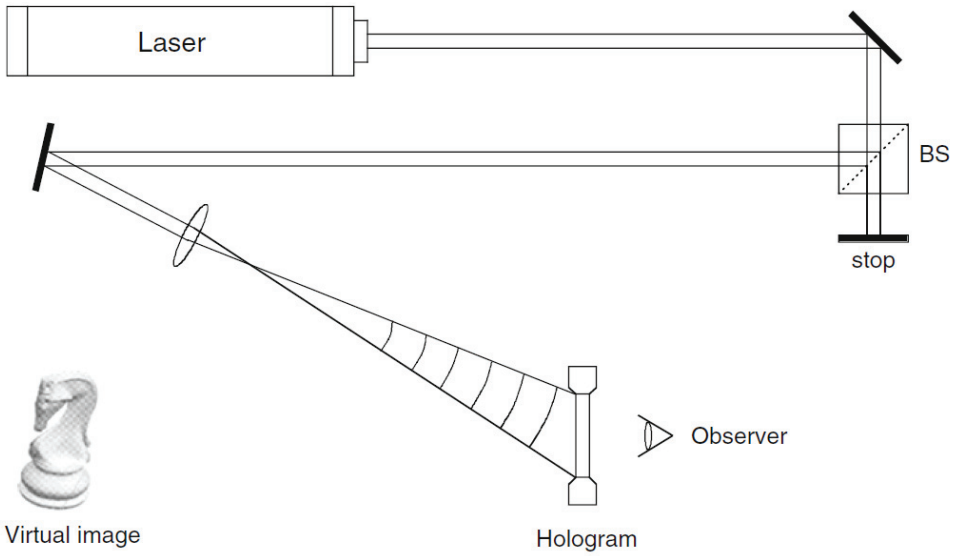

Figure 1.8 Hologram reconstruction

Laser Induced Fluorescence (LIF) or planar laser induced fluorescence (PLIF) is a very sensitive laser imaging technique for species concentration, mixture fraction and temperature measurements in fluid mechanical processes, sprays and combustion systems. For fluorescence, the molecule is excited not by chemical reaction but by absorption of light photon (s), typically from a laser source (laser-induced fluorescence, LIF) [77]. It has the advantage of strong red shifted signal but it is quenching at high pressures and difficult to calibrate. The fluorescence intensity can be used to estimate concentration because it is proportional to the molecular density [78]. LIF has been applied to perform mass distribution measurements in patternation applications [79, 80]. Seitzman and Hanson [81] reviews the theoretical basis of planar laser-induced fluorescence imaging and describes strategies for making instantaneous two-dimensional measurements of species concentration (or mole fraction), temperature and velocity in combustion gases. Figure 1.9 shows the experimental arrangement for a typical PLIF measurement [81].

Laser induced exciplex fluorescence (LIEF) which was developed [82-84] quantitatively measure vapor phase and liquid phase of spray simultaneously. This advanced LIF-technique allowed a simultaneous spectrally separated 2-D measurement of liquid and vapor phase in spray and combustion systems, which gained widely attention

by other researchers [85]. Senda et al. [86-88] used LIEF to investigate the vapor concentration of impinging spray and gave some fundamental principles of imping spray evolution. More recently, Bruneaux [89] measured the structures of concentrations of liquid phase and vapor phase by applying LIEF. Bruneaux [90] used LIEF to investigate the mixing process in high pressure diesel free jets and show the experimental setup for LIEF in Figure 1.10. The results show that a constant air entrainment rate when injection pressure is increased and the nozzle hole diameter has a significant effect on the global mixing rate. Bruneaux [91] also used LIEF to investigate the combustion structure of free and wall-impingement diesel jets. One of the advantages with LIEF as compared with LIF is that it enables imaging of the vapor phase without interference from the liquid phase [92]. However, the LIEF technique has the limitation of quenching by oxygen, careful considerations of used fuel type and ambient conditions is necessary.

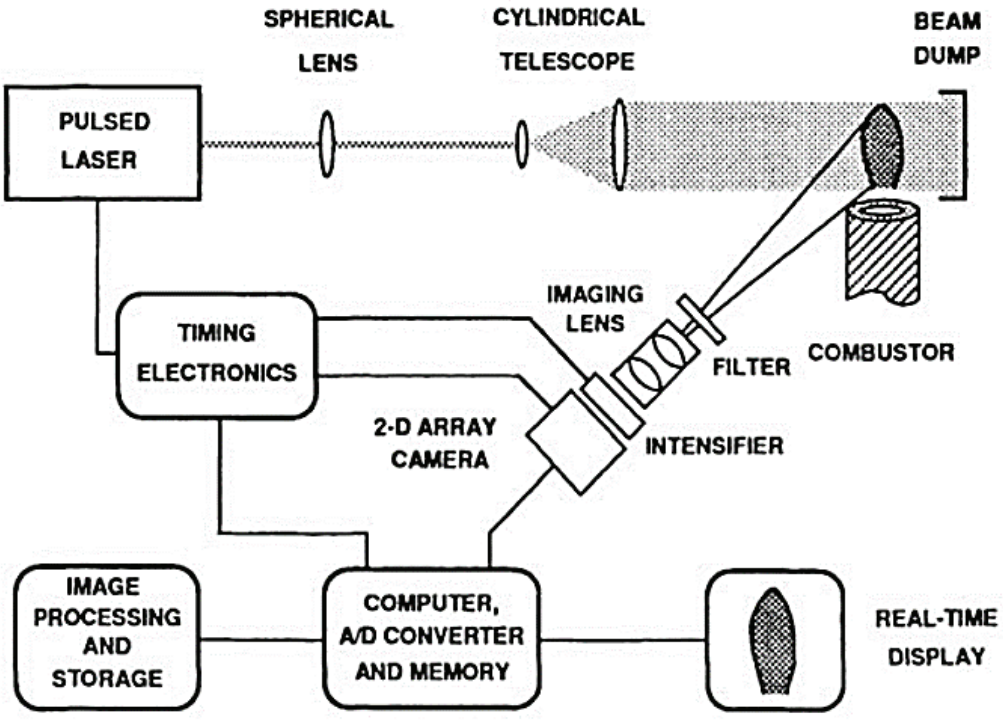

Figure 1.9 Experimental arrangement for a typical PLIF measurement

Laser Rayleigh Scattering (LRS) is applied to analyze vapor phase concentration as the scattered light intensity is proportional to the number density of gas molecules, and

also it can be applied to measure vapor concentration under low gas density because the lager scattering cross section. However, it is difficult to eliminate noise which comes from Mie scattering for LRS technique. It is meaningless if Mie scattering occurs when applying LRS technique because the energy of Mie scattering is ten to twenty orders of magnitude stronger than that of Rayleigh scattering. Thus the LRS technique must be applied in the environment of virtually free of particles. Espey et al. [93] used planar LRS technique successfully to obtain the quantitative images of fuel vapor concentration, the experimental setup is shown in Figure 1.11.

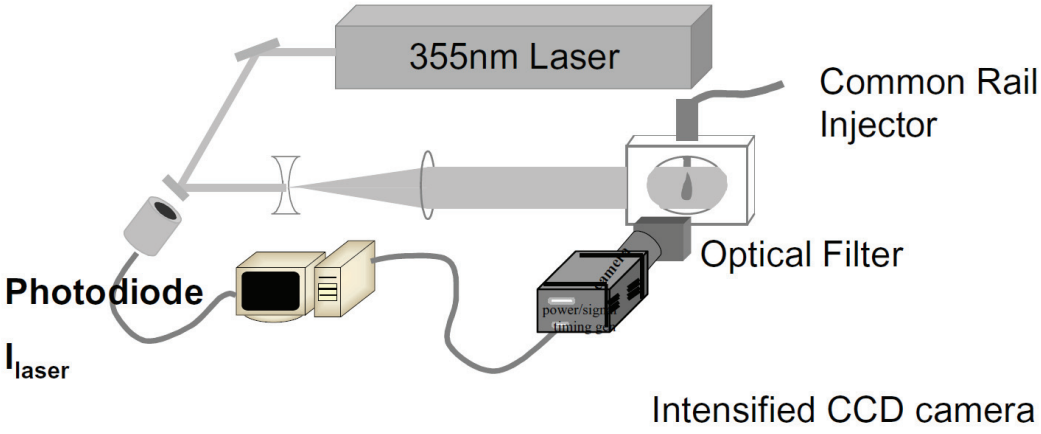

Figure 1.10 Experimental setup for LIEF visualizations

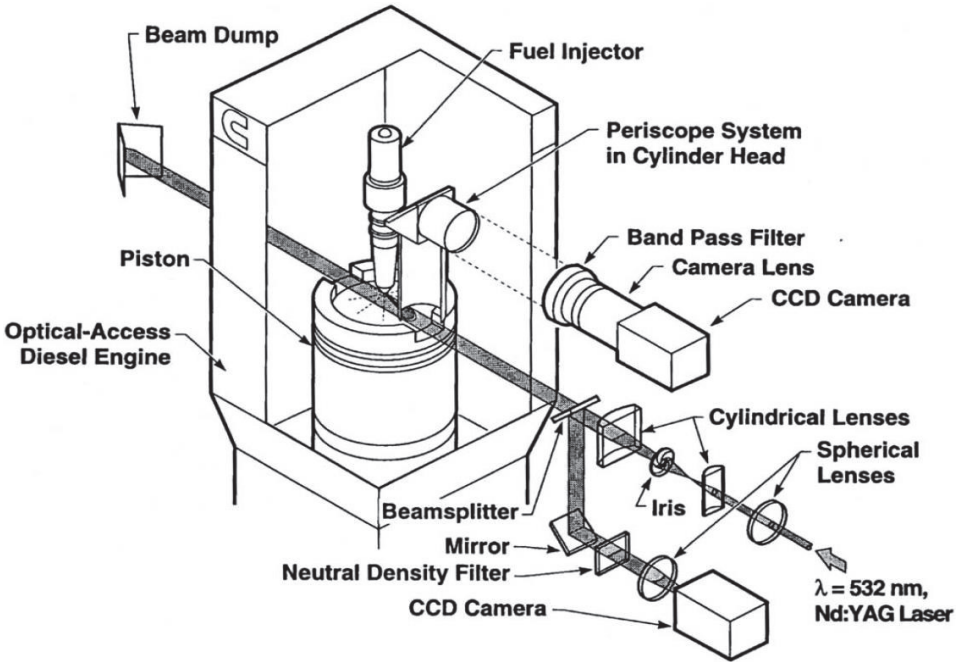

Figure 1.11 Schematic of the optical setup for LRS measurements

Spontaneous Raman Scattering (SRS) is a technique to calculate air/fuel ratio and measure gaseous species concentrations. Johnston [94] investigated the pre-combustion fuel/air distribution in a stratified charge engine, and the results reveal that the air/fuel ratio distribution changes hugely after fuel injection. Sawersyn et al. [95] investigated spatial distributions of different species by adopting SRS. And then Miles and Hinze [96] carried out an investigation of molar fraction of gaseous species. Reising [97] also used SRS to measure the thermal non-equilibrium in high-speed mixing and combustion. Figure 1.12 shows the schematic of the Raman set up from Reising [97].

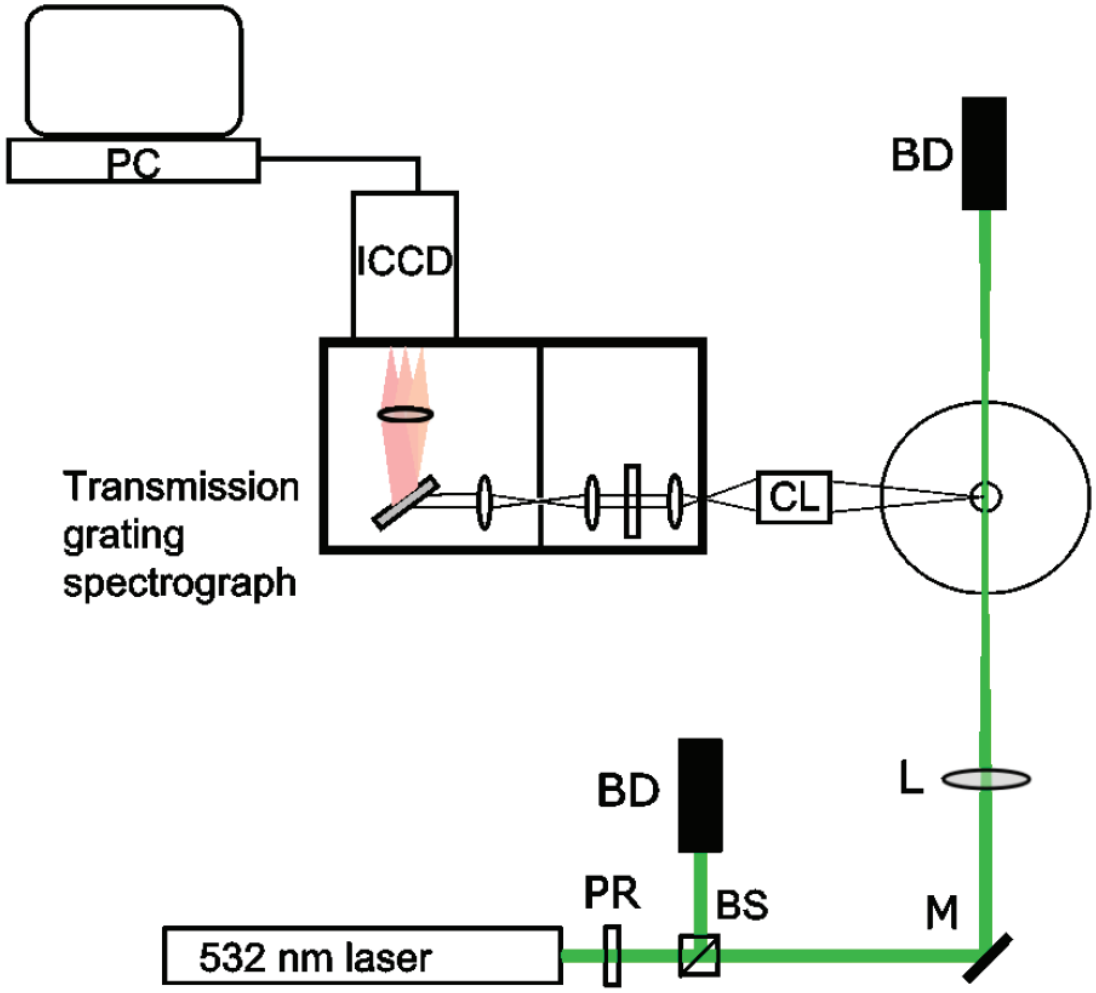

Figure 1.12 Schematic of the Raman set up

Laser Absorption-Scattering (LAS) technique will be used to investigate the fuel spray evaporation characteristics in this dissertation and will be introduced detail in

Chapter 2. Chraplyvy [98] firstly proposed the LAS technique in 1981, 3.39 μm and 0.6328 μm were applied to measure vapor and liquid scattering respectively. Suzuki et al. [99] applied 280 nm (absorption) and 560 nm (scattering) beams pass through an evaporative α-methylnaphthalene (α-MN) spray which developed LAS technique and simultaneously measured vapor concentration and liquid droplets. Zhang [100] and Gao et al. [101] continued improving the LAS technique, they selected Dimethylnaphthalene (DMN) as the test fuel and systematically described the analyzing methods of symmetric and non-symmetric sprays. The most comprehensive applications of LAS technique were carried out by Matsuo et al. [102] and Itamochi et al. [103], the tracer fuel (2.5 vol% of α-MN and 97.5 vol% of n-tridecane) was adopted.

There are also several techniques which are available for the measurements of ambient gas flowing velocity, spray droplet size and spray flow velocity, such as Laser Doppler Anemometer (LDA), Phase Doppler Anemometry (PDA), Phase Doppler Particle Analysis (PDPA), Particle Image Velocimetry (PIV), Particle Image Analysis (PIA) and so on. LDA is usually used to measure the flow velocity or turbulent scale. There are some researchers adopted LDA to engine measurement [104, 105]. PDA or PDPA can receive the size and velocity date, number density, volume flux and time resolved information. PIV is a measurement technique for obtaining the instantaneous whole field velocities. PIA Series provides size measuring based on the shape of the measured particles or crystals. PIA probes work in real time and under insitu conditions and detect size and shape of the particles [106].

Table 1.1 Summary of optical techniques for in-cylinder mixture formation measurement

Technique	Applications	Advantages	Limitations
Mie Scattering	Liquid fuel distribution	Simple setup	Sensitive to large droplets
Schlieren and Shadowgraph	Observation of overall spray	Simple setup	Sensitive to both liquid and vapor phases
LRS	Density measurement Vapor concentration	Strong signal Simple setup 2-D imaging	Interference from Mie and spurious scattering Limited to gaseous fuel
SRS	A/F ratio Residual gas fraction	Multi-species detection Multi-point detection Most accurate A/F readings Unaffected by windows fouling	Weak signal
LIF	Fuel concentration	Strong red shifted signal 2-D image of fuel	Quenching at high pressures Difficult to calibrate
FARLIF	A/F ratio	Direct A/F measurements 2-D imaging	Careful calibration required High pressure operation
LIEF	Fuel vaporization	2-D imaging	Quenching by

	& atomization	Simultaneous detection of vapor and liquid	oxygen
LAS	Fuel vaporization & atomization	Quantitative concentration measurements Droplet size information	Poor spatial resolution

CHAPTER 2 EXPERIMENTAL APPERATUS AND MEASURING METHODS

2.1 MIE SCATTERING METHOD FOR NON-EVAPORATION CONDITION

The spray development was initially observed by applying the Mie scattering method. Mie scattering refers primarily to the elastic scattering of light from atomic and molecular particles whose diameter is larger than about the wavelength of the incident light [107]. As shown in Figure 2.1, a high-speed video camera (Photron Co., ultima APX RS) was used to record the reflected light from the spray droplets. The frame rate was 10000 fps and the resolution was 512 × 512 pixels, with the exposure time of 1/200,000 s. The visible Nikkor 105 mm f/4.5 lens was mounted in front of the camera. A Xenon lamp (Ushio Inc., SX-UID 510XAMQ) and two reflect mirrors were used to form the incident light.

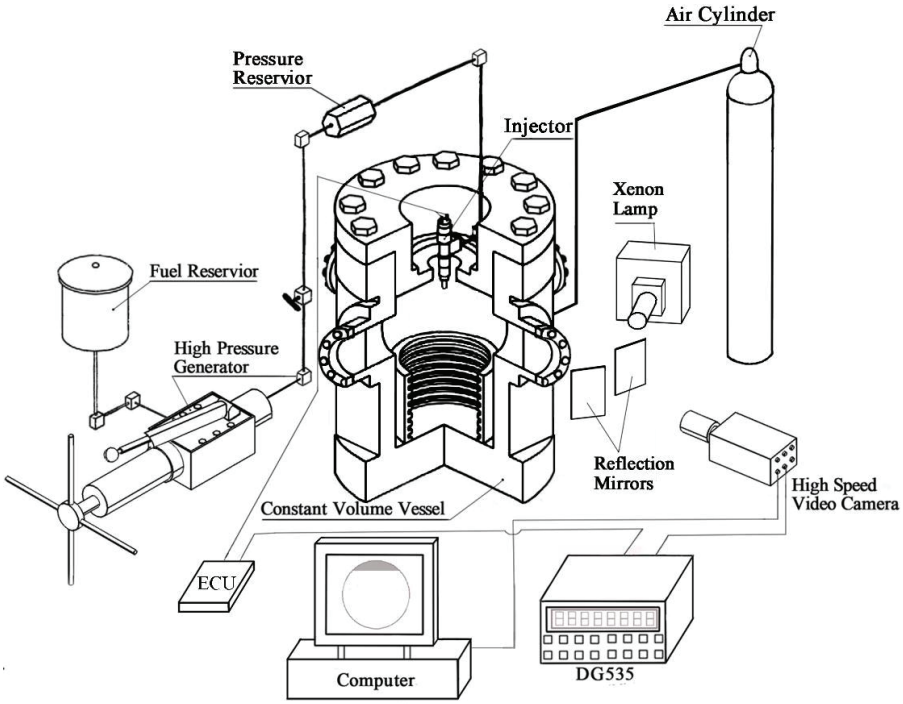

Figure 2.1 Experimental setup for Mie scattering method

2.2 TRACER LAS TECHNIQUE FOR EVAPORATION OBSERVATION

The principles of the LAS technique have been discussed in detail in our previous papers [100, 108, 109]. The vapor mass and liquid mass concentration can be achieved by using Bouguer-Lambert-Beer's law, and then the equivalence ratio can be calculated. The vapor mass and liquid mass calculation process will show as bellow. At first, measurement accuracy of vapor mass was evaluated by analyzing the completely evaporating spray in our previous paper [102, 103]. The comparison between analyzed mass of vapor of completely evaporating spray and injected mass was shown. To estimate errors under various evaporation condition, another injector and higher injection pressure were used.

2.2.1 Principles of tracer LAS Technique

In the ultraviolet and visible LAS technique, laser beam comprising two wavelengths (ultraviolet light and visible light) are applied. The ultraviolet (UV) light (wavelength=λ_A)

and visible (Vis) light (wavelength=λ_T) function as the absorption wavelength and scattering wavelength, respectively. The intensities of the two lights are attenuated by passing them through the fuel spray, as illustrated in Figure 2.2. The intensity attenuation of Vis and UV light can be expressed as $log\ (I_0 / I_t)_{\lambda T}$ and $log(I_0 / I_t)_{\lambda A}$, where I_0 and I_t represent incident light intensity and transmitted light intensity, respectively.

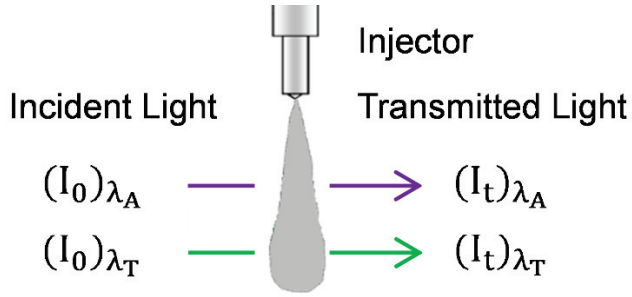

Figure 2.2 Principle of LAS technique

Figure 2.3 shows the flow diagram of axisymmetric analyzing process, the main analyzing process will be introduced briefly here.

Vis light is attenuated only by droplet scattering; UV light is attenuated by droplet scattering as well as liquid and vapor phase absorption. These phenomena can be expressed as Eq. (2.1) and Eq. (2.2), respectively:

$$log\left(\frac{I_0}{I_t}\right)_{\lambda_A} = log\left(\frac{I_o}{I_t}\right)_{L_{sca}} + log\left(\frac{I_o}{I_t}\right)_{L_{abs}} + log\left(\frac{I_o}{I_t}\right)_{V_{abs}} \tag{2.1}$$

$$log\left(\frac{I_0}{I_t}\right)_{\lambda_T} = log\left(\frac{I_o}{I_t}\right)_{L_{sca}} \tag{2.2}$$

Where $log\ (I_0 / I_t)_{Lsca}$, $log\ (I_0 / I_t)_{Labs}$ and $log\ (I_0 / I_t)_{Vabs}$ represent the attenuation by liquid scattering, liquid absorption and vapor absorption, respectively. As discussed in previous researches [110-112], liquid absorption $log\ (I_0 / I_t)_{\lambda T}$ in Eq. (2.1) is negligible. Therefore, vapor absorbance $log\ (I_0 / I_t)_{Vabs}$ can be calculated by subtracting the scattering light attenuation from the absorption light attenuation as illustrated in Eq. (2.3):

$$log\left(\frac{I_0}{I_t}\right)_{V_{abs}} = log\left(\frac{I_o}{I_t}\right)_{\lambda_A} - log\left(\frac{I_o}{I_t}\right)_{\lambda_T} \tag{2.3}$$

The vapor absorbance is obtained by the Lambert - Beer's law as expressed by Eq. (2.4):

$$log\left(\frac{I_0}{I_t}\right)_{V_{abs}} = \frac{\varepsilon}{M} \cdot C_V \times 10^2 \cdot l \tag{2.4}$$

Where ε [l/(mol· cm)] is the molar absorption coefficient, C_V [kg/m^3] is the mass concentration of vapor per unit volume, and l [m] is the optical path length. The onion - pealing model (for estimating l) which is used to approximate ε (T_{mix}) in the spray is applied. The details are described in our previous paper [100].

The scattering transmittance by droplets can be calculated based on Bauguer – Lambert -Beer's law as expressed in Eq. (2.5):

$$\left(\frac{I_t}{I_0}\right)_{L_{sca}} = \left(\frac{I_t}{I_0}\right)_{\lambda_T} = exp\left[-R \cdot Q_{ext} \int_0^l \int_0^\infty \frac{\pi}{4} D^2 \cdot N \cdot f(D) \cdot dDdl\right] \tag{2.5}$$

Where R is a correctional factor, Q_{ext} is the extinction coefficient, D is the droplet diameter, N is the number densify of droplets and f (D) is the droplet size distribution function.

The droplets concentration C_d [kg/m^3] is defined as

$$C_d = \frac{1}{L} \int_0^L \int_0^\infty \frac{\pi}{6} \rho_f \cdot D^3 \cdot N \cdot f(D) \cdot dDdl \tag{2.6}$$

Here ρ_f[kg/m^3] is the density of the injected fuel.

Then Eq. (2.7) can be obtained by combining Eq. (2.5) and Eq. (2.6):

$$C_d = \frac{2}{3} \rho_f \cdot D_{32} \frac{ln\left(\frac{I_0}{I_t}\right)_{\lambda_T}}{R \cdot Q_{ext} \cdot l} \tag{2.7}$$

Here D_{32} is the Sauter mean diameter [m] defined by Eq. (2.8):

$$D_{32} = \frac{\sum_i N_i \cdot D_i^3}{\sum_i N_i \cdot D_i^2} \tag{2.8}$$

Then Eq. (2.9) can be obtained by applying the measured attenuation of Vis light [58].

$$D_{32} = \frac{0.63 \cdot R \cdot Q_{ext} \cdot M_f}{\rho_f \cdot \sum_i \log\left(\frac{I_0}{I_t}\right)_{\lambda_T} \cdot \Delta S} \tag{2.9}$$

where M_f [mg] is the mass of injected fuel and ΔS [m^2] is the unit projection area.

Finally, mass concentration of droplet and vapor is obtained by applying Eq. (2.10) and Eq. (2.11).

$$C_d = 0.42\rho_f \cdot \frac{M_f \cdot ln\left(\frac{I_0}{I_t}\right)_{\lambda_T}}{\rho_f \cdot l \cdot \sum_i \log\left(\frac{I_0}{I_t}\right)_{\lambda_T} \cdot \Delta S} \tag{2.10}$$

$$C_V = \frac{M \cdot \left[log\left(\frac{I_0}{I_t}\right)_{\lambda_A} - log\left(\frac{I_0}{I_t}\right)_{\lambda_T}\right]}{\varepsilon \cdot l \times 10^2} \tag{2.11}$$

The spray in a Diesel engine is non-axisymmetric. The onion-peeling model is unavailable to analyze the non-axisymmetric spray when LAS technique is applied. Therefore, Zhang and Nishida [73] modified the LAS technique, which rendered it capable of analyzing the concentrations of non-axisymmetric sprays (Figure 2.4).

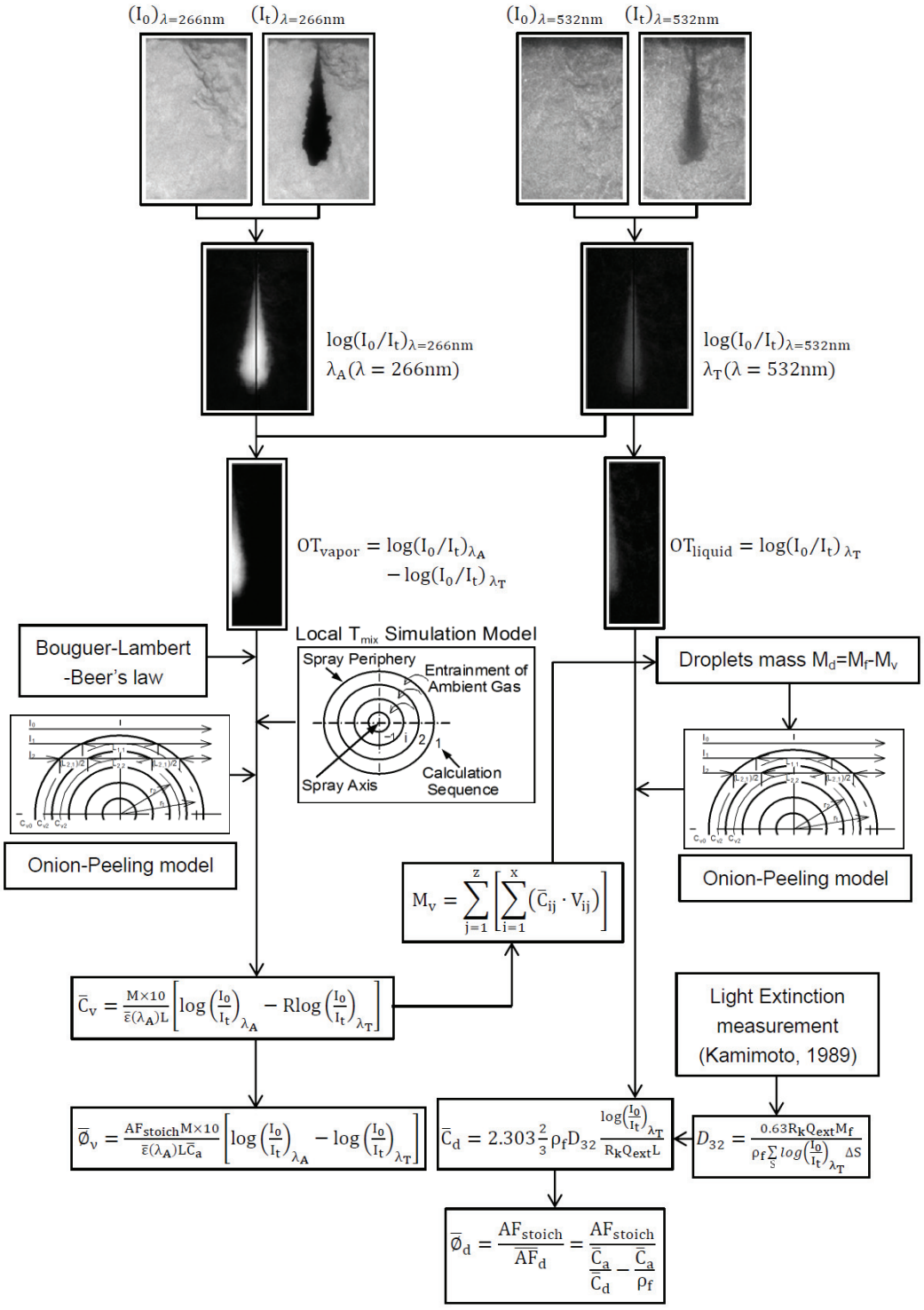

Figure 2.3 Flow diagram of axisymmetric analyzing process

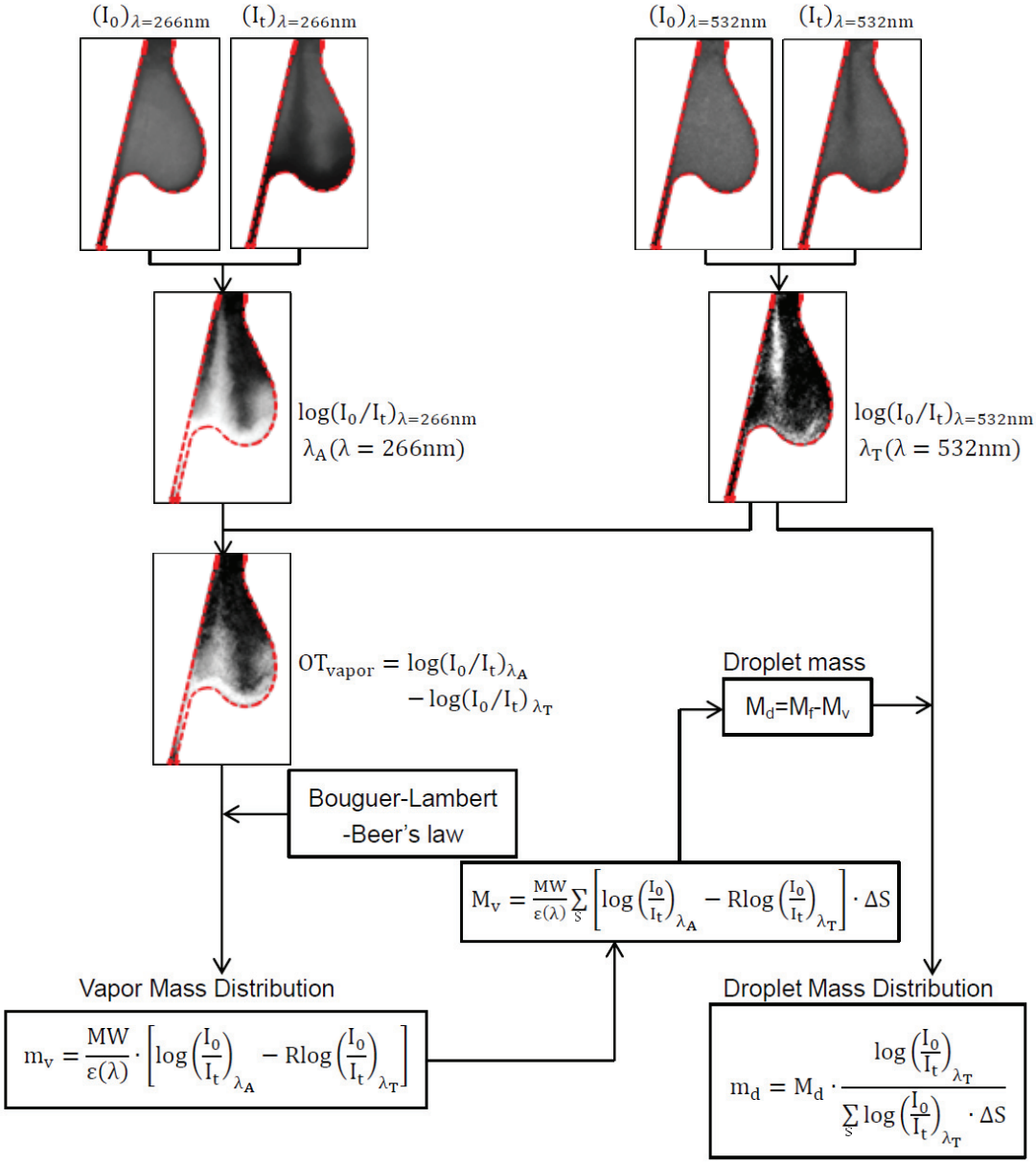

Figure 2.4 Flow diagram of non-axisymmetric analyzing process

2.2.2 Experiment Setup

In Figure 2.5, UV (ultraviolet, fourth harmonic, 266 nm) and Vis (visible, second harmonic, 512 nm) beams were generated using a pulsed YAG laser (Continuum NY 61-10). Firstly, the two beams were separated by a dichroic mirror and expanded. Then the two beams were combined and passed through the diffuser (Shinetsu film, polypropylene film) to homogenize the light intensity distribution prior to entering the

chamber. Subsequently, the two beams pass through the spray. Then, the two beams were separated and recorded by two CCD cameras (C4880, Hamamatsu Photonics).

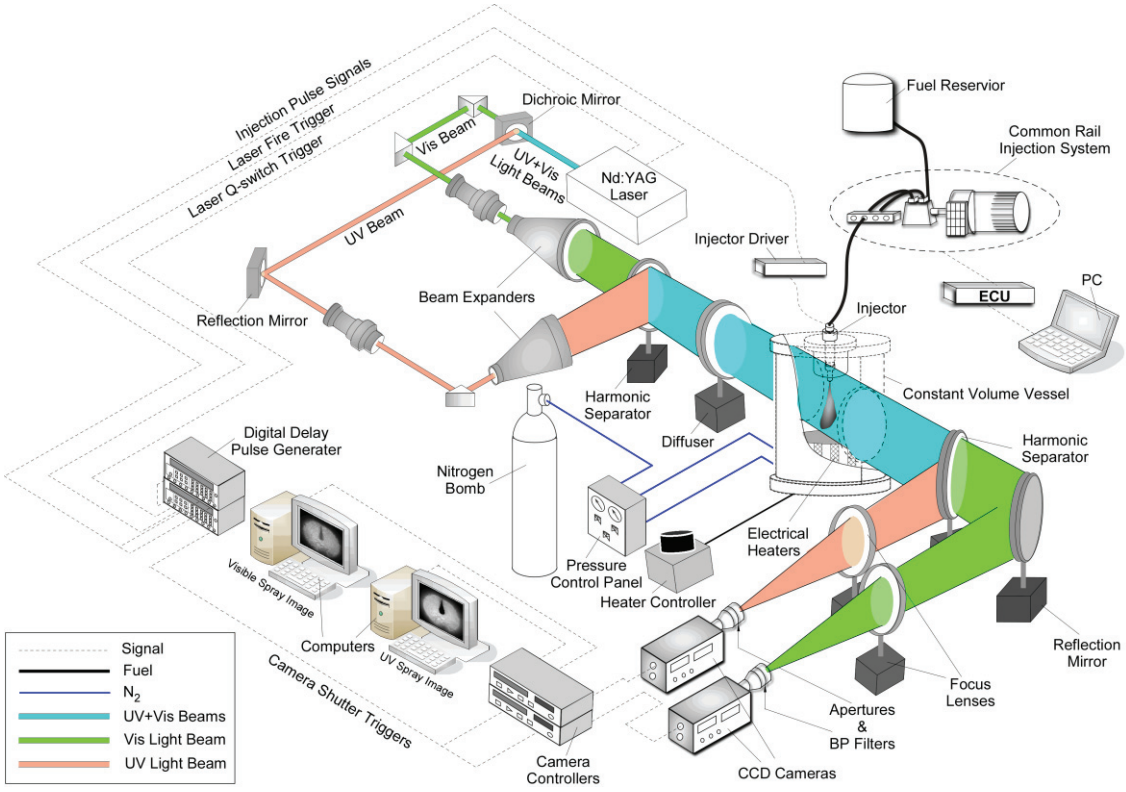

Figure 2.5 Experimental setup of LAS system

In developing the Mazda Skyactiv-D engine [27], Mazda's stated objectives in selecting a low r_c were decreased peak firing pressure and lower engine-out emissions through improved premixing. Nevertheless, this engine provides an impressive 59 KW/L and a peak BMEP of over 25 bar, while meeting Euro 6 NOx emissions regulations without after-treatment. In the Mazda design, the focus was on reduction of NOx [26, 27]. It is difficult to realize ideal combustion timing and duration due to NOx and PM restrictions (Diesel knocking noise is included in this problem.) for Japan domestic diesel passenger cars. Cost increase due to use of NOx after treatments to conform to strict emissions regulations

To solve these problems, the Mazda focused on the realization of the SKYACTIV-D technical concept shown in Figure 2.6 [113], in which an ultra-low compression ratio of 14.0 (the previous model for European market had 16.3) and high-efficiency boosting were combined.

In this concept, the outer "egg-shaped" vortex transports hot combustion products

to the cylinder center where they mix rapidly with cooler surrounding charge, thereby quenching thermal NO_x production. The thermal efficiency is also increased due to a shortening of the combustion duration [26]. This egg-shaped two-dimensional (2-D) piston cavity was employed to form impinging spray. The impinging distance between the nozzle tip and impingement point is 30 mm. The specifications of the 2-D cavity are presented in Figure 2.7 and the EGG shape combustion chamber concept are presented in Figure 2.8 [113].

a) At the early stage, by contriving the curvature of the collision part of the spray and the side wall of the combustion chamber, a strong flow is formed toward the bottom surface of the combustion chamber where the rich air-fuel mixture is most likely to stay stagnant and suppresses the rich air-fuel mixture locally stagnation.

b) At the middle stage, the bottom and the slope of the chamber sustains a strong flow created at the initial stage, guides burned gas to the center of the cylinder, promotes mixing with fuel gas. Here, oxygen is led into burned gas and oxidation of soot by oxygen introduction into burned gas and suppresses thermal NO by cooling the burned gas.

c) At the latter stage, by directing the flow from the center of the cylinder towards the squish area and connect with the reverse squish flow during the expansion stroke, and the surplus air in the squish area during the expansion stroke is effectively used.

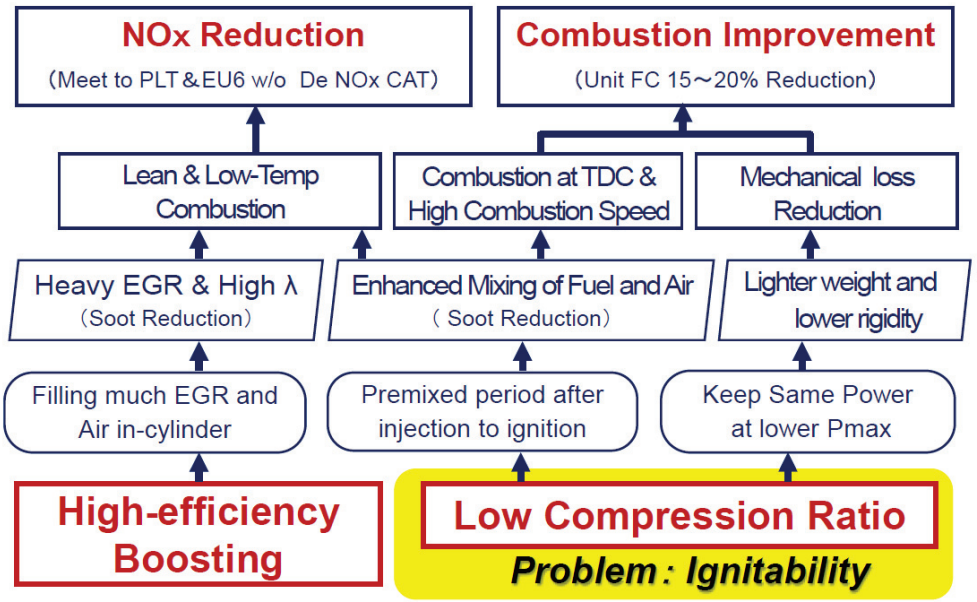

Figure 2.6 SKYACTIV-D Technology Concept

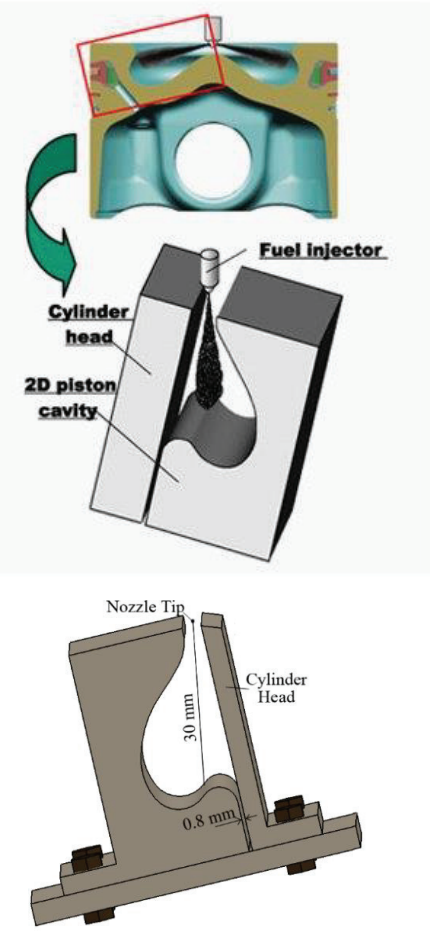

Figure 2.7 Specification of 2-D cavity

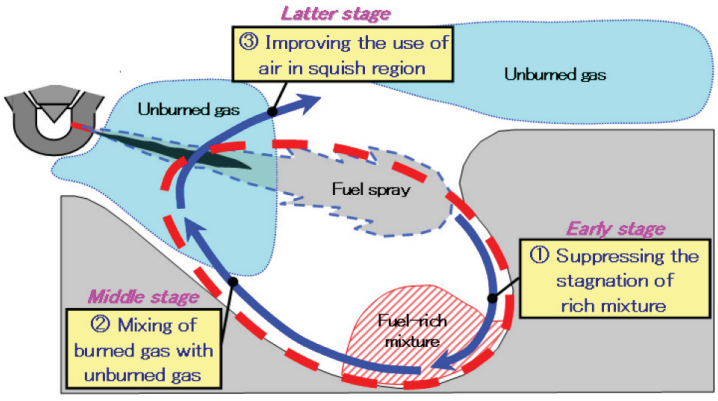

Figure 2.8 EGG Shape Combustion Chamber Concept

2.2.3 Fuel for LAS Technique

A blend fuel of 2.5 vol% of α-MN and 97.5 vol% of n-tridecane was adopted.

To image diesel fuel sprays by means of LAS technique, the test fuel must have

following properties:

(1) Similar physical properties with Diesel fuel;

(2) Strongly absorbs UV light but not absorbs Vis light;

(3) UV absorption satisfies Lambert-beer's law and molar absorptivity has less temperature dependences.

The physical properties of candidate test fuels and diesel fuel (Japanese Industrial Standard No.2 (JIS#2) diesel fuel) are shown in Table 2.1. Candidate fuels are selected based on first requirement (1).

The fuel n-Pentadecane seems to be the most suitable to replace diesel fuel. However, depression of freezing point of this fuel is occurred under high pressure condition such as diesel injection pressure [114, 115]. And for n-Tetradecane, n-Pentadecane and n-Hexadecane, these three fuels freeze under room temperature. Because of this, these four fuels are not suitable for the test fuel.

Compare the physical properties of the remanent fuels n-Tridecane and α-Methylnaphthalene, density of n-Tridecane is closer to diesel fuel. Therefore, n-Tridecane was provisionally selected as the test fuel.

As shown in Figure 2.9, n-Tridecane satisfies the requirement (2) which mentioned above, absorbs UV light but not absorbs Vis light. However, the absorbance of UV light at 266 nm is little weaker than that of 1, 3-DMN.

Accordingly, α-Methylnaphthalene (α-MN) which has strong absorbance of UV light is added to the test fuel, which works as "tracer" to get strong absorption at UV light.

For n-Tridecane and α-MN, these two fuels have superior compatibility and similar vapor-pressure curve function with temperature [116]. Thus, α-MN is suitable for the tracer added to n-Tridecane.

In this investigation, the tracer LAS fuel contains 2.5 volume percent of α-MN and 97.5 volume percent of n-Tridecane. Based on this, the calculated physical properties and measured absorbance spectrum of the tracer fuel are also shown in Table 2.1 and

Figure 2.9. Third Requirement (3) will be discussed in next chapter.

Table 2.1 Properties of candidate test fuels

Substance	Formula	Boiling point [℃]	Density [kg/m^3]	Kinetic viscosity [mm^2/s]
α-Methyl-naphthalene	$C_{11}H_{10}$	244.7	1016	2.58
1,3-Dimethyl naphthalene	$C_{12}H_{12}$	262.5	1018	3.95
n-Tridecane	$C_{13}H_{28}$	235.0	756	2.47
n-Tetradecane	$C_{14}H_{30}$	253.7	760	3.04
n-Pentadecane	$C_{15}H_{32}$	270.6	770	3.73
n-Hexadecane [cetane]	$C_{16}H_{34}$	287.0	780	4.52
Tracer fuel [α-MN 2.5% + n-Tridecane 97.5%]	-	235.8	767	2.48
Diesel JIS#2	-	~273	~830	~3.86

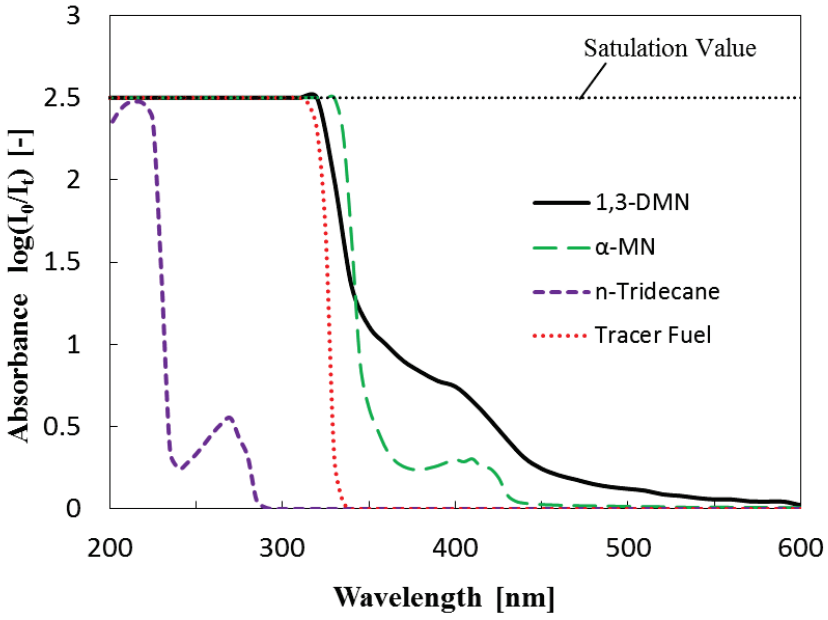

Figure 2.9 Absorption spectrum of liquid fuels

2.2.4 Molar Absorption Coefficient of Tracer Fuel

Molar absorption coefficient measuring system is shown in Figure 2.10.

The system is composed of a high Pressure/temperature cell (optical path length is 100mm), a fiber optic spectrometer (Ocean Optics, S2000) and a deuterium lamp (Ocean Optics, D1000). The UV beam is provided by the deuterium lamp and spectrum is measured by the fiber optic spectrometer. The fuel vapor is filled in the cell after adjusting measurement temperature and pressure inside the cell.

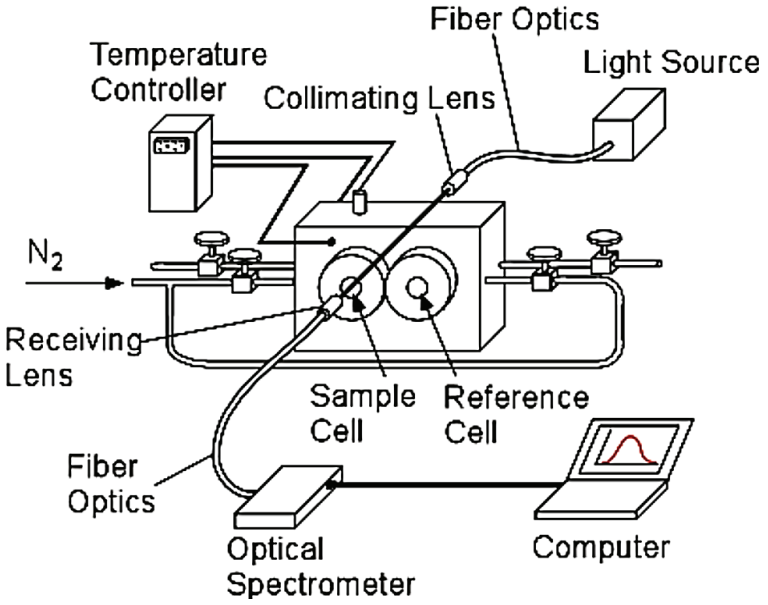

Figure 2.10 Experimental apparatus for vapor phase absorption measurement

The absorbance is calculated by applying Eq. (2.12).

$$Absorbance = log\left(\frac{I_0 - DK}{I_t - DK}\right)_{\lambda_A} \quad (2.12)$$

Where DK is the dark intensity measured without light source.

Strength of the absorption is represented by molar absorption coefficient ε in Eq. (2.5).

The measured absorbance of the tracer fuel (2.5% a-MN + 97.5% n-Tridecane) is shown in Figure 2.11.

Figure 2.11 shows good linear relationship between the molar concentration and absorbance which coincides with Lambert-beer's law and also satisfy the third

requirement (3). The experimental data adopted here comes from our lab previous paper [52].

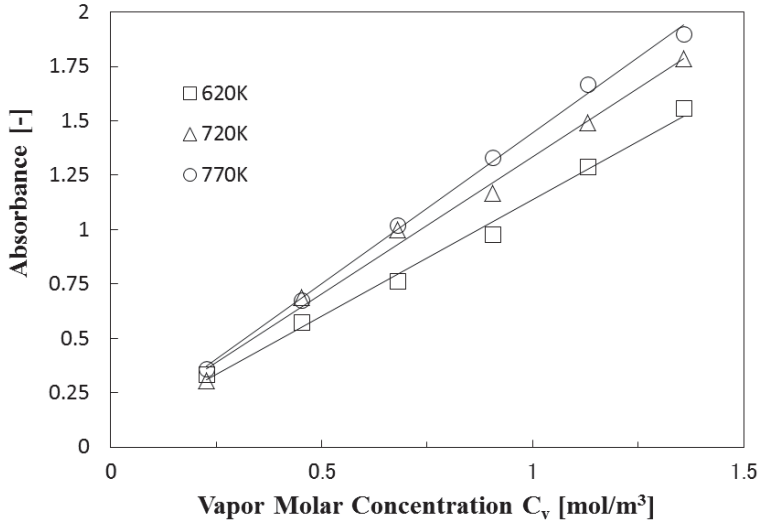

Figure 2.11 Vapor absorbance dependences on vapor concentration of the tracer fuel (P_a =3.6 MPa, T_{mix}=620, 720 and 770 K)

The molar absorption coefficient ε is calculated by the Lambert-Beer's law as shown in Eq. (2.13) (the same meaning as Eq. (2.5))

$$\varepsilon = \frac{log\left(\frac{I_0}{I_t}\right)_{\lambda_A}}{C_V \cdot M \times 10^2 \cdot l} \tag{2.13}$$

The molar absorption coefficients of the tracer fuel under various temperatures are shown in Figure 2.12. It is found that molar absorptivity has less temperature dependences and meets the third requirement (3).

In analyzing procedure, the mixture temperature in the spray is calculated by bulk temperature [100]. Thus, the molar absorption coefficient is expressed as a function of temperature which is shown in Eq. (2.14).

$$\varepsilon(T_{mix}) = 10^{(0.000591948 \cdot T_{mix} + 1.69738)} \tag{2.14}$$

As mentioned at the part of principle, liquid absorption $\log(I_0/I_t)_{\lambda T}$ in Eq. (2.1) is ignored. In this section, it is confirmed by the non-evaporation spray.

Figure 2.13 shows UV and Vis spray images under non-evaporation ambient condition (Ta=300 K, Pa=1.4 MPa). Figure 2.14, 2.15 and 2.16 give the optical thickness

distributions along the lines which are shown in Fig 2.13. If liquid phase absorption can be ignored, the attenuation of Vis and UV light in Eq. (2.1) and Eq. (2.2) should have the same value because of no existence of fuel vapor under non-evaporating condition.

As a result, the optical thickness of UV and Vis light extremely correspond with each other which indicates liquid phase absorbance in Eq. (2.1) is very small compared with scattering extinction and can be neglected.

According to the above discussions, the tracer fuel satisfies all the requirements of LAS technique.

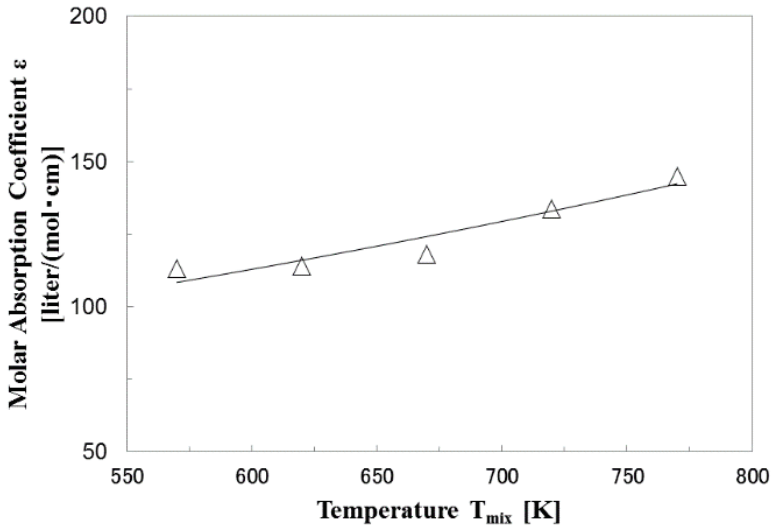

Figure 2.12 Molar absorption coefficient dependence on temperature (P_a=3.6 MPa)

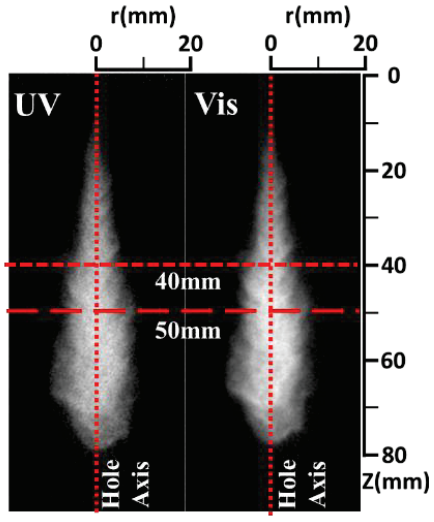

Figure 2.13 Spray images of non-evaporating spray

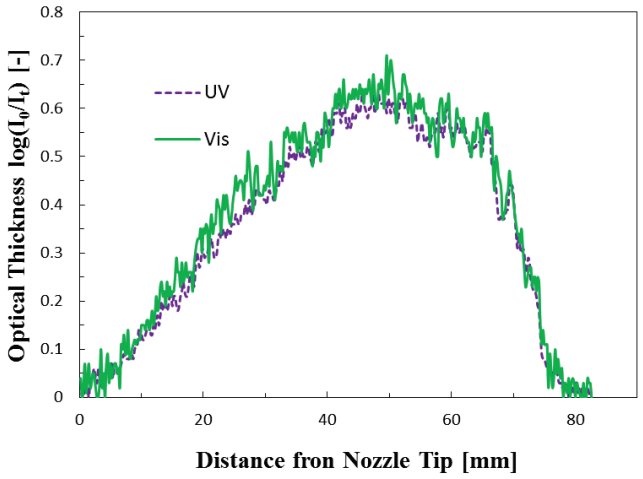

Figure 2.14 Optical thickness distribution along nozzle hole axis

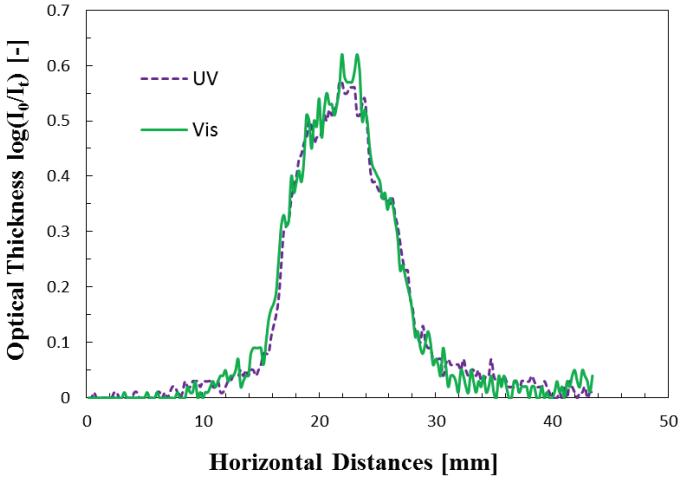

Figure 2.15 Optical thickness distribution along horizontal axis of 40mm downstream

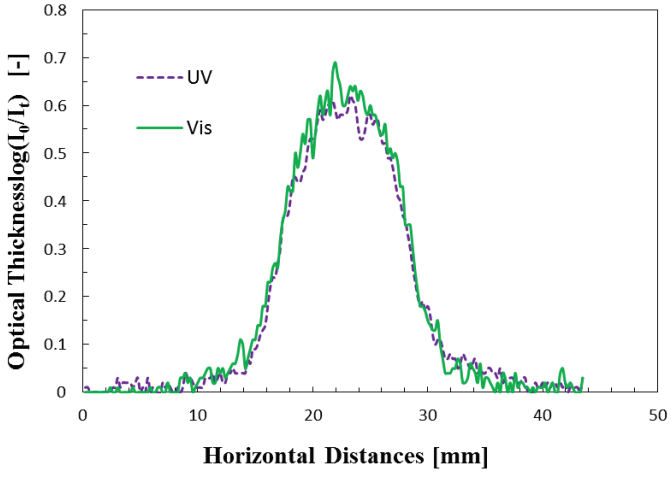

Figure 2.16 Optical thickness distribution along horizontal axis of 50mm downstream

2.3 TWO-COLOR PYROMETRY FOR COMBUSTION

Figure 2.17 illustrates the experimental apparatus for the two-color pyrometry observation of combustion.

The combustion images were captured by the high-speed camera, which was same as that used in the Mie scattering experiment. The frame rate was 10000 fps and the resolution was 512 × 512 pixels, with an exposure time of 1/10000 s. The temperature and soot concentration (represented by KL factor) were calculated by the two-color pyrometry method. Red, Green and Blue channels were got from the natural flame color images. Red and Green channels were adopted because these two channels have spectral responses with insignificant overlap.

2.3.1 Principle of Two-color Pyrometry

According to the Wien's equation, the monochromatic emissive power of a black body N(λ ,T) depends on the temperature and the specific wavelength, which can be expressed as:

$$N(\lambda, T) = C_1 \lambda^{-5} exp(-C_2/\lambda T_a) \tag{2.15}$$

Where C_1 and C_2 are the first Planck's constant and the second Planck's constant respectively; λ is the wavelength and T_a is the temperature of the black body.

Under non-blackbody emission condition, the mission power is expressed as:

$$N(\lambda, T) = \varepsilon_\lambda C_1 \lambda^{-5} exp(-C_2/\lambda T_a) \tag{2.16}$$

Where T is the temperature of the non-black body; ε_λ is the monochromatic emissivity of a non-black body.

In practice, ε_λ is estimated for soot particles based on the empirical correlation developed by Hottel and Broughton [117],

$$\varepsilon_\lambda = 1 - e^{(-KL/\lambda^a)} \tag{2.17}$$

Combining Eq (2.15), Eq (2.16) and Eq (2.17) gives,

$$KL = -\lambda^a ln\left[1 - \exp\left(-C_2/\lambda \cdot \left(\frac{1}{T_a} - \frac{1}{T}\right)\right)\right] \quad (2.18)$$

If there are two specific wavelengths λ_1 and λ_2 that are measured simultaneously, the value KL which is proportional to the integrated soot concentration can be eliminated:

$$\left[1 - \exp\left(-C_2/\lambda \cdot \left(\frac{1}{T_{a1}} - \frac{1}{T}\right)\right)\right]^{\lambda_1^a} = \left[1 - \exp\left(-C_2/\lambda \cdot \left(\frac{1}{T_{a2}} - \frac{1}{T}\right)\right)\right]^{\lambda_2^a} \quad (2.19)$$

Provided the black body temperatures T_{a1} and T_{a2} at two specific wavelength $\lambda_1$and λ_2 can be obtained according to the calibration data, the actual temperature and the KL value calculated.

2.3.2 Calibration Method

According to the Eq. (2.16), the power of monochromatic emissive after passed through the neutral filter with transmittance of τ_i can be expressed as,

$$N(\lambda, T) = \tau_i \varepsilon_\lambda C_1 \lambda^{-5} exp(-C_2/\lambda T) \quad (2.20)$$

Combining Eq. (2.15) and Eq. (2.20) gives:

$$1/T - 1/T_a = \lambda/C_2 \cdot ln(\tau_i \varepsilon_\lambda) \quad (2.21)$$

When the transmittance is 1, the temperature T will be received by using a thermodetector and then T_a will be calculated through equation 1. The empirical correlation of $\varepsilon_\lambda = a_0 + a_1\lambda + a_2 T + a_3 \lambda T$ is used in this calculation.

The luminous intensity I perceived by camera sensor could be defined as:

$$\mathrm{I} = \mathrm{a}\varepsilon_\lambda C_1 \lambda^{-5} exp(-C_2/\lambda T) + b \quad (2.22)$$

Where a and b are constants which depend on the camera sensor. Taking the logarithm at both sides of Eq. (2.22) gives,

$$ln(1-b) = -C_2/\lambda T + ln(a\varepsilon_\lambda C_1 \lambda^{-5}) \quad (2.23)$$

According to this equation, the relationship between $ln(1-b)$ and 1/T follow linearity when the illuminant happens. The slope equals to $-C_2/\lambda$, in reverse, the effective wavelength of this system could be defined as follows:

$$\lambda_{effective} = -C_2/slpoe \tag{2.24}$$

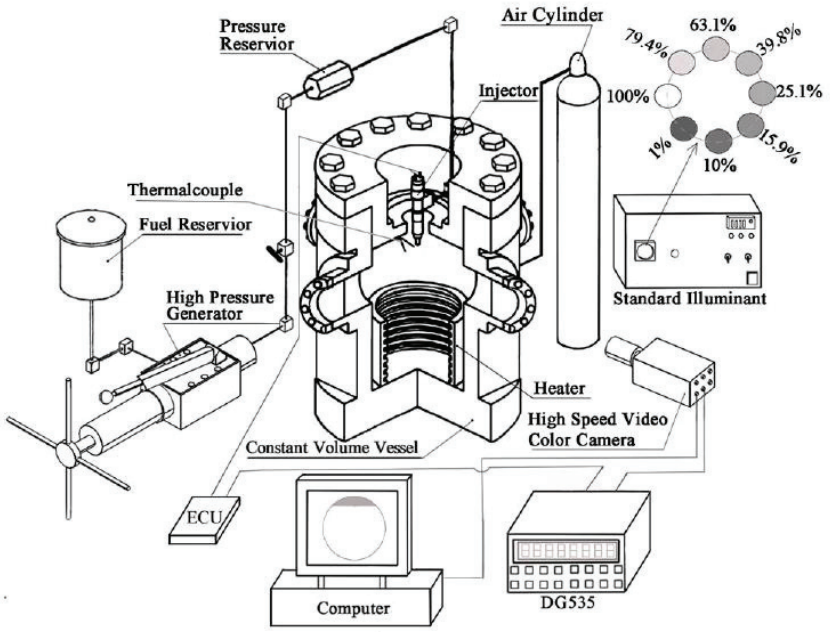

Figure 2.17 Experimental setup for natural luminosity and two-color pyrometry

In this investigation, a high-speed video color camera is used and the intensity of Red, Green and Blue channels could be obtained. Three effective wavelengths of color camera (GX-8, Nac Image Technology Inc.) could be acquired:

$$\lambda_{red} = 577.38\,nm, \lambda_{green} = 541.12\,nm, \lambda_{blue} = 517.82\,nm$$

Only the red and blue channels are selected for our two-color calculation because these two channels have spectral responses with insignificant overlap [118].

When the source of the light is a standard illuminant as shown in the right top part of Figure 2.17, the ε_λ in will becomes the value of 1, and the T will be replaced by T_a. After the camera recorded eight kinds of luminous intensity which are attenuated by eight kinds of neutral filters and calculate those data by using the Eq. (2.24) then the calibration line like Figure 2.18 will be obtained.

From Figure 2.18 the temperatures of black body at two effective wavelengths are received. And the actual temperature could be calculated by applying Eq. (2.19).

In this study, in fact, some natural luminosity, as a result, the two color experiments

were carried out by applying another high speed color camera (Nac Image Technology Inc. GX-1). In this system, the actual temperature was calculated by two apparent temperatures at two specific wavelengths. The calibration method was different with that of GX-8 camera as introduced above which was implemented employing standard illuminant. The calibration process of GX-1 camera used a tungsten lamp to play a role as standard illuminant. The correlation of the voltage and the apparent temperature at the wavelength of 662 nm of the tungsten lamp was identified in advance, then the apparent temperature at the effective wavelength can be calculated by Eq. (2.25):

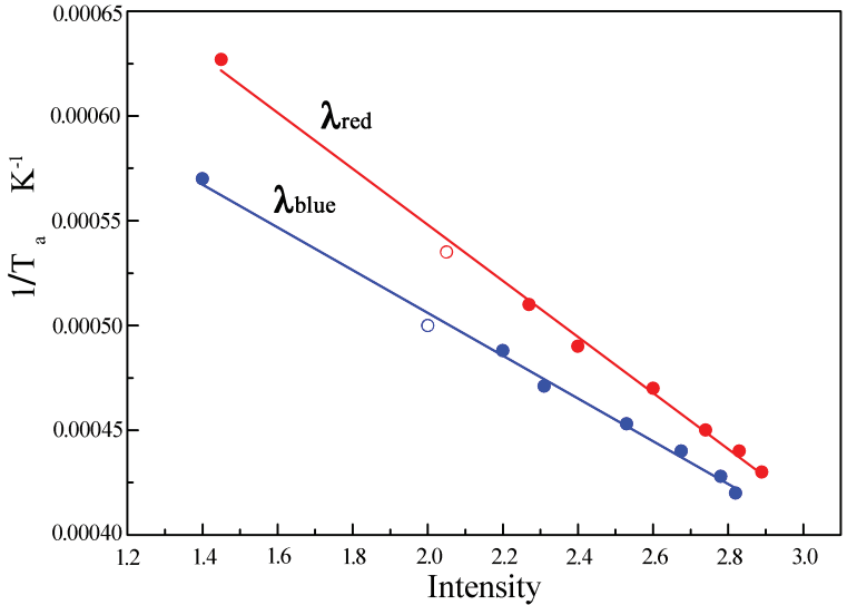

Figure 2.18 Calibration graph sample. The vertical axis represents the black body's temperature; the horizontal axis represents the actual intensity $\ln(1-b)$ which is received by camera sensor, b is a constant of the camera.

Table 2.2 Larabee empirical equations

350 to 450 nm	$\varepsilon_{\lambda T} = 0.6075 - 0.3000\lambda - 0.3265 \times 10^{-4}T + 0.5900 \times 10^{-4}\lambda T$
450 to 680 nm	$\varepsilon_{\lambda T} = 0.4655 - 0.01558\lambda - 0.2675 \times 10^{-4}T - 0.7305 \times 10^{-4}\lambda T$
680 to 800 nm	$\varepsilon_{\lambda T} = 0.6552 - 0.2633\lambda - 0.7333 \times 10^{-4}T + 0.7417 \times 10^{-4}\lambda T$
λ is the effective wavelength and T is the tungsten temperature	

The effective wavelengths were calculated by Eq. (2.24), and the result revealed that the effective wavelength of red channel and green channel of GX-1 camera are 754 nm

and 596 nm respectively. The emissivity ε is a function of wavelength and the tungsten temperature, it can be calculated by the Larabee empirical equations as shown in Table 2.2.

2.4 OH* CHEMILUMINESCENCE METHOD

OH* chemiluminescence is widely considered as the indicator of high temperature reaction in a flame. The OH* chemiluminescence was evident in the spectral analysis of premixed diesel combustion when implementing the HCCI mode [119]. The energetic reactions and high temperatures in a diesel flame that occur during the stoichiometric combustion of typical hydrocarbon fuels form excited state species that include excited state OH (OH*) [112]. The primary kinetic path for forming OH* is the exothermic reaction $CH + O2 \rightarrow CO + OH^*$ [112]. Once formed, OH* returns rapidly to its ground state, a portion through chemiluminescent emission and a portion through collisional quenching. For the typical mixing-controlled diesel flame, a distinct OH peak was observed at 310 nm, and a strong gray-body emission dominated the spectrum at wavelengths longer than 340 nm [120].

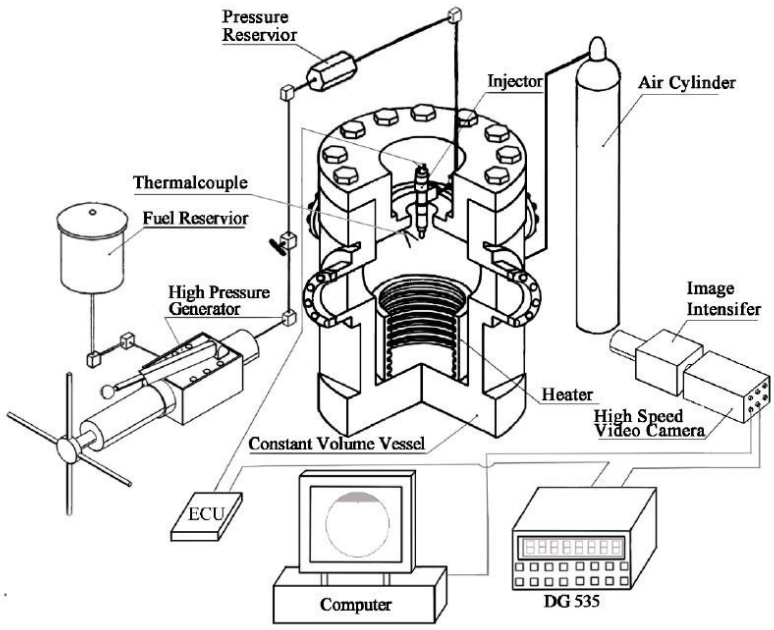

Figure 2.19 Experimental setup for OH* chemiluminescence

Figure 2.19 shows the experimental setup for the OH* chemiluminescence method. A high-speed camera (Photron Co., ultima FASTCAM-APX RS) with a Nikkor lens (Nikon, 105 mm, f/4.5) was used to capture the images. A band-pass filter (310 nm centered, 10 nm FWHW) was used to isolate the OH* chemiluminescence. The soot gray-body emission is considered to be separated from the OH* chemiluminescence. An image intensifier system (LaVision Inc., HS-IRO) was employed because the OH* intensity is too weak to detect.

CHAPTER 3 MIXTURE AND COMBUSTION CHARACTERISTICS OF SMALL INJECTION AMOUNT FUEL SPRAY

3.1 INTRODUCTION

Homogeneous charge compression ignition (HCCI) is a form of internal combustion in which well-mixed fuel and oxidizer (typically air) are compressed to the point of auto-ignition. HCCI engines achieve extremely low levels of oxides of nitrogen emissions (NOx) without a catalytic converter. Decreasing compression ratio is an effective way realize HCCI combustion mode in a diesel engine [121]. But there is a strict problem that the combustion under cold start process and idle mode are unstable in a low compression ratio diesel engine. Multi-polit injection strategy is an effective way to solve this problem [122]. HC and CO emissions are sufficiently low when a small quantity of fuel is injected [13]. Therefore, the spray behaviors of small injection mass is worthwhile to be concentrated on.

3.2 EXPERIMENTAL CONDITIONS

Table 3.1 shows the experimental conditions. In order to measure the spray mixture formation and the combustion characteristics, high-temperature, high-pressure conditions were adopted. For the evaporation conditions, the ambient gas was nitrogen which can prevent self-ignition. The test fuel used was tracer LAS fuel (Tridecane 97.5% / α-MN 2.5%). The ambient gas was air in the combustion conditions (O_2: 21%, N_2: 79%).

Single-hole piezo actuator was used for the meet of high injection pressure. The injection pressure was selected as 100, 150, 170 MPa for the evaporation conditions and 100 MPa for the combustion conditions. But the injection mass was kept at 2.97 mg for two conditions.

For the evaporation conditions, the ambient temperature and pressure were selected as 760 K and 3.6 MPa respectively. The ambient and pressure for the combustion conditions were 900 K and 4.1 MPa respectively in order to achieve the same ambient density 16 kg/m^3.

Table 3.1 Experimental conditions

	Evaporating	Combustion
Ambient Gas	N_2	Air
Temperature: T_a [K]	760	900
Pressure: P_a [MPa]	3.6	4.1
Density: ρ_a [kg/m^3]	16	
Fuel	Tracer LAS Fuel	JS#2 Diesel Fuel
Injection Amount: M_f [mg]	0.27, 0.89, 2.97	
Injection Pressure: P_{inj} [MPa]	100, 150, 170	100
Injector Type	Single Hole Piezo Actuator	
Nozzle Hole Diameter [mm]	0.133	

3.3 SPRAY MIXTURE CONCENTRATION DISTRIBUTIONS

This part discusses the results of the vapor/liquid distributions of the various conditions, such as varying of the injection amount and the injection pressure. The Figures show the different results of the vapor/liquid equivalence distributions, the evaporation ratio and the ratio of entrained gas to total fuel as time elapses under various injection amounts and injection pressures.

3.3.1 Effect of Injection Amount

Figure 3.1 shows the vapor/liquid equivalence distributions as time elapses under various injection amounts, the liquid phase evaporates and the vapor phase becomes lean as time elapses. It is necessary to explain that in this paper the midpoint of the top edge of every image is defined as the position of nozzle tip of the injector. The injection

amounts differed from 0.27, 0.89 and 2.97 mg but the injection pressure always fixed at 100 MPa. In each plot of the figure, left half is the liquid phase, while the right half shows the vapor phase. The values in the plot mean the equivalence ratio value. The values become bigger as the image color on the left bottom plot becomes richer.

At 0.2 ms ASOI, there is no great difference for the spray penetration. The liquid equivalence ratio is rich, but vapor equivalence ratio is lean under the three injection amounts conditions. When the injection amount increases, the liquid equivalence ratio becomes richer. For the results of 0.89 and 2.97 mg, the liquid equivalence ratios are almost same. But it can be seen that the vapor equivalence ratio of the 2.97 mg is richer than that of 0.89 mg.

At 0.3 ms ASOI, there is also no significance difference of the spray tip penetration for three injection amounts. It can be seen that the vapor phase is around stoichiometric at this time when the injection amount is 0.27 mg.

At 0.5 ms ASOI, it shows that larger injection amount gives the longer spray tip penetration. The vapor phase is around stoichiometric at the injection amount of 0.89 mg. It still shows rich liquid equivalence ratio of 2.97 mg at this time.

At 1.0 ms ASOI, the spray tip penetration difference of the three injection amounts is significant. The larger injection amount gives the longer spray tip penetration. The rich vapor concentration phase (equivalence ratio around 1.6) is formed at the injection amount of 2.97 mg.

At 1.5 ms ASOI, the spray tip penetration difference of the three injection amounts is also significant. The larger injection amount gives the longer spray tip penetration. Compare with the result of 1.0 ms, it can be seen that the vapor equivalence ratio distribution becomes lean.

According to Figure 3.1, the liquid equivalence ratio decreases but the vapor equivalence ratio increases at first and then decreases as time elapses. The larger the injection amount is, the later the time of stoichiometric vapor phase is. Moreover, the larger injection amount gives the higher vapor equivalence ratio.

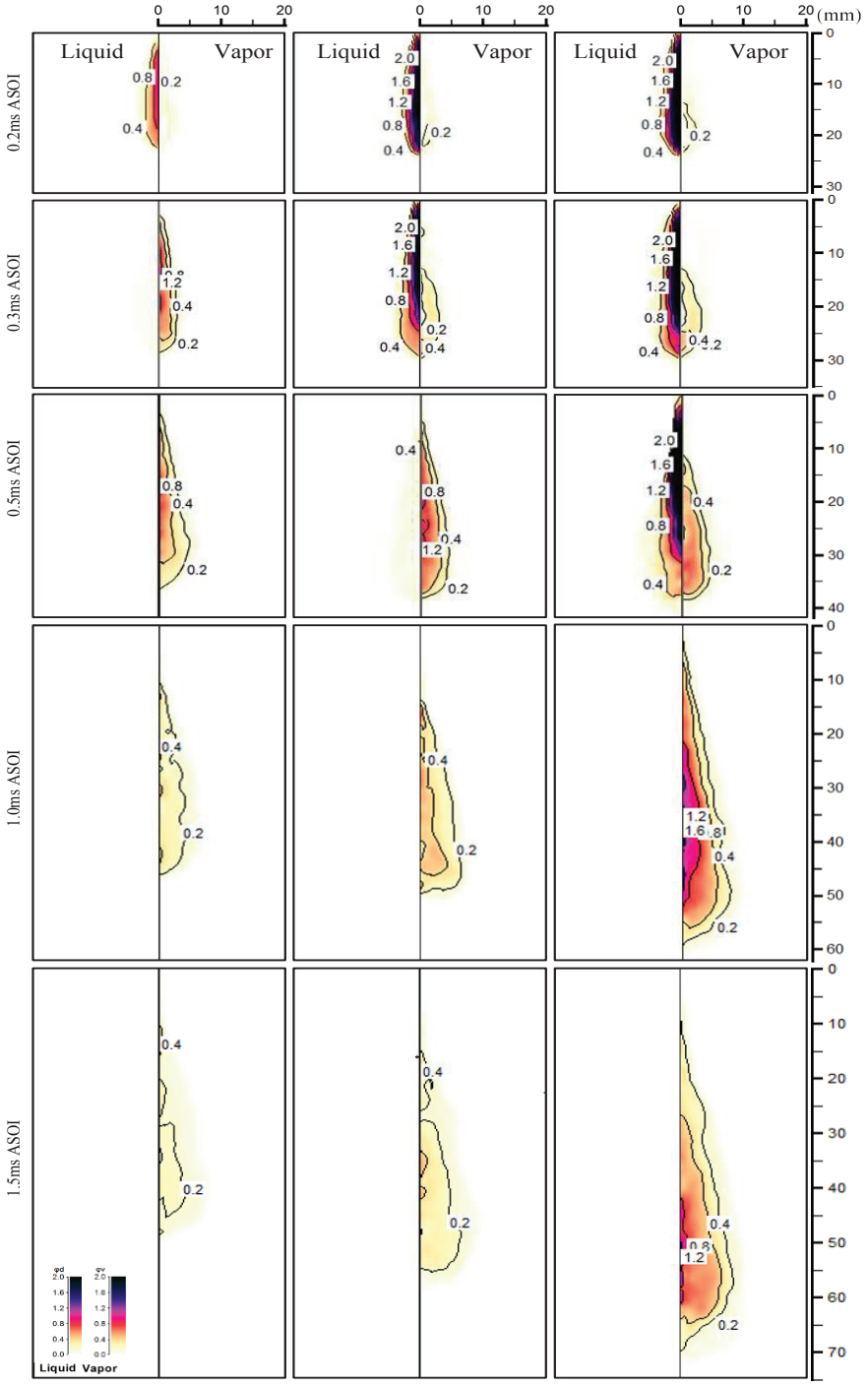

(a) Q=0.27 mg (b) Q=0.89 mg (c) Q=2.97 mg

Figure 3.1 Vapor/liquid equivalence ratio distributions

Injection durations of three injection amounts are shown in Figure 3.2 and Figure 3.3. The larger the injection amount is, the longer injection duration will be. The temporal variations of ratio of vapor to total fuel under different injection amounts are shown in Figure 3.2. The evaporation ratio signifies the ratio of fuel evaporation, which equals the

vapor mass at a particular time divided by the injected fuel mass at this time. The results obtained show that the evaporation ratio becomes higher as the injection amount is smaller. When the injection amount is 0.27 mg, the fuel is full evaporates at time 0.5 ms ASOI. At the injection amount of 0.89 mg and 2.97 mg, the fuel full evaporates time is 0.9 ms and 1.3 ms ASOI respectively. The smaller the injection amount is, the faster the fuel full evaporates. The gradient of evaporation ratio of small injection amount is bigger than that of big injection amount. It implies that the small injection amount can improve the fuel evaporation process. The EOI of 0.27 mg is 0.19 ms ASOI, 0.32 ms ASOI for 0.89 mg and 0.75 ms ASOI for 2.97 mg. It can be calculated that it continues 0.31 ms from EOI to the fuel full evaporates timing for 0.27 mg, 0.58 ms for 0.89 mg and 0.55 ms for 2.97 mg. It can be seen that it takes shorter time for small injection amount to finish the evaporation process.

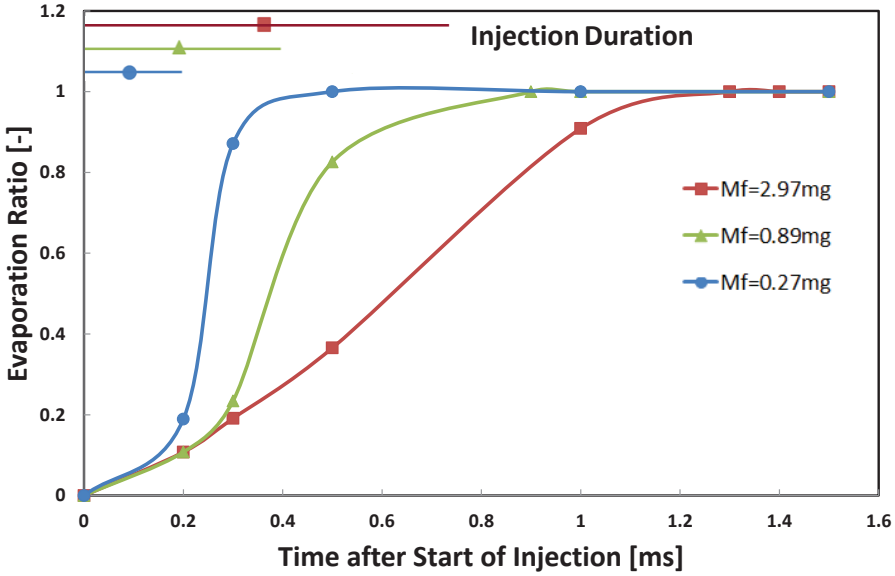

Figure 3.2 Evaporation ratio

The spray is considered to be many parts of symmetrical column. The space volume of spray considered to be the sum of these spray column. The spray mass can be calculated by space mass minus the temporary spray mass. Then the ratio can be calculated. The calculate process will be briefly introduced here. Figure 3.3 shows the definition of spray

volume.

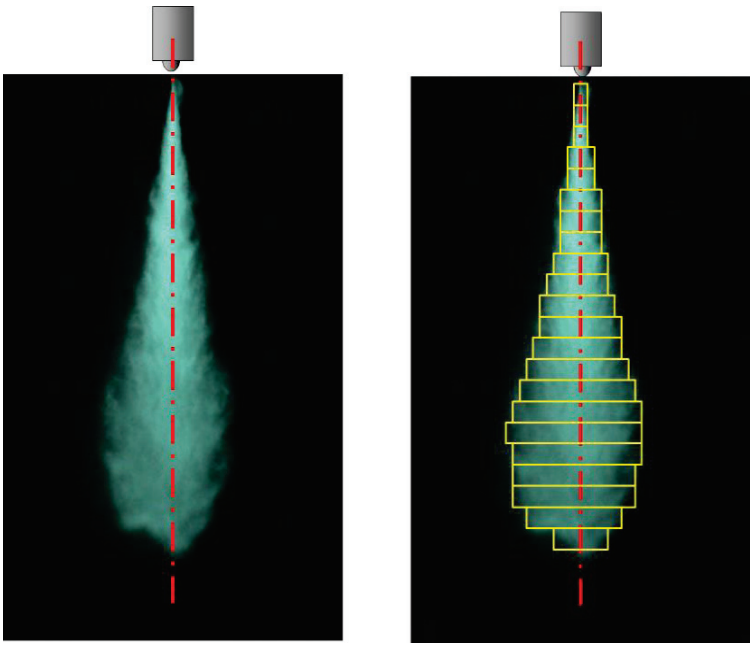

Figure 3.3 Definition of Spray Volume

$$V = \sum \pi r^2 h$$

Where V [mm^3] is the spray volume, r [mm] is the radius and h [mm] is the spray column height.

Then the spray mass can be calculated by:

$$M_a = \rho_a \left(V - \frac{m_f \cdot t}{\rho_f} \right)$$

Where M_a [mg] is entrainment ambient gas mass, ρ_a [kg/m^3] is the ambient gas density, ρ_f [kg/m^3] is the fuel density, m_f [mg/s] is fuel mass injection rate and t [s] is the timing.

In Figure 3.4, it shows the ratio of entrained gas to total fuel under different injection amounts. Figure 3.4 shows that the ratio of entrained gas to total fuel is bigger when the injection amount is smaller. The ratio of entrained gas to total fuel increases as the time elapses under three injection amounts. Nevertheless, the smaller injection amount gives the bigger entrained gas and accelerates the fuel evaporation. The results contribute to the rich air-fuel mixture formation. The ratio gap between 0.89 mg and 2.97 mg is smaller

than that of between 0.27 mg and 0.89 mg. The gradient of ratio increases as the injection amount decreases. It implies that the small injection amount can obtain much more relative entrained gas, which can make the fuel evaporates quickly and improve the fuel evaporation process.

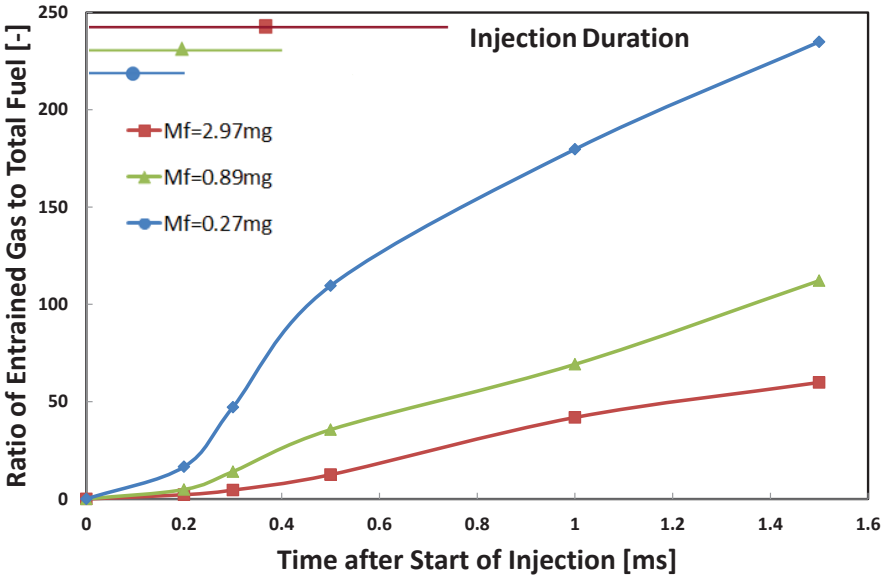

Figure 3.4 Ratio of entrained gas to total fuel

After the comparison of Figure 3.1, 3.2 and 3.4, it can be concluded that a larger injection amount gives a longer spray tip penetration. Small injection amount can obtain much more relative entrained ambient gas. Small injection amount can improve the fuel evaporation process. After the comparison of Figure 3.2 and 3.4, it can be seen that the fuel evaporation is not greatly enhanced by the longer injection duration but greatly enhanced by the shorter injection duration.

Figure 3.5 shows the relationship between the mass frequency to total fuel and equivalence ratio to total fuel (Φ_{all}) under different injection amounts, which can investigate the fuel vapor homogeneous extent.

In Figure 3.5 (a), it shows the relationship between the mass frequency to total fuel and Φall under 0.27 mg. It shows that small Φ_{all} becomes rich as time elapses. And the peak of mass frequency to total fuel moves to the lean Φ_{all} area as time elapses. It can be

seen that the rich Φ_{all} achieves 1.26 when time goes to 0.2 ms ASOI. When time goes to 1.5 ms ASOI, the mass frequency to total fuel achieves 0.55 when the Φ_{all} is 0.2. And the Φ_{all} is smaller than 0.36 at 1.5 ms ASOI.

In Figure 3.5 (b), it shows the relationship between the mass frequency to total fuel and Φall under 0.89 mg. It also shows that small Φ_{all} becomes rich as time elapses. And the peak of mass frequency to total fuel also moves to the lean Φ_{all} area as time elapses. It can be seen that the rich Φ_{all} achieves 2.26 when time goes to 0.2 ms ASOI. When time goes to 1.5 ms ASOI, the mass frequency to total fuel achieves 0.37 when the Φ_{all} is 0.26. And the Φ_{all} is smaller than 0.46 at 1.5 ms ASOI.

In Figure 3.5 (c), it shows the relationship between the mass frequency to total fuel and Φ_{all} under 2.97 mg. It also shows that small Φ_{all} becomes rich as time elapses. And the peak of mass frequency to total fuel also moves to the lean Φ_{all} area as time elapses. It can be seen that the rich Φ_{all} achieves 3.0 when time goes to 0.2 ms ASOI. When time goes to 1.5 ms ASOI, the mass frequency to total fuel is smaller than 0.2. And the Φ_{all} is smaller than 1.26 at 1.5 ms ASOI.

Compares with the three injection amount results of Figure 3.5, it can be seen that the Φ_{all} becomes smaller when the injection amount decreases. The peak of mass frequency to total fuel moves to the lean Φ_{all} area as time elapses. The maximum frequency to total fuel increases as the injection amount decreases. Based on these, the air-fuel mixture becomes rich when the injection amount decreases. Especially for the time 1.5 ms, the difference of the mixture formation is significant between three injection amounts. This tendency is same with the results in Figure 3.4. Figure 3.5 also shows the smaller injection amount gives the bigger entrained gas. And the results contribute to the rich air-fuel mixture formation.

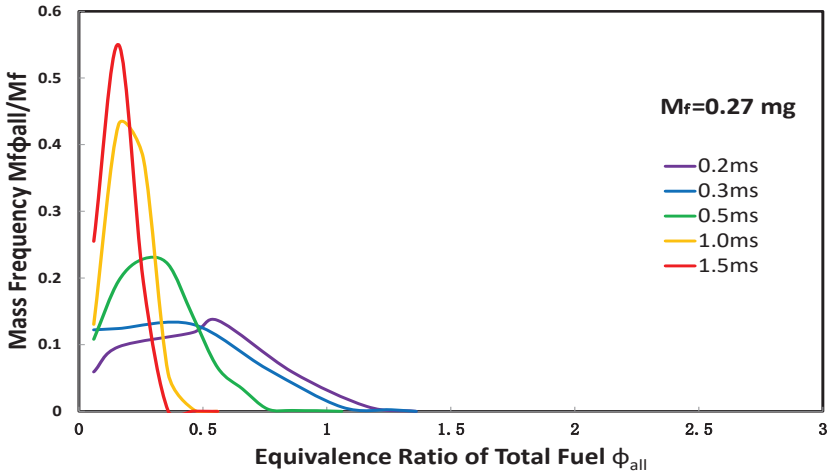

(a) M_f=0.27 mg

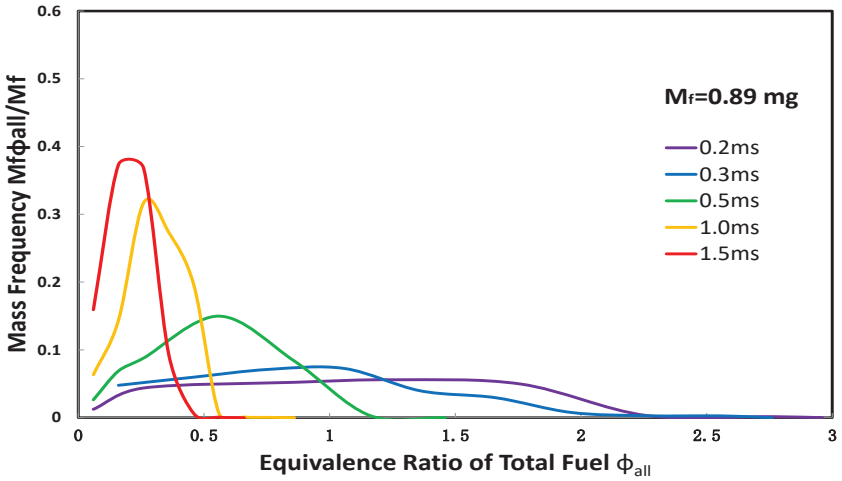

(b) M_f=0.89 mg

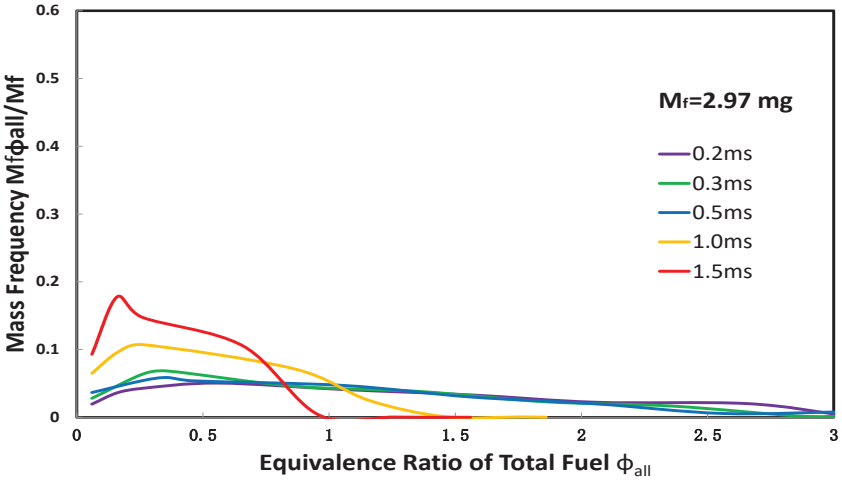

(c) M_f=2.97 mg

Figure 3.5 Mass frequency to total fuel versus Φ_{all}

3.3.2 Effect of Injection Pressure

Not only the injection amount but also the injection pressure has the effect on the spray characteristics. It is necessary to discuss about the effect of injection pressure on the spray characteristics.

Figure 3.6 shows the vapor/liquid equivalence ratio distributions as time elapses under various injection pressures with the injection amount of 0.27 mg. Figure 3.7 shows the results of the equivalence ratio distributions of 2.97 mg. The varied injection pressures were 100, 150 and 170 MPa, the injection amount was 0.27 mg in the Figure 3.6 and 2.97 mg in the Figure 3.7.

Both the 0.27 mg and 2.97 mg show that the higher injection pressure gives the leaner vapor phase equivalence ratio. This is because the higher the injection pressure is, the higher injection velocity it achieves. It contributes for the atomization of the fuel droplets which makes the fuel evaporates quickly and lower equivalence ratio.

In Figure 3.6, it can be seen that the higher injection pressure gives the shorter spray tip penetration at the injection amount of 0.27 mg. On the other hand, from the images of Figure 3.7, the tendency is opposite. The higher injection pressure gives the longer spray tip penetration at the injection amount of 2.97 mg.

According to Figure 3.2, the smaller injection amount gives the higher evaporation ratio than the bigger injection amount. And it can be seen from Figure 3.6 that the smaller injection amount gives the bigger entrained gas than the higher injection amount and accelerates the fuel evaporation.

Furthermore, a higher injection pressure has a higher injection velocity which promotes fuel atomization and enhances the fuel evaporation. Based on these, the fuel evaporates quickly under small injection amount and high injection pressure. As for this, it results in leaner air-fuel mixture formation which has a little momentum makes the spray tip penetration of 170 MPa becomes shorter than that of 100 MPa. On the contrary, the higher injection pressure gives the higher injection velocity which has a significant

effect on the spray tip penetration than the fuel evaporation velocity under a big injection amount. The spray tip penetration of the higher injection pressure is longer than that of the lower injection pressure under a bigger injection amount.

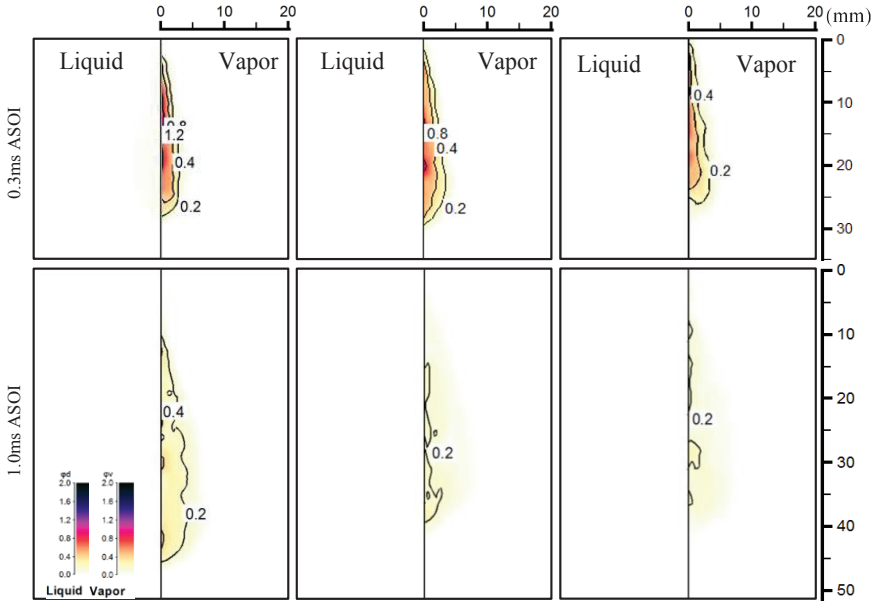

Figure 3.6 Vapor/liquid equivalence ratio distributions under various injection pressures

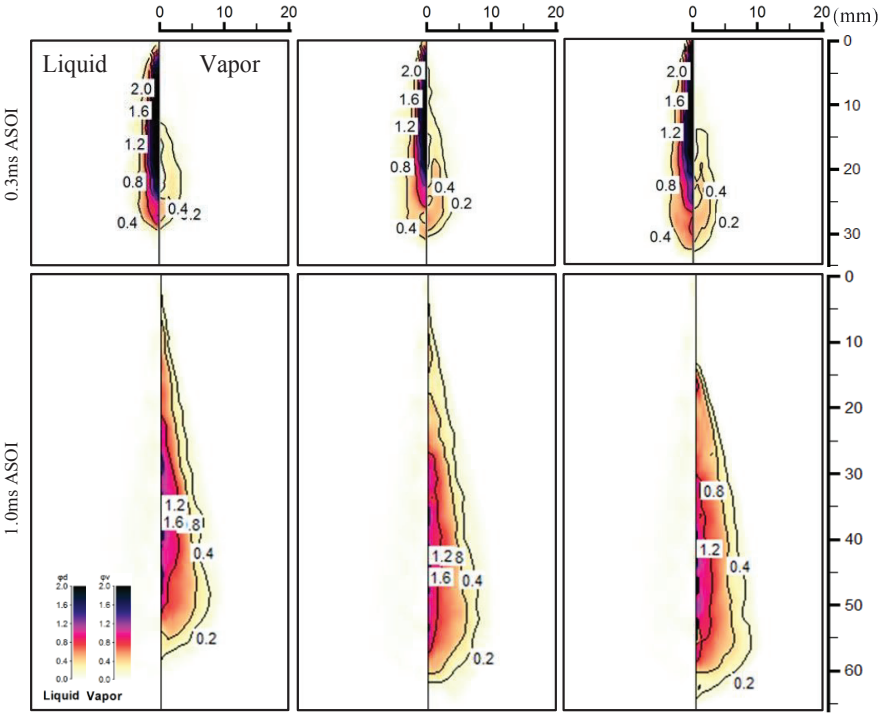

Figure 3.7 Vapor/liquid equivalence ratio distributions under various injection pressures

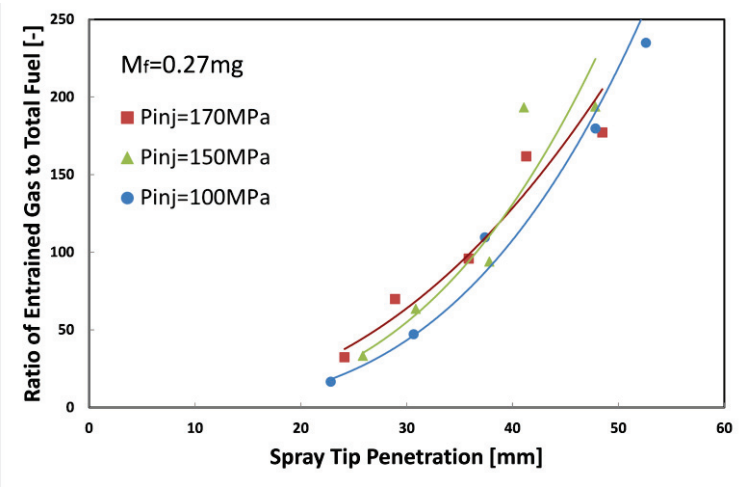

(a) M_f=0.27 mg

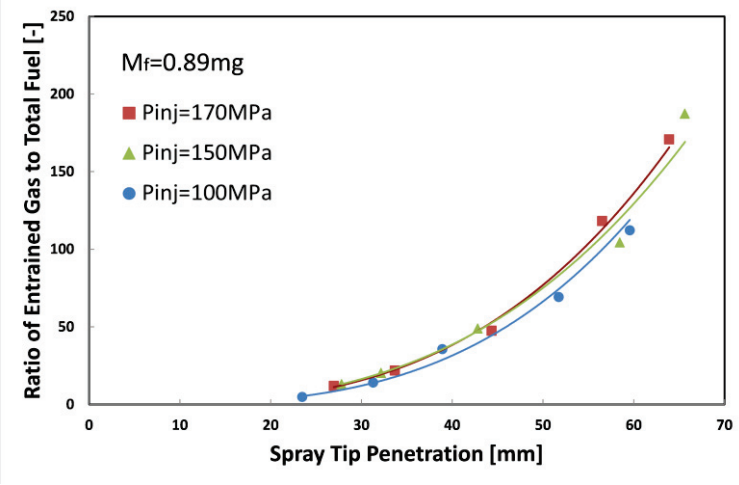

(b) M_f=0.89 mg

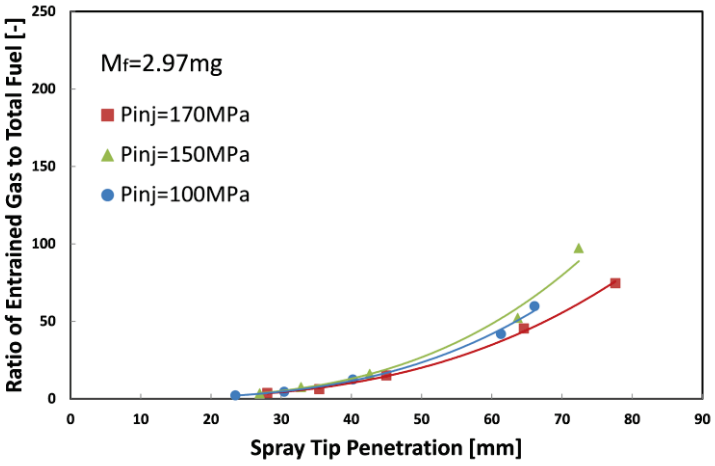

(c) M_f=2.97 mg

Figure 3.8 Entrained gas ratio versus spray tip penetration

Figure 3.8 shows the tendency between ratio of entrained gas to total fuel and spray

tip penetration under different injection pressures and different injection amounts. Entrained gas ratio and spray tip penetration are two important factors on the fuel-air mixture formation. It is necessary to discuss about the relationship between these two.

In Figure 3.8 (a), the entrained gas ratio of 100 MPa is bigger than that of 150 MPa and 170 MPa at the late period of the spray mixture formation. And the spray tip penetration of 100 MPa is also longer than that of 150 MPa and 170 MPa.

In Figure 3.8 (b), the entrained gas ratio of 150 MPa is bigger than that of 100 MPa and 170 MPa at the late period of the spray mixture formation. And the spray tip penetration of 150 MPa is also longer than that of 100 MPa and 170 MPa.

In Figure 3.8 (c), the entrained gas ratio of 150 MPa is bigger than that of 100 MPa and 170 MPa at the late period of the spray mixture formation. But the spray tip penetration of 170 MPa is longer than that of 100 MPa and 150 MPa.

It can be seen from the Figure 3.8, the spray tip penetration of 2.97 mg is longer than that of 0.27 mg and 0.89 mg at late period of spray mixture formation. But the ratio of entrained gas to total fuel is too small. The spray tip penetration of 0.89 mg under 150 MPa is longer than other conditions of 0.27 mg and 0.89 mg at late period of spray mixture formation. And the ratio of entrained gas to total fuel is also enough.

Figure 3.9 shows the tendency between evaporation ratio and spray tip penetration with various injection amounts 0.27 mg, 0.89 mg and 2.97 mg under various injection pressures 100, 150 and 170 MPa.

In Figure 3.9 (a), the spray tip penetration of 170 MPa (24 mm) is too short when the fuel all evaporates. But for the 100 MPa, it achieves 37 mm when the fuel all evaporates. The difference of three injection pressures at injection amount 0.27 mg is significant.

In Figure 3.9 (b), the difference of the spray tip penetration when the fuel all evaporates under three injection pressures at 0.89 mg decreases than that of 0.27 mg.

In Figure 3.9 (c), the spray tip penetration when the fuel all evaporates under three injection pressures are almost same.

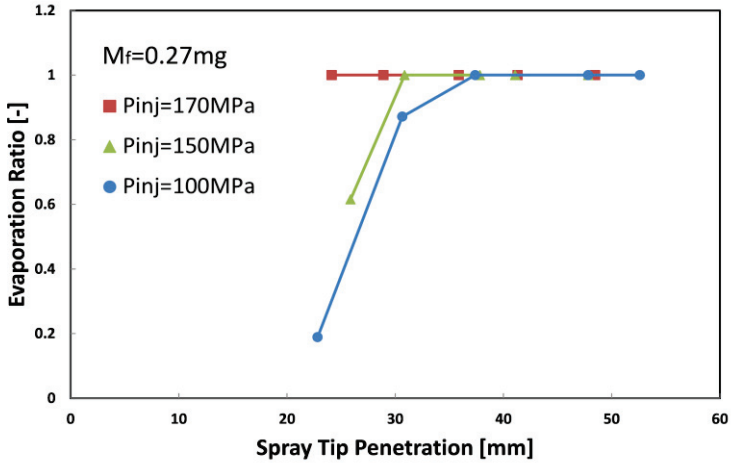

(a) M_f=0.27 mg

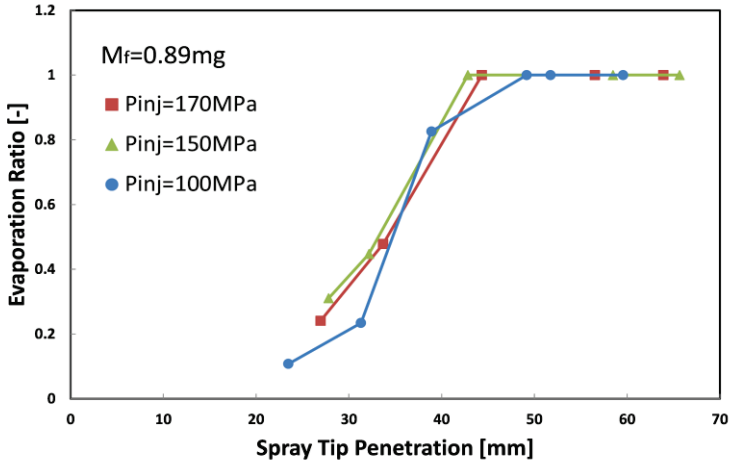

(b) M_f=0.89 mg

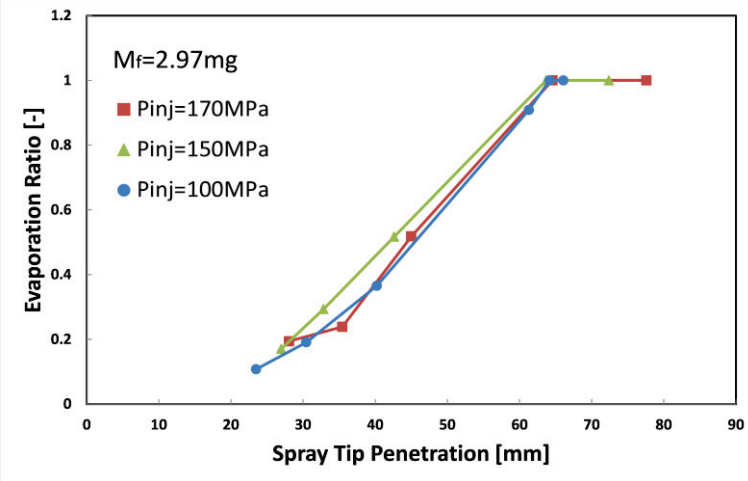

(c) M_f=2.97 mg

Figure 3.9 Evaporation ratio versus spray tip penetration

It can be seen that the spray tip penetration becomes longer when the fuel all

evaporates as the injection amount increases. It means the bigger injection amount gives the longer spray tip penetration at the time that fuel all evaporates. The difference of the spray tip penetration when the fuel all evaporates under three injection pressures decreases when the injection amount increases. For the small injection amount, the effect of injection pressure on the spray tip penetration when the fuel all evaporates is significant. At the condition of same injection amount, the spray tip penetration becomes shorter when the fuel all evaporates as the injection pressure increases. It means the bigger injection pressure promotes the evaporation process.

3.4 COMBUSTION PROCESS

This part shows the results of combustion process under the conditions of the constant injection pressure 100 MPa and different injection amounts (0.27 mg, 0.89 mg and 2.97 mg).

Figure 3.10 shows the distributions of KL factor and flame temperature obtained by analyzing the images captured from the high-speed video camera using the two-color pyrometry method. The upper row images of each injection amount are the KL factor and the bottom row images of each injection amount are the flame temperature. The timing of the images from left to right is ignition, combustion medium, combustion peak ending time.

According to Figure 3.10, it can be seen that some regions where the KL factor is high but the flame temperature is low. But there are still some regions that the KL factor is high but the flame temperature is also high. The high KL factor locates in the flame tip region. The volume of the flame and the KL factor intensity increase as the time elapses. And the volume of the flame and the KL factor intensity also increase when the injection amount increases. The soot emissions can decrease as the injection amount decreases. And compare with the results of Figure 3.1, it can be seen that the spray tip vapor equivalence ratio around the ignition timing increases when the injection amount

increases. Because of this, the KL factor intensity around the ignition timing increases when the injection amount increases. The high KL factor region can be observed at the center of flame at 1.44 ms ASOI under the injection amount of 2.97 mg. The ignition time of three injection amounts 0.27 mg, 0.89 mg and 2.97 mg is 0.84 ms, 0.94 ms and 0.94 ms ASOI respectively.

According to Figure 3.1, it can be concluded that the high vapor concentration will occur in the spray center at 1.5 ms of 2.97 mg. And according to Figure 3.5, the bigger injection amount gives the smaller entrained gas. And the results contribute to the rich air-fuel mixture formation. Even the ambient temperature of spray mixture formation and combustion process is different, but the tendency is same. Based on this, the high KL factor region will occur when the time going to 1.5 ms.

It can be observed that the time from ignition to combustion peak increases when the injection amount increases and the ignition time of 0.27 mg is a little ahead than 2.97 mg. This is because the evaporation ratio of small injection amount is higher than the evaporation ratio of big injection amount at the same time. It makes the air-fuel mixture ignitable concentration appears early and the ignition delay becomes shorter.

Figure 3.11 shows the integrated KL factor under various injection amounts and the Figure 3.12 shows the integrated KL factor per unit injection amount. As it can be seen in the Figure 3.11 and 3.12, 2.97 mg is shown with the main y-ordinates (left), 0.89 mg and 0.27 mg are shown with the auxiliary y-ordinates (right).

The integrated KL factor and the integrated KL factor per unit injection amount reduce very significantly when the injection amount decreases. This reflects that the small injection amount can reduce the soot concentration. According to Figure 3.4, it can be seen that the ratio of entrained gas to total fuel becomes bigger when the injection amount becomes smaller. Because of this, the lean homogenous fuel-air mixture is formed which makes the combustion more sufficient result in lower soot concentration.

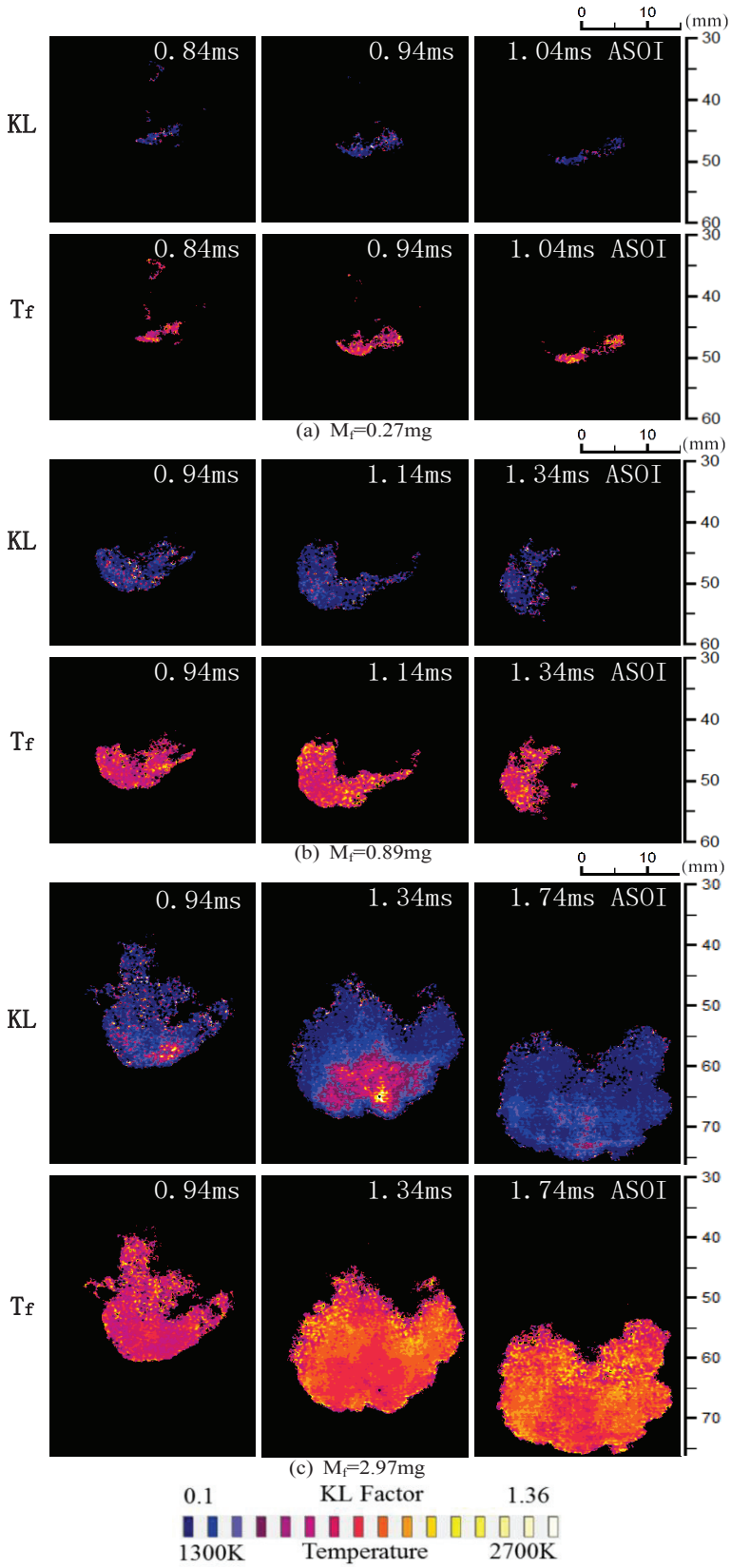

Figure 3.10 Distributions of KL Factor and Flame Temperature

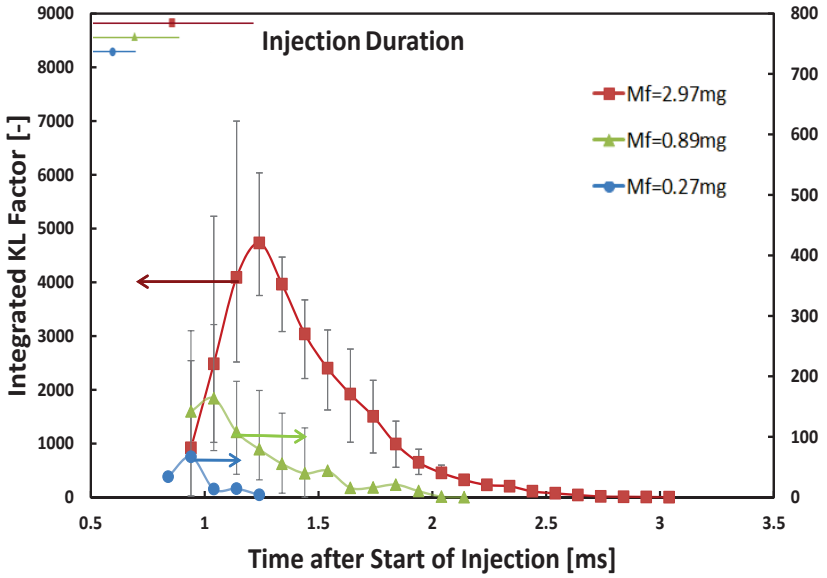

Figure 3.11 Integrated KL factor under various injection amounts

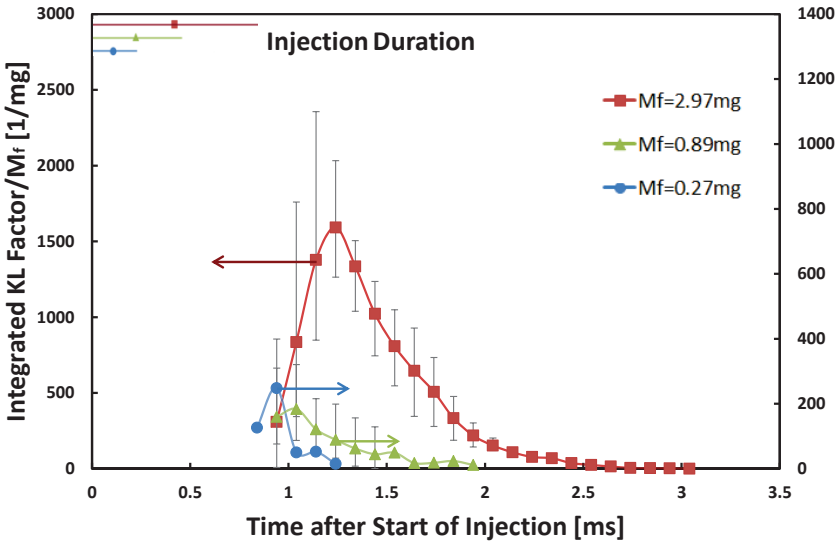

Figure 3.12 Integrated KL factor per unit injection amount

Figure 3.13 shows the mean flame temperature under various injection amounts versus the time after start of injection. The mean flame temperature also decreases very significantly when the injection amount decreases from 2.97 mg to 0.27 mg. This is the same tendency with the change of integrated KL factor. But compare the results of 0.89 mg and 0.27 mg, the difference between the mean flame temperatures is not very significant. Contact Figure 3.11 and 3.13, the high integrated KL factor shows the high mean flame temperature at the same time.

Figure 3.14 shows integrated KL factor per unit injection amount versus ratio of entrained gas to total fuel under 100 MPa injection pressure with various injection amounts. The time chosen is 0.93 ms, 1.04 ms, 1.24 ms, 1.54 ms and 1.84 ms ASOI, which is after end of injection. It can be seen that the entrained gas ratio becomes smaller when the injection amount increases. It means the air-fuel ratio is low for the big injection amount. As for this, the combustion of big injection amount is not sufficient.

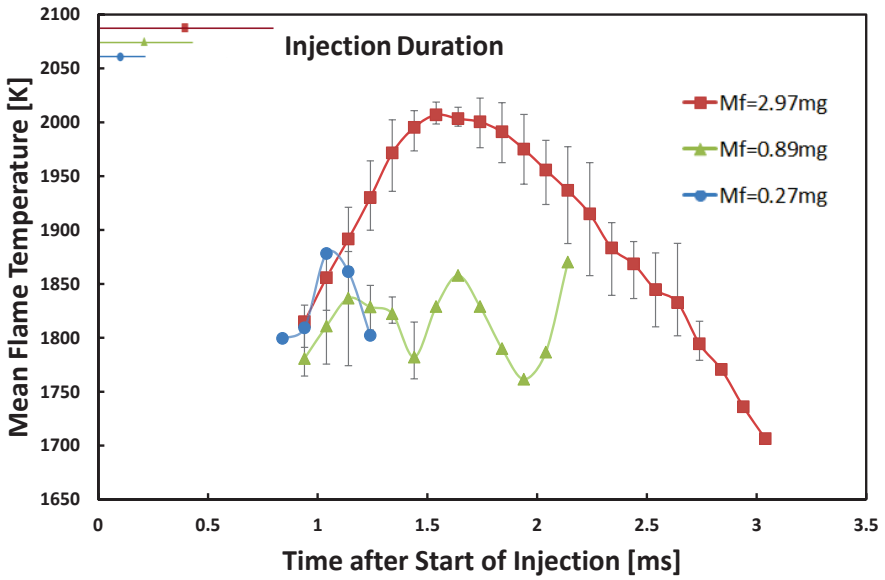

Figure 3.13 Mean flame temperature under various injection amounts

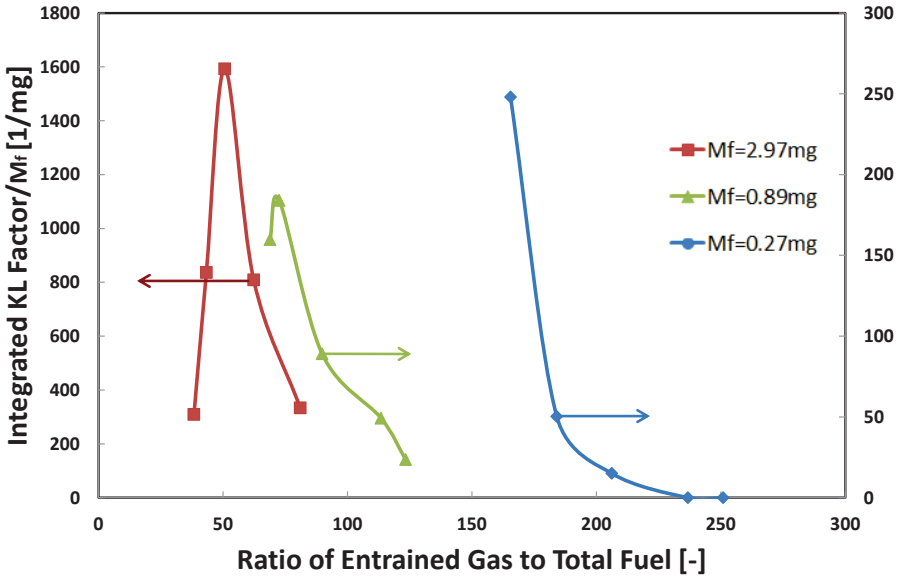

Figure 3.14 Integrated KL factor per unit injection amount versus ratio of entrained gas to total fuel (0.93 ms, 1.04 ms, 1.24 ms, 1.54 ms and 1.84 ms ASOI)

3.5 SUMMARY

The experiments were carried out in a constant volume vessel. The spray mixture formation processes were analyzed by the tracer LAS technique under various injection parameters and same ambient conditions. The combustion processes were analyzed by the two-color pyrometry method with various injection amounts but fixed injection pressure (100 MPa) and same ambient conditions. The main conclusions are summarized as follows:

Spray Mixture Formation Process

1. The smaller injection amount gives the shorter time to achieve stoichiometric vapor phase, the leaner air-fuel mixture and the shorter spray tip penetration under same injection pressure and same ambient conditions.
2. The performance of fuel-air mixture formation under the condition of 0.89 mg injection amount and 150 MPa injection pressure is higher than other conditions.
3. The effect of injection pressure shows that the spray tip penetration becomes longer when the injection pressure decreases at the small injection amount (0.27 mg). The tendency is opposite at the injection amount of 2.97 mg.

Therefore, the injection amount and the injection pressure have a significant effect on spray tip penetration and equivalence ratio which have an effect on the soot, nitrogen oxides.

Combustion Process

1. The volume of the flame and the KL factor intensity increase when the injection amount increases. It's a significant way to reduce soot formation with increasing the injection amount.
2. The high KL factor region occurs at the time when high vapor concentration appears. The lower vapor concentration gives lower KL factor intensity.
3. The time from ignition to combustion peak is shorter under the smaller injection amount condition.

4. The integrated KL factor and the integrated KL factor per unit injection amount decrease very greatly when the injection amount decreases from 2.97 mg to 0.89 mg. And the mean flame temperature also decreases as the injection amount decreases.
5. The integrated KL factor (represents the soot concentration) becomes higher when the injection amount increases. The combustion of big injection amount is not sufficient.

Consequently, it's an efficient way to reduce the soot formation by adopting small injection amount.

CHAPTER 4 CHARACTERISTICS OF FREE SPRAY DEVELOPMENT, MIXTURE FORMATION AND COMBUSTION UNDER HIGH-PRESSURE SPLIT INJECTION

4.1 INTRODUCTION

Numerous attempts [123-128] have been made to understand the mechanism of diesel spray. However, it is not likely that the determinants described in the above studies can individually explain the spray atomization. In this section, the effect of split injection on the spray development, the evaporation process phenomena of split injection and the effect of split injection on the soot evaluation (formation and oxidation domain) process were investigated.

4.2 EXPERIMENTAL CONDITIONS

Table 4.1 summarizes the experimental conditions. The fuel for non-evaporation conditions was JIS#2 diesel, that for the evaporation conditions was the tracer LAS fuel (n-tridecane 97.5%, α-MN 2.5%), and that for the combustion conditions was JIS#2 diesel. To compare the results of the spray mixture formation processes and the combustion processes, temperature and pressure were selected as 870 K and 4.2 MPa, respectively. According to this, ambient gas density is 16.8 kg/m^3. This ambient condition reproduces the thermodynamic environment near top dead center (TDC) in the combustion chamber of a low compression ratio diesel engine, which can realize homogeneous combustion effectively. Moreover, the ambient temperature and pressure were selected as 300 K and 1.5 MPa, respectively, which made the ambient density of non-evaporation, evaporation and combustion the same. The ambient gas for the non-evaporation and evaporation

conditions was nitrogen. The ambient gas for the combustion conditions was air (O_2: 21%, N_2: 79%).

The injection process comprises two parts: pre-injection and main injection. The main injection processes in this study are of two types, based on the two injection pressures of 100 MPa and 160 MPa. For split main injection, the main injection was achieved as two pluses of 160 MPa. The single main injection process is represented as Pre + S100 and Pre + S160 for short, where "S" denotes the single pulse main injection. The split main injection process was based on the mass fraction ratio of the two pulses of the main injection of 75:25. Accordingly, the split main injection process is represented as Pre + D160_75-25, where "D" denotes the double pulse (split-) main injection. The injection mass of the pre-injection was 0.9 mm^3 and the injection mass of the main injection was 5 mm^3 under three injection strategies.

Table 4.1 Experimental conditions

	Non-Evaporation/ Evaporation Conditions	Combustion Conditions
Ambient Gas	N_2	Air
Temperature: T_a [K]	300/870	870
Pressure: P_a [MPa]	1.5/4.2	4.2
Density: ρ_a [kg/m^3]	16.8	
Fuel	JIS#2 Diesel Fuel/ Tracer LAS Fuel	JIS#2 Diesel Fuel
Injection amount [mm^3]	0.9 (Pre-injection)+5.0 (Main injection)	
Injection Pressure: P_{inj} [MPa]	100 (Pre+Single injection) 160 (Pre+Split injection)	
Injector Type	Single Hole Piezo Actuator	
Nozzle Hole Diameter [mm]	0.111	
Nozzle Hole Number	1	

4.3 INJECTION RATE

Figure 4.1 illustrates the results of the injection rate measurement of the single main injection and split main injection processes. As illustrated in Figure 4.1, considering Pre + S100 injection strategy as the base condition, the end of injection (EOI) of the high-

pressure split main injection strategy (Pre + D160_75-25) was similar to that of Pre + S100 injection strategy. Furthermore, for the high injection case, single main injection of 160 MPa (Pre + S160) was also adopted. The EOI of Pre + S100 and Pre + D160_75-25 was approximately 2.8 ms after the start of injection (ASOI), and the EOI of Pre + S160 was approximately 2.5 ms ASOI, and the end of pre-injection of the three injection strategies was approximately 0.6 ms ASOI. As mentioned above, the injection volume of pre-injection was 0.9 mm^3 and that of main injection was 5.0 mm^3. The total volumes of the tracer LAS fuel and diesel were identical.

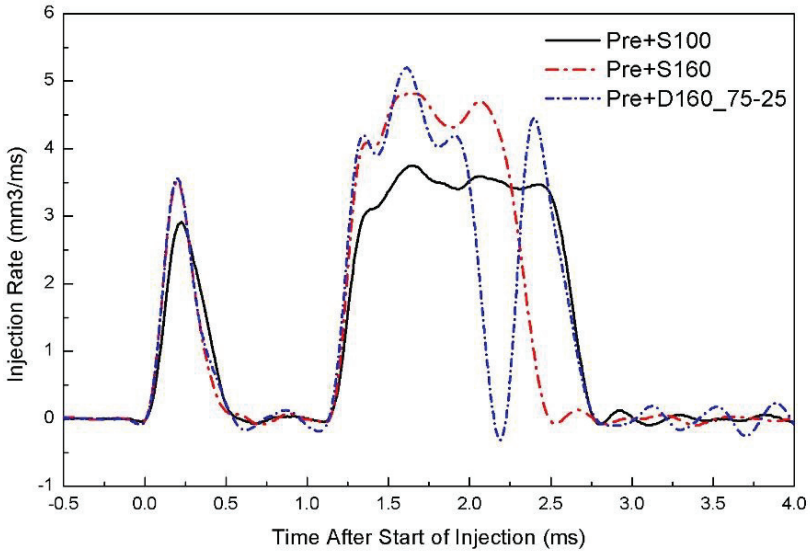

Figure 4.1 Injection Rates of Pre + S100, Pre + S160 and Pre + D160_75-25

4.4 NON-EVAPORATION CHARACTERISTICS

The spray developments of the three injection strategies are presented in Figure 4.2. The timings chosen for Pre + S100 and Pre + S160 are 0.4 ms ASOI (around the end of pre-injection), 1.2 ms ASOI (start of main injection, SOMI for short), 1.4 ms ASOI (0.2 ms after SOMI), 2.5 ms ASOI (1.3 ms after SOMI for Pre + S100, EOI for Pre + S160), and 2.8 ms ASOI (EOI for Pre + S100, 0.3 ms, AEOI for Pre + S160). The timings chosen for Pre + D160_75-25 are 0.4 ms ASOI (around the end of pre-injection), 1.2 ms ASOI (start of 1st main injection, SO1MI for short), 1.4 ms ASOI (0.2 ms after SO1MI), 2.5 ms ASOI (0.3 ms after start of 2nd main injection, SO2MI for short), and 2.8 ms ASOI

(EOI).

The spray tip penetration of pre-injection at 0.4 ms ASOI for high injection pressure is significantly longer than that of low injection pressure. It implies that higher injection pressure provides larger momentum. It can be observed that the main injection of the three injection strategies appears at 1.2 ms ASOI. The injected fuel of the main injection of Pre + S160 and Pre + D160_75-25 is larger than that of Pre + S100 at 1.2 ms ASOI because of the high injection pressure. The main injection fuel can be observed at 1.4 ms ASOI under three injection strategies. The injection has already finished at 2.5 ms ASOI under Pre + S160, while the second main injection of Pre + D160_75-25 can be observed. According to the spray images, the spray tip penetration of Pre + S100 is shorter than that of Pre + S160 and Pre + D160_75-25, which is due to the low injection pressure of Pre + S100. The effect of main injection fuel on the spray tip penetration will be discussed in the next Figure.

Figure 4.3 presents the spray tip penetration of the three injection strategies. The spray tip penetration of the high injection pressure strategies is longer than that of the low injection pressure strategy, as the higher injection pressure provides larger momentum that makes the spray penetrate longer.

The main injection fuel will catch up with the tip of the pre-injection at 2.1 ms ASOI for Pre + S160 and Pre + D160_75-25 but 2.2 ms ASOI for Pre + S100. It implies that higher injection pressure provides larger momentum. The spray tip penetration gradient becomes bigger after the main injection fuel catches up with the tip of the pre-injection. It means the split injection gives the fuel more momentum to penetrate quickly. The spray tip penetration of Pre + S160 is almost same with that of Pre + D160_75-25 till 1.2 ms ASOI as the same injection pressure. However, the spray tip penetration of Pre + S160 is a little longer than that of Pre + D160_75-25 from 1.2 ms ASOI to 1.9 ms ASOI as the injection mass of Pre + S160 is larger than that of Pre + D160_75-25 during this period. It implies that split injection can suppress the spray tip penetration which can void the effect of spray and cylinder head interaction. Suppresses the spray tip penetration can decrease the soot formation.

The main injection fuel will catch up with the tip of the pre-injection fuel at 2.1 ms ASOI, which makes the spray tip penetration of Pre + D160_75-25 to catch up with that of Pre + S160. The second main injection fuel of Pre + D160_75-25 will reach the tip of

the first main injection fuel at 3.9 ms ASOI. The spray tip penetration of Pre + D160_75-25 becomes shorter than that of Pre + S160 from 2.9 ms ASOI to 3.9 ms ASOI, because the effect of the first main injection on the spray tip penetration has already finished, and the second main injection fuel still does not have an effect on the spray tip penetration.

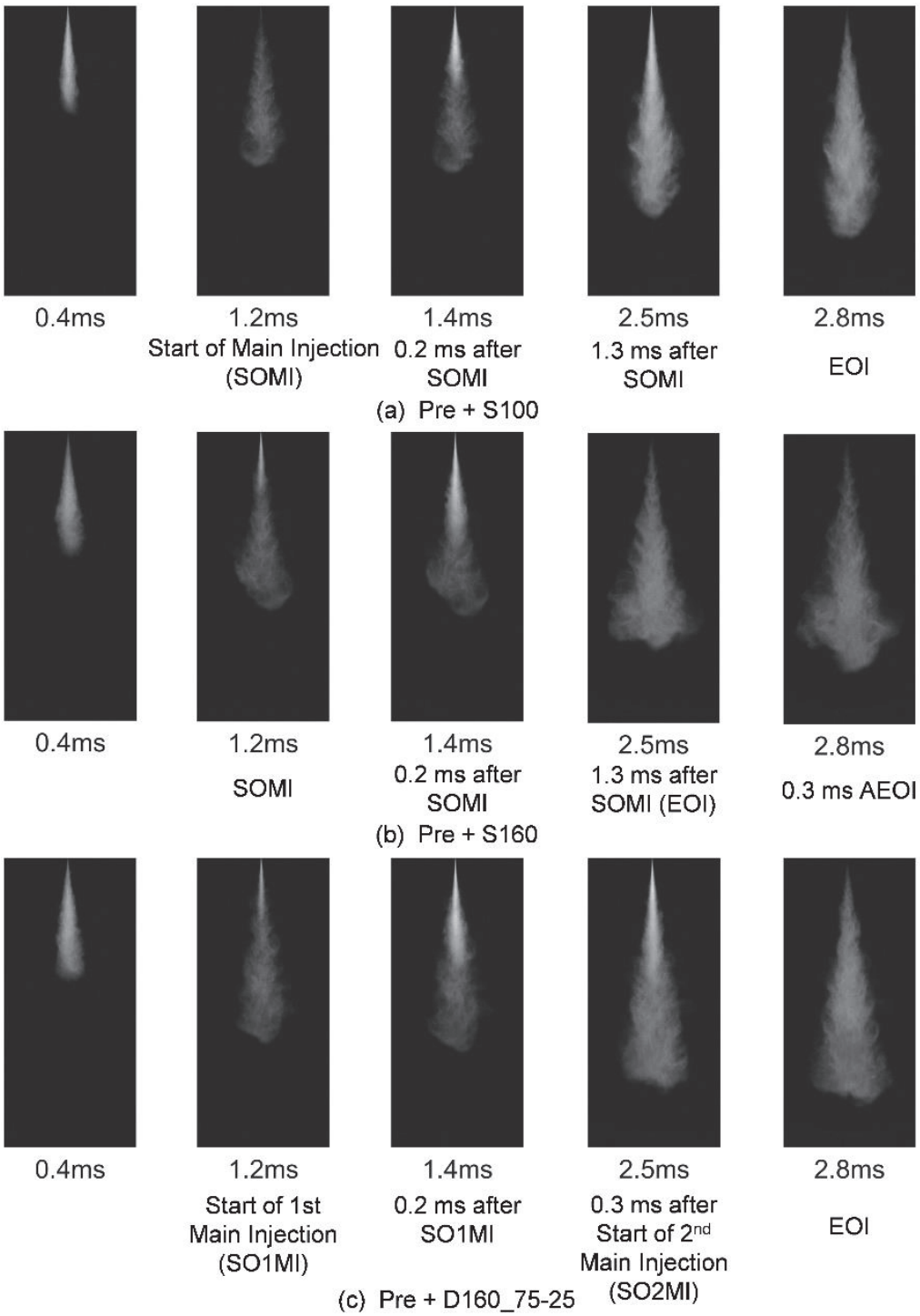

Figure 4.2 The spray developments of three injection strategies

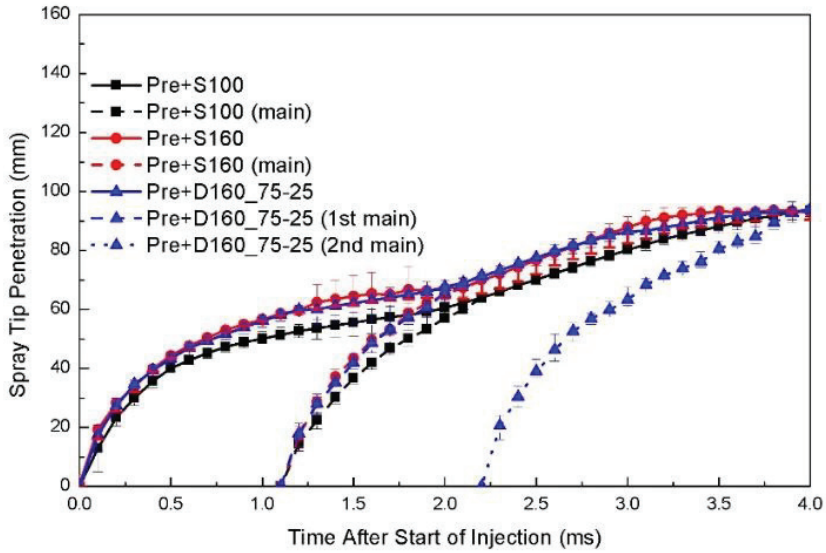

Figure 4.3 Spray tip penetrations

Figure 4.4 shows the equivalence ratio of the overall fuel versus time under the three injection strategies. The equivalence ratio is defined as the ratio of the actual fuel/nitrogen ratio to the stoichiometric fuel/air ratio.

The equivalence ratio of low injection pressure is higher than that of high injection pressure during the interval between the pre- and main injection. As the injected fuel mass is the same during this interval, it is safe to say that the ambient air entrainment of the low injection pressure is smaller than that of the high injection pressure when the injection mass is very small.

The equivalence ratio of the three injection strategies decrease first and then increase during the whole injection phase. Moreover, the maximum ratio of Pre + S100 during the pre-injection phase is 0.3, which is larger than that of Pre + S160 and Pre + D160_75-25. However, for the Pre + S160 and Pre + D160_75-25, the equivalence ratio is almost the same and the data of Pre + S160 is just slightly higher than that of Pre + D160_75-25. The equivalence ratio of the overall fuel for the three injection strategies is almost the same during the start of the main injection phase. Then, the equivalence ratio of the overall fuel of the high injection pressure is higher than that of the low injection pressure. The equivalence ratio of Pre + D160_75-25 at 2.8 ms ASOI (EOI of Pre + D160_75-25) is smaller than that of Pre + S160 at 2.5 ms ASOI (EOI of Pre + S160). It implies that split main injection provides much more ambient gas amount,

which improves the spray breakup and atomization process as the injected mass is same at these two timings.

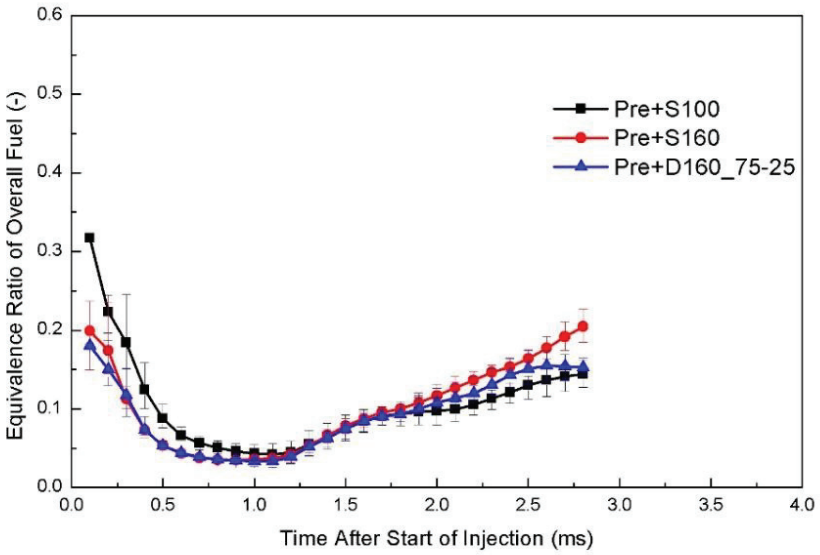

Figure 4.4 Equivalence ratio of overall fuel

4.5 EVAPORATION CHARACTERISTICS

Figure 4.5 shows the liquid/vapor equivalence ratio of the three injection strategies. The left and right columns of each graph are the liquid and vapor phase equivalence ratios, respectively. The timings chosen for Pre + S100 are 1.14 ms ASOI (start of the main injection), 1.8 ms ASOI (during the main injection), and 2.8 ms ASOI (EOI) from left to right. The timings chosen for Pre + S160 are 1.2 ms ASOI (start of the main injection), 1.7 ms ASOI (during the main injection), and 2.8 ms ASOI. The timings chosen for Pre + D160_75-25 are 1.14 ms ASOI (start of the first main injection), 1.8 ms (during the first main injection), 2.19 ms ASOI (start of the second main injection), 2.39 ms ASOI (0.2 ms after the start of the second main injection), and 2.8 ms ASOI (EOI).

The liquid phase equivalence ratio of Pre + D160_75-25 is leaner than that of Pre + S160 around 1.8 ms ASOI. The split main injection decreases the first main injection mass, which makes the fuel to evaporate easier than that in single main injection. The split main injection fuel can be observed obviously at 2.19 ms and 2.39 ms ASOI under Pre +

D160_75-25. The vapor-phase equivalence ratio of Pre + D160_75-25 is more homogeneous than that of Pre + S160 at 2.8 ms ASOI. It implies that the split injection can improve the fuel evaporation process. Comparing the liquid phase equivalence ratio of Pre + D160_75-25 and Pre + S100 at 2.8 ms ASOI, the high injection pressure can improve the fuel evaporation process. The spray tip penetration increases as the time elapses under the three injection strategies. Moreover, the spray tip penetration of Pre + S160 and Pre + D160_75-25 is longer than that of Pre +S100 because higher injection pressure provides higher momentum. The spray tip penetration of Pre + S160 at 2.8 ms ASOI is longer than that of Pre + D160_75-25 because the vapor expansion of Pre + S160 is stronger than that of Pre + D160_75-25 as the EOI of Pre + S160 is 2.5 ms ASOI.

Figure 4.6 shows the spray tip penetration of non-evaporation and evaporation conditions under the three injection strategies. The dashed lines represent the spray tip penetration of the non-evaporation condition, while the others are the spray tip penetration of the evaporation conditions.

The spray tip penetration of evaporation condition is shorter than that of non-evaporation condition. The fuel vapor expansion which causes larger flower resistance by ambient for evaporation condition. The spray tip penetration gap between non-evaporation and evaporation conditions under high injection pressure is smaller than that of low injection pressure. It implies that high injection pressure can decrease the effect of flower resistance by ambient. The spray tip penetration increases as time elapses under three injection strategies. The spray tip penetration of Pre + S160 and Pre + D160_75-25 under evaporation condition are longer than that of Pre + S100, as the higher injection pressure provides a larger spray momentum. The split main injection does not make the spray tip penetration longer than the single main injection, which is same with the results of evaporation condition.

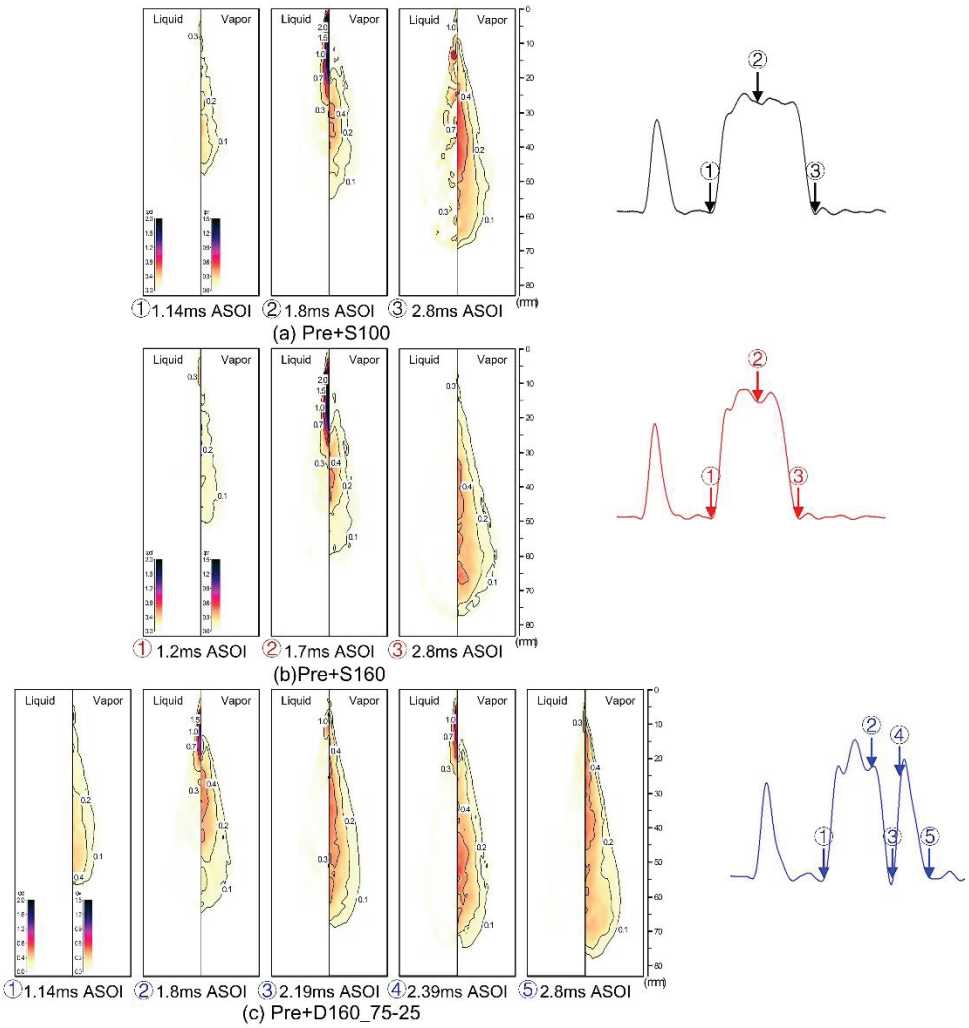

Figure 4.5 Liquid and vapor phase equivalence ratio distributions

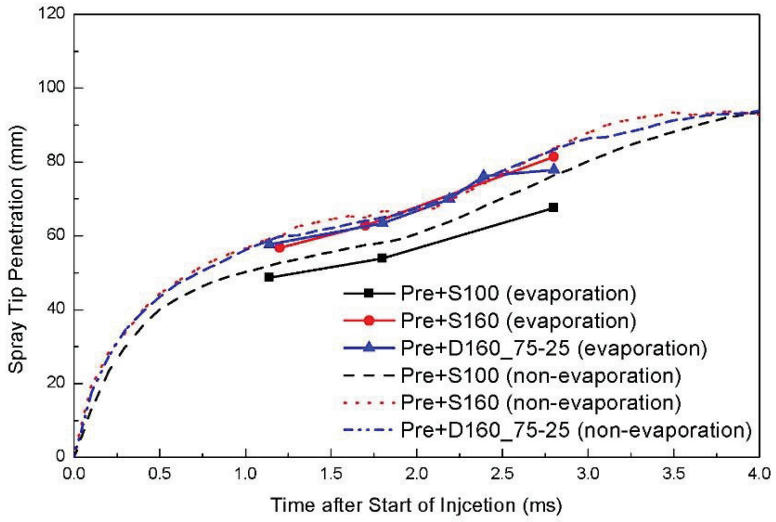

Figure 4.6 Comparison of Spray tip penetration under non and evaporation conditions

Figure 4.7 shows the equivalence ratio of the overall fuel under non-evaporation and evaporation conditions with the three injection strategies. According to the previous dissertation paper [100], the vapor mass and liquid mass concentration can be achieved by using Bouguer-Lambert-Beer's law, and then the overall fuel equivalence ratio can be calculated. The dashed lines represent the results of non-evaporation, while the others are the results of the evaporation conditions. The equivalence ratio of the overall fuel of the three injection strategies is almost the same during the start of the main injection phase under non-evaporation conditions. Furthermore, the differences among the equivalence ratio of the overall fuel from the three injection strategies during this phase are also small under evaporation conditions. From the evaporation condition results, the equivalence ratio of the overall fuel of Pre + S100 at 2.8 ms ASOI is higher than that of Pre + D160_75-25. As the injected mass is the same under these two injection strategies, the ambient gas mass of Pre + S100 is bigger than that of Pre + D160_75-25. It implies that the higher injection pressure can obtain richer entrained ambient gas under evaporation condition. The equivalence ratio of the overall fuel increases from 2.19 ms ASOI to 2.39 ms ASOI under Pre + D160_75-25. The tendency of the equivalence ratio of the overall fuel increases under Pre + S100 and Pre + D160_75-25. However, the equivalence ratio of the overall fuel of Pre + S160 at 2.8 ms ASOI is definitely smaller than that of 1.7 ms ASOI. Because the fuel injection of Pre + S160 has already finished at 2.5 ms ASOI and fuel continues to evaporate as time elapses. This contributes more ambient gas entrained into the spray, which causes low equivalence ratio.

Figure 4.8 presents the relationship between the mass frequency of the vapor fuel and the equivalence ratio of vapor at EOI under the three injection strategies. The mass frequency of vapor fuel of Pre + S100 is smaller than that of Pre + S160 and Pre + D160_75-25. It means that the high injection pressure causes the fuel to evaporate more quickly than that of the low injection pressure. The equivalence ratio width of Pre + S100 is longer than that of Pre + D160_75-25 and the equivalence ratio width of Pre + D160_75-25 is shorter than that of Pre + S160. It means that the vapor phase of Pre +

D160_75-25 is significantly more homogeneous than that of Pre + S160 and the vapor phase of Pre + S160 is considerably more homogeneous than that of Pre + S100. This is similar to the results in Figure 4.5. The split main injection and high injection pressure can make the vapor distribution more homogeneous, which is consistent with the results of a previous paper [67].

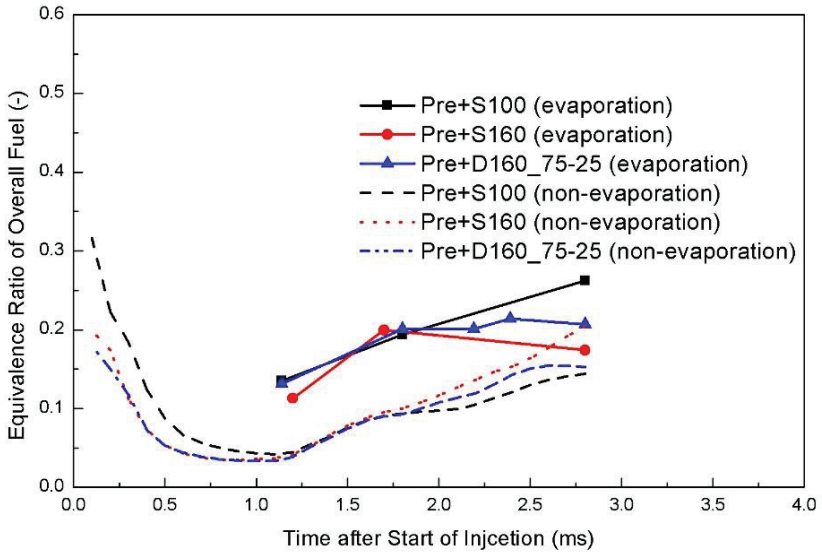

Figure 4.7 Comparisons of equivalence ratio of overall fuel under non and evaporation conditions

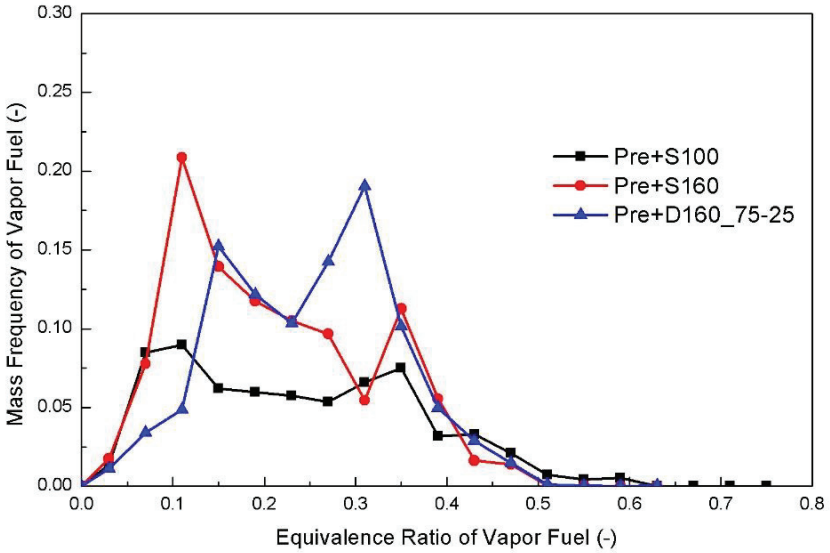

Figure 4.8 Mass frequency of vapor fuel at EOI

4.6 COMBUSTION CHARACTERISTICS

This section presents the results of the combustion process under the three injection strategies. Figure 4.9 presents the distributions of the KL factor and the soot temperature obtained by analyzing the images captured from the high-speed video camera using the two-color pyrometry method.

The upper row images for each injection strategy present the temperature, while the bottom row images present the KL factor. The timings chosen for Pre + S100 from the left to the right are 1.6 ms ASOI (main ignition, short for MIG), 2.0 ms ASOI (0.4 ms after MIG), 2.7 ms ASOI (the integrated KL peak timing, short for tpeak), and 3.1 ms ASOI (0.4 ms after tpeak). The timings chosen for Pre + S160 from the left to the right are 1.6 ms ASOI (MIG), 2.0 ms ASOI (0.4 ms after MIG), 2.3 ms ASOI (tpeak), and 2.7 ms ASOI (0.4 ms after tpeak).

Furthermore, the timings chosen for Pre + D160_75-25 from the left to the right are 1.6 ms ASOI (MI), 2.0 ms ASOI (0.4 ms after MIG), 2.2 ms ASOI (tpeak for the first main injection flame, short for tpeak1), 2.4 ms ASOI (0.2 ms after tpeak1), 2.6 ms ASOI (the valley for the integrated KL, short for tvalley), 2.9 ms ASOI (tpeak for the second main injection flame, short for tpeak2), and 3.3 ms ASOI (0.4 ms after tpeak2). These timings correspond to that of Figure 4.10.

The line was used to describe the area of KL factor and temperature at 1.6 ms ASOI as the ignition timing is too weak to observe it clearly. The auto-ignition occurs near the spray tip, which is the same as the results of Zhang et al. [109]. The large KL factor region is near the tip region because of the large momentum.

Moreover, the low temperature is shown in this region. The second main injection flame is evident at 2.6 ms ASOI and 2.9 ms ASOI for Pre + D160_75-25. The first main injection flame is finished at 0.4 ms Atpeak2 (3.3 ms ASOI), and the KL factor of Pre + D160_75-25 is lower than that of Pre + S160 and Pre + S100 at 0.4 ms Atpeak2.

The high KL factors are observed around the flame tip region. The KL factors of Pre + S100 are significantly higher than that of the high injection pressure strategies. This means that high injection pressure can decrease the soot. The KL factor of the single main injection pressure strategies first increases, and then decreases. However, for the

split main injection strategy, the KL factor first increases from the MIG to the tpeak1; then, it decreases as the time elapses until the tvalley; then, it increases to the tpeak2; and finally, it decreases as the time elapses until 0.4 ms after tpeak2. It is evident that the split injection has an effect on the soot formation.

In the temperature images, a relatively high temperature appears in the midstream region of the sooting flame at 0.4 ms after tpeak for the three injection strategies because of the oxidation of the soot in this region [130], which is an exothermic process. Moreover, the relative high temperature also appears in the midstream region from tpeak1 to tvalley under Pre + D160_75-25, also resulting in soot oxidation in this region during the period from 2.2 ms ASOI to 2.5 ms ASOI.

In this chapter, the integrated KL factor was calculated by integrating the pixel values over the images, and the mean temperature was calculated by the average of pixel values over the images, which represents the soot temperature. These results were averaged over three different runs at the same experiment condition.

Figure 4.10 illustrates the integrated KL factor ASOI under the three injection strategies. The integrated KL factor of the high injection pressure strategies is obviously smaller than that of the low injection pressure strategy. The higher injection pressure is the main reason behind this. The integrated KL factor of the single main injection strategies increases first and then decreases, but the trend of the split main injection strategy is to increase, decrease, increase, and then decrease. This is due to the ignition of the second main injection fuel, which increases the KL factor after 2.6 ms ASOI. The KL factor of Pre + D160_75-25 is smaller than that of Pre + S160 from the ignition timing to 2.8 ms ASOI. This happens because the injection amount of the first main injection of Pre + D160_75-25 is smaller than that of Pre + S160. Then, the KL factor of Pre + D160_75-25 becomes larger than that of Pre + S160 because of the second main injection combustion of the split main injection. The KL factor of Pre + D160_75-25 at 2.8 ms ASOI (EOI of Pre + D160_75-25) is smaller than that of Pre + S160 at 2.5 ms ASOI (EOI of Pre + S160). According to the discussions above, it can be concluded that the split main injection can decrease the soot, which agrees with the studies of Nishioka et al., [131]; Nehmer and Reitz [132]. Further, the gradient of the KL factor of Pre + D160_75-25 from 2.9 ms to 4.0 ms ASOI is bigger than that of Pre + S160 from 2.2 ms to 3.3 ms ASOI. It implies that the split injection decreases the soot quickly.

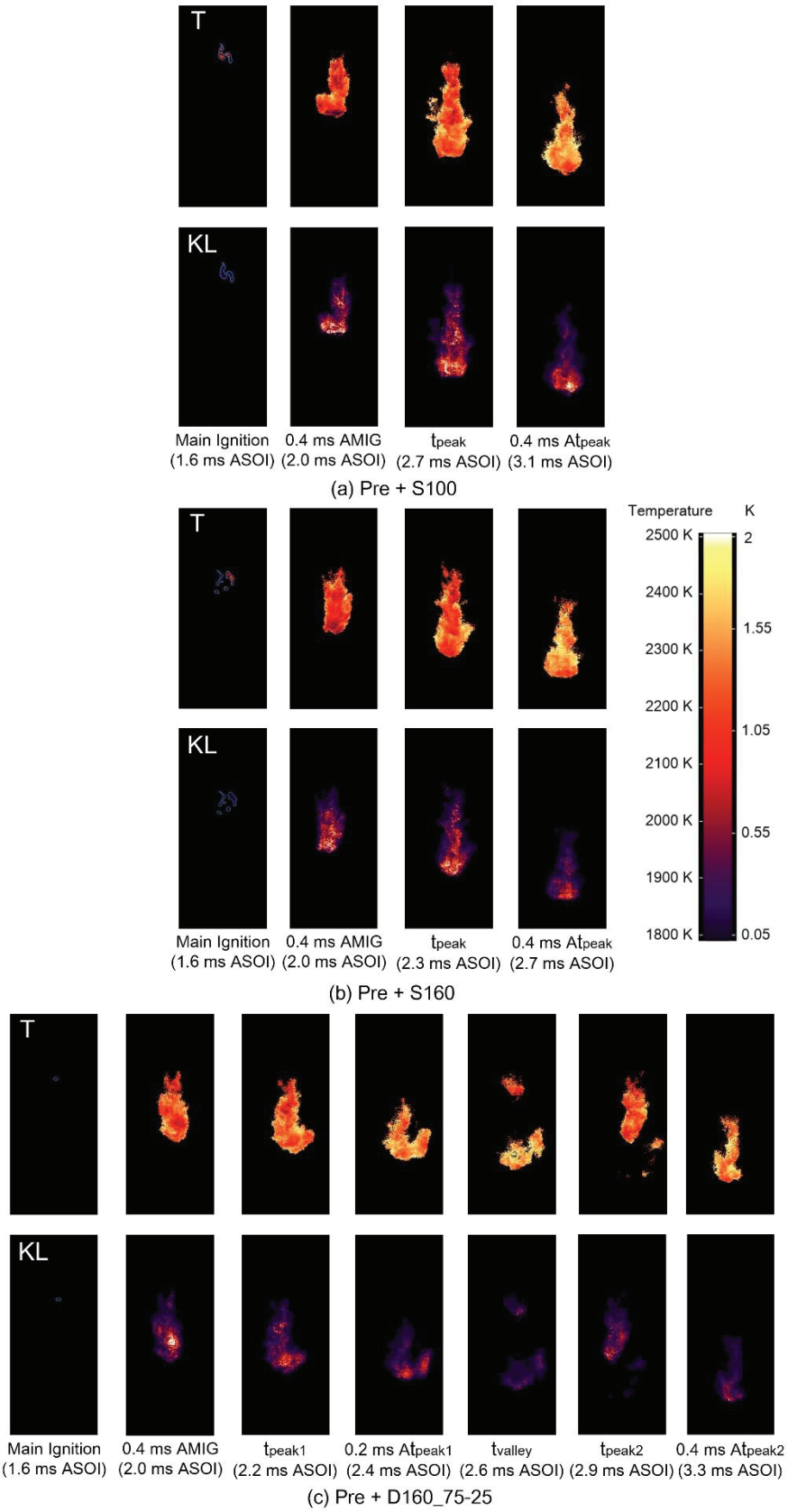

Figure 4.9 KL factor and temperature distributions under three injection strategies

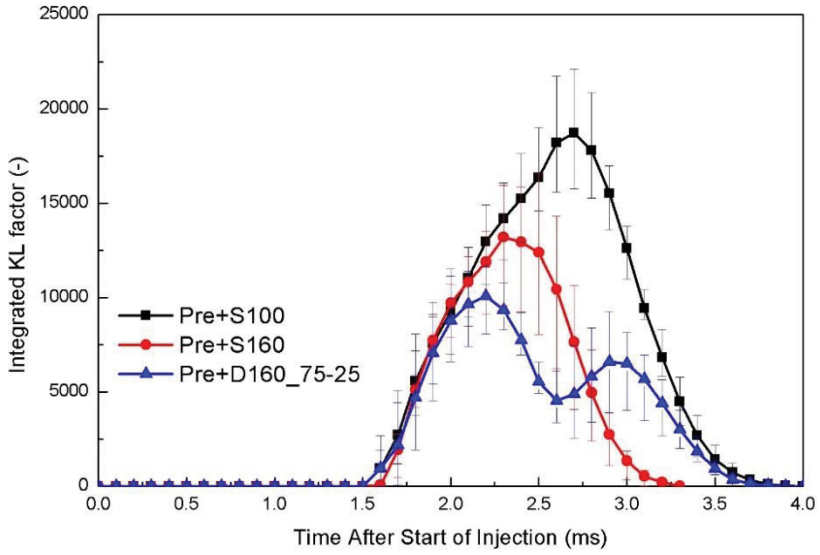

Figure 4.10 Integrated KL factor under three injection strategies

Figure 4.11 shows the plot of each pixel's KL value versus temperature at EOI + 0.2 ms under the three injection strategies. Figure 4.11 (a) shows the KL factor distribution at EOI + 0.2 ms under the three injection strategies (3.0 ms for Pre + S100 and Pre + D160_75-25, 2.7 ms for Pre + S160). The KL factor images are divided into three regions, flame tip, middle and flame tail, as the dashed lines shown in the images. Figure 4.11 (b) presents the KL factor versus temperature in these three regions, with a large amount of scatter pixels of the KL values between 0 to 3.0 for Pre + S100, 0 to 2.0 for Pre + S160, and 0 to 1.5 for Pre + D160_75-25 from the whole flame region. The KL factor of Pre + S100 is much denser than that of Pre + S160 and Pre + D160_75-25. This implies that the high injection pressure could decrease the soot. Furthermore, the KL factor of Pre + S160 is much denser than that of Pre + D160_75-25. It implies that the split main injection can obtain more entrainment which decreases the soot. It means that the split injection could decrease the soot. The small KL factor is located in the flame tail region and the high KL factor is located in the flame tip region with the three injection strategies. The high KL factor in the flame tip region of the high injection pressure is smaller than that of the low injection pressure, and the high KL factor of the split main injection pressure is smaller than that of the single main injection pressure. It indicates that the high injection pressure and split injection could decrease the maximum soot. It has overlap among the three regions. The overlap ratio of the split main injection

strategy is higher than that of other two injection strategies. The split injection makes the soot distribution more homogeneous. The high KL factor is located in the low temperature region. The maximum KL factor becomes small as the temperature increases. The exponential trendlines are represented in the graphs by yellow lines. The exponentially trend increases from the spray tail to the flame tip region. The exponentially trend of the high injection pressure is higher than that of the low injection pressure strategy. It means that the degree of homogeneity of KL versus temperature of the high injection pressure is higher than that of low injection pressure. The exponentially trend of Pre + D160_75-25 in the flame tip region is lower than that of Pre + S160. However, the exponentially trend of Pre + D160_75-25 in the flame tail and middle regions is higher than that of Pre + S160. The split injection has a positive effect on the degree of homogeneity of KL versus temperature in the whole flame region.

Figure 4.12 presents the integrated KL factor versus the mean temperature under the three injection strategies. It also presents the soot evaluation under the three injection strategies. It can be seen in the figure that the soot evaluates in a clockwise direction, as shown by the arrows.

The soot evaluation includes three phases under Pre + S100. In the first phase, the integrated KL factor and the mean temperature increase because of the initial combustion, dominated by the soot formation process. The KL factor decreases but the mean temperature increases in the second phase because the combustion is dominated by the soot oxidation process. Both the integrated KL factor and mean temperature decrease in the third phase because of the end of combustion.

The soot evaluation under Pre + S160 is similar to that of Pre + S100. The first phase is the soot-formation domain process, the second phase is the soot-oxidation domain phase, and the last phase is the late combustion phase. The start timing of the first phase of Pre + S100 and Pre + S160 is the same, but the end of the first phase is different. The duration of the first phase of Pre + S160 is shorter than that of Pre + S100, which is due to the high injection pressure. The high injection pressure decreases the soot formation domain process. However, the second phase duration of the two single main injections are the same, implying that the high injection pressure does not decrease the soot oxidation domain process. Finally, the late combustion phase finished quickly under Pre + S160 because of the high injection pressure. The high injection pressure

decreases the combustion duration.

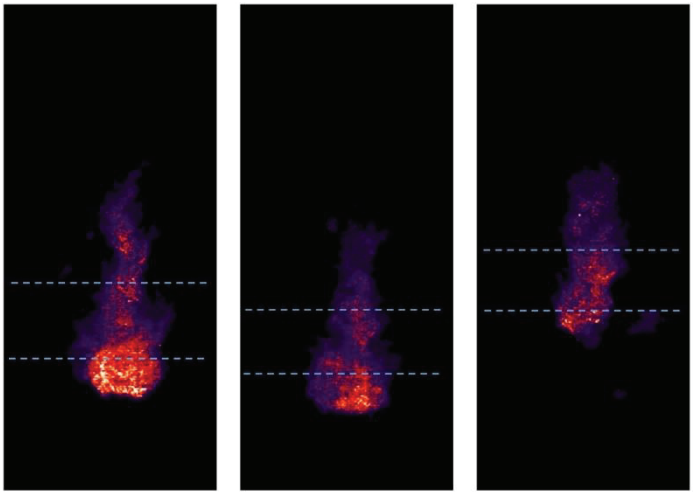

(a) KL factor distribution at EOI + 0.2 ms

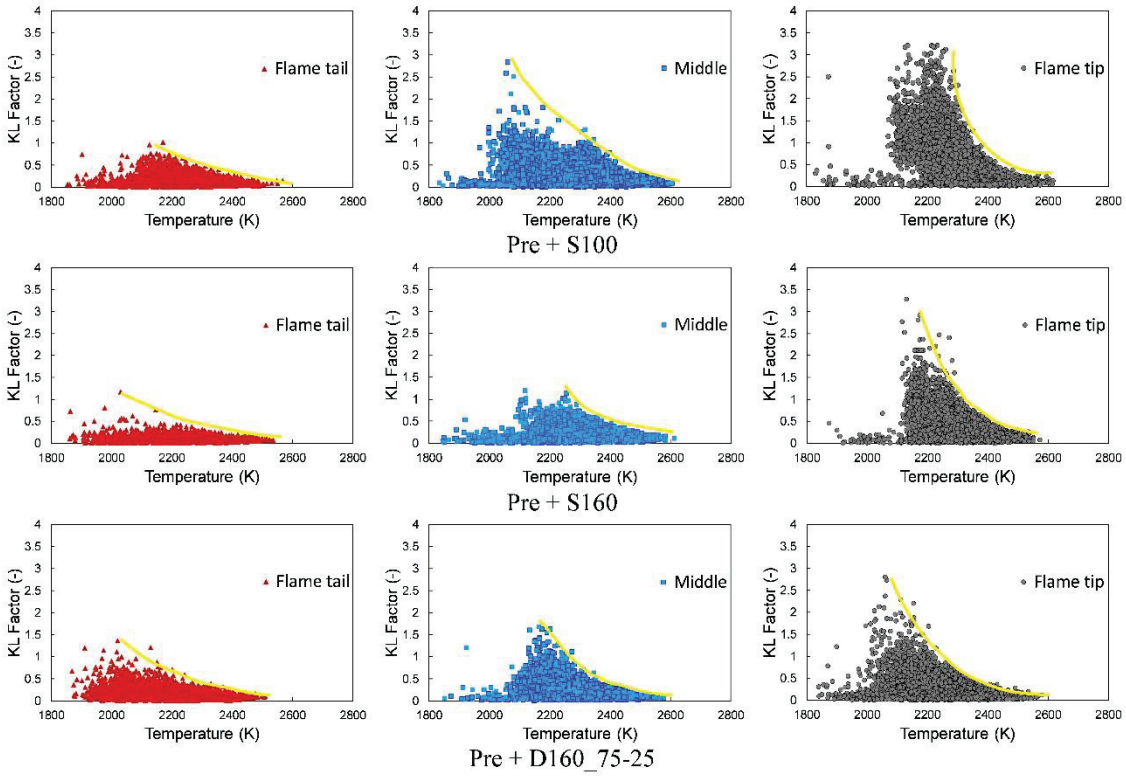

(b) KL factor versus temperature in three regions

Figure 4.11 KL factor versus temperature at EOI + 0.2ms

The soot evaluation under Pre + D160_75-25 is divided into six phases. The first

phase is the soot-formation domain process, which is the same as that of Pre + S100 and Pre + S160. The second phase is the soot-oxidation domain process, which is the same as that of Pre + S100 and Pre + S160. However, the duration of Pre + D160_75-25 is shorter than that of Pre + S100 and Pre + S160 because of the split main injection. Then, the KL factor and mean temperature decrease because of the end of the first main injection combustion. This phase is also the same as the third phase of Pre + S100 and Pre + S160. The KL factor increases but the mean temperature decreases during the fourth phase, which is the soot formation phase. Then, the KL factor decreases but the mean temperature increases during the fifth phase, which is the soot oxidation phase. Finally, the sixth phase is the end of the main injection combustion, which is the same as that of the single main injection strategies. The split main injection soot evaluation circles two times, with 1, 2, and 3 being one circle and 4, 5, and 6 being the other one. This happens as the split main injection is divided into two parts.

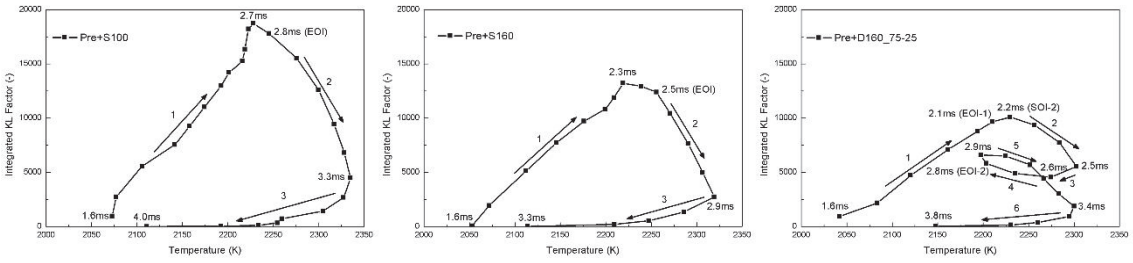

Figure 4.12 The integrated KL factor versus the mean temperature

4.7 SUMMARY

In this section , free spray experiments were carried out to observe the fuel non-evaporation, evaporation, and combustion characteristics. The non-evaporation processes applied the Mie scattering method under three injection strategies (Pre + S100, Pre + S160, and Pre + D160_75-25). The evaporation processes were analyzed by the tracer LAS technique and the combustion processes were analyzed by the two-color pyrometry method. The main conclusions are presented as follows:

The split injection can be distinctly observed during the injection phase. Split injection provides much more ambient gas amount, which improves the spray breakup

and atomization process under the non-evaporation condition. Split injection gives the fuel more momentum to penetrate quickly. High injection pressure can improve the fuel evaporation process and obtain rich entrained ambient gas. Split injection can make the vapor phase more homogeneous and make the soot distribution more homogeneous. Dense soot is generated in the flame tip region. The combustion can be enhanced, and the soot emissions can be improved by using the split injection. High injection pressure and split injection could decrease the maximum soot. Split injection has a positive effect on the degree of homogeneity of KL versus temperature in the whole flame region. The soot evaluation process finishes at the same time when the injection strategies have the same SOI and EOI.

CHAPTER 5 CHARACTERISTICS OF FUEL EVAPORATION, MIXTURE FORMATION AND COMBUSTION OF 2-D CAVITY IMPINGING SPRAY UNDER HIGH-PRESSURE SPLIT INJECTION

5.1 INTRODUCTION

Numerous researchers [46-49] studied the air entrainment of an impinging spray and determined that spray/wall interaction also plays a role in air entrainment before impingent occurs. However, the structure of the impinging wall in a practical engine is complicated, the real impinging spray is not like the simplified flat wall impinging spray. Therefore, it is worthwhile to investigate the spray mixture formation and combustion process by employing a 2-D piston cavity which was designed based on the Mazda Skyactiv-D engine.

5.2 EXPERIMENTAL CONDITIONS

Table 5.1 summarizes the experimental conditions. Expect the injection strategies, other experimental conditions are same with that of free spray in Chapter 4. The injection process comprises two parts: pre-injection and main injection. The single main injection process is represented as Pre + S100 for short, where “S” denotes single pulse main injection and “100” denotes 100 MPa injection pressure. The split main injection process was based on the mass fraction ratio of the two pulses of the main injection, 50:50 and 75:25. Accordingly, the split main injection process is represented as Pre + D160_50-50 and Pre + D160_75-25, where, “D” denotes double pulse (split-) main injection, “160” denotes 160 MPa injection pressure. The injection mass of the pre-injection was 0.9 mm^3, and the injection mass of the main injection was 5 mm^3 under the three injection strategies.

This corresponds to the injection amount per injection hole in the multi-nozzle of medium / high load diffusion type combustion region of the actual engine. The interval between the pre-injection and the main injection used in the actual engine was also set as 0.6 ms.

5.3 INJECTION RATE

Figure 5.1 illustrates the result of the injection rate measurement of the single main injection and split main injection processes, which was obtained using the single cylinder multiple injection rate measurement system. The Zuech type rate of injection meter was adopted to measure the injection rate, and the methodology is illustrated in the paper [64].

As illustrated in Figure 5.1, considering Pre + S100 injection strategy as the base condition, the end of injection (EOI) of the high pressure split main injection strategies (Pre + D160_50-50 and Pre + D160_75-25) were similar with that of the Pre + S100 injection strategy. The timing of the EOI was approximately 2.8 ms after start of injection (ASOI), and the end of the pre-injection was approximately 0.5 ms ASOI under the three injection strategies. As mentioned above, the injection volume of the pre-injection is 0.9 mm^3 and that of the main injection is 5.0 mm^3. The total volume of the tracer LAS fuel and diesel were identical.

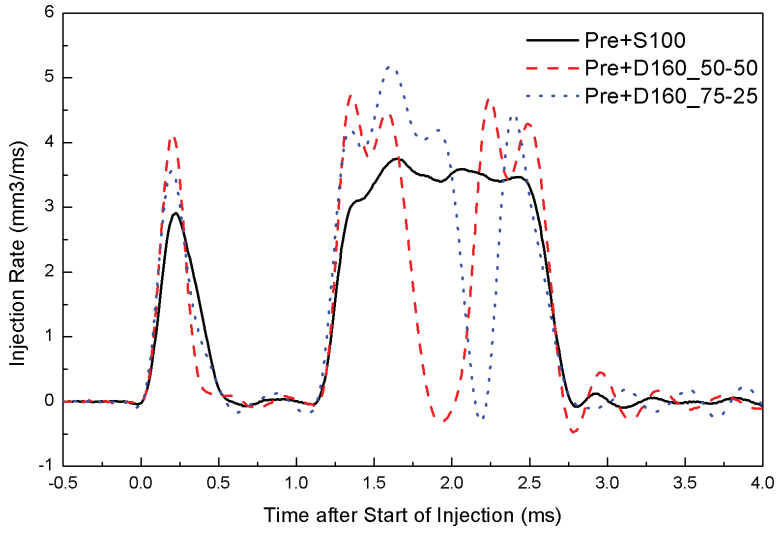

Figure 5.1 Injection rates of Pre + S100, Pre + D160_50-50 and Pre + D160_75-25

5.4 EVAPORATION CHARACTERISTICS

Figure 5.2 presents the spatial distribution of the liquid phase optical thickness and vapor mass per unit projected area of spray impingement in the 2-D piston cavity under the three injection strategies.

The times selected for Pre + S100 are 1.14 ms ASOI (start of main injection), 1.8 ms ASOI (KL first observed timing), and 2.8 ms ASOI (end of injection) from left to right. The times selected for Pre + D160_50-50 are 1.16 ms ASOI (start of first main injection), 1.9 ms ASOI (KL first observed timing), 1.96 ms ASOI (start of second main injection), 2.16 ms ASOI (0.2 ms after the start of second main injection) and 2.8 ms ASOI (end of injection). The times selected for Pre + D160_75-25 are 1.14 ms ASOI, 1.8 ms ASOI, 2.19 ms ASOI, 2.39 ms ASOI and 2.8 ms ASOI (end of injection). The meaning of times for Pre + D160_75-25 are same with that of Pre + D160_50-50 from start to end.

From Figure 5.2, it is observed that the spray penetrates not only along the wall surface but also along the lip after the impingement. A relatively high droplet density is located in the proximity of the impingement point region and at the deep groove region of the cavity. This is because of the spray–wall interaction, large momentum loss after impingement, and droplet stagnation at those regions. The vapor distribution of the split main injection is significantly more homogeneous than that of the single main injection.

The spray momentum divides into two parts after the impingement point. That is why the rich vapor mass locates not only in the cavity groove but also near the lip area near 1.8 ms ASOI. The droplet densities of Pre + S100 in the proximity of the impingement point region and at the deep groove region of cavity are smaller than those of Pre + D160_50-50 and Pre + D160_75-25. The velocity of Pre + S100 is smaller than that of high injection pressure strategies, which results in the weaker spray–wall interaction of Pre + S100, causes weaker stagnant strength. The vapor mass of Pre + D160_50-50 is leaner than that of Pre + D160_75-25 near 1.8 ms ASOI, which is because the injected mass for Pre + D160_50-50 is smaller than that of Pre +D160_75-25 near 1.8

ms ASOI. Accordingly, the injection mass and spray–wall interaction have the effect on fuel evaporation. The vapor mass distribution of Pre + D160_50-50 and Pre + D160_75-25 are significantly more homogeneous than that of Pre + S100 owing to the higher injection pressure. Moreover, the vapor mass distribution of Pre + D160_50-50 is significantly more homogeneous than that of Pre + D160_75-25 due to smaller injected mass of Pre + D160_50-50.

According to the 1.96 ms ASOI and 2.16 ms ASOI of Pre + D160_50-50, 2.19 ms ASOI and 2.39 ms ASOI of Pre + D160_75-25, the second main injection is evident from the comparison of the third and fourth columns in the liquid images. The vapor fuel is mainly distributed at the impingement point and cavity wall. It is evident that the vapor mass distributions of high injection pressure strategies are richer than those of Pre + S100 at 2.8 ms ASOI.

The vapor fuel around the impingement point of Pre + D160_50-50 at 2.8 ms ASOI is richer than that of Pre + D160_75-25 because of the bigger injection mass of second main injection of Pre + D160_50-50. Oppositely, the vapor fuel around the spray tip of Pre + D160_50-50 at 2.8 ms ASOI is leaner than that of Pre + D160_75-25 because of the leaner injection mass of first main injection of Pre + D160_50-50. The injection mass ratio of split main injection has a significant effect on the vapor distribution.

For Pre + S100; moreover, the spray–wall interaction becomes strong at the EOI because of the big injection mass and low injection pressure, which results in a higher droplet density at the deep groove region of the cavity at the EOI than that at other times. The vapor fuel is mainly distributed around the impingement point of the cavity wall. And compare with 2.16 ms ASOI and 2.8 ms ASOI of Pre + D160_50-50, the droplets become dense in the cavity groove and the vapor of spray tip becomes rich. It implies that the second main injection fuel catches up with the previous spray from 2.16 ms ASOI to 2.8 ms ASOI. And the same tendency can be observed from 2.39 ms ASOI to 2.8 ms ASOI of Pre + D160_75-25.

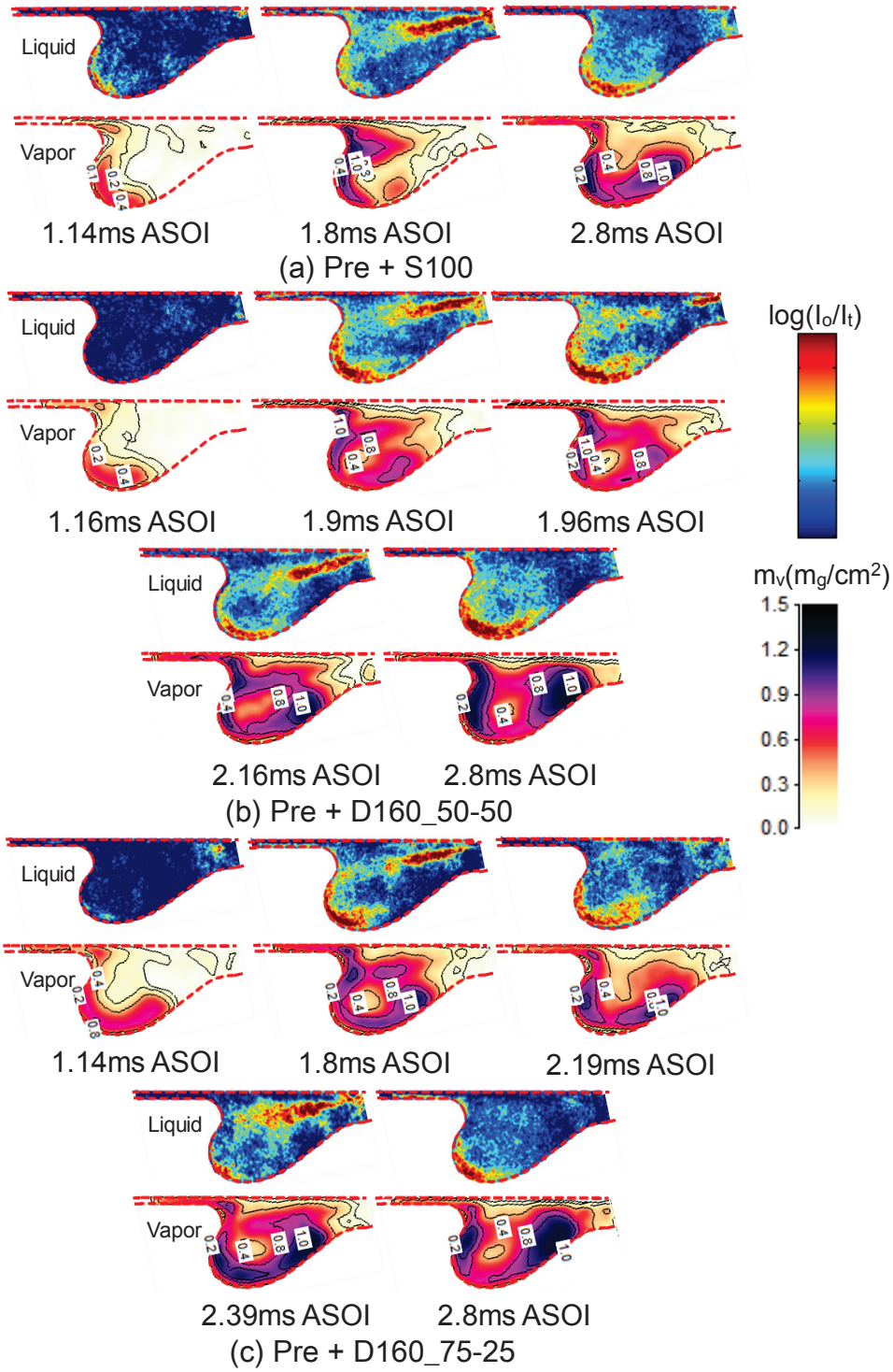

Figure 5.2 Spatial distributions of liquid phase optical thickness and vapor mass per unit projection area

Figure 5.3 presents the evaporation ratio under the three injection strategies as time elapses. The evaporation ratio of Pre + S100 at 1.14 ms ASOI is smaller than that of Pre

+ D160_50-50 and Pre + D160_75-25. It implies that a high injection pressure promotes the fuel evaporation process.

The evaporation ratio of Pre + S100 decreases under these three timings. A probable reason is that the increase in the velocity of the injected fuel mass is higher than the evaporation rate when the injection amount is substantially larger. Another reason is that the wall heat loss happens, which reduces the temperature inside the cavity.

The evaporation ratio of Pre + D160_50-50 also decreases from 1.16 ms ASOI to 1.9 ms ASOI. But the evaporation ratio of 1.96 ms ASOI is bigger than that of 1.9 ms ASOI. The timing 1.96 ms ASOI is during the interval which means the fuel can evaporate without new injected fuel, causes the evaporation ratio increases compared with that of 1.9 ms ASOI. It means the split injection can improve the fuel evaporation process. And then the evaporation ratio decreases from 1.96 ms ASOI to 2.16 ms ASOI because of the second main injection. The evaporation ratio of Pre + D160_75-25 also decreases except at 2.39 ms ASOI.

For Pre + D160_75-25, it can be observed that the evaporation ratio at 2.39 ms ASOI is marginally higher than that at 2.19 ms ASOI. A probable reason for this is that the marginal injection amount of the second main injection results in an increase in velocity of injected fuel mass which is lower than the evaporation rate. It indicates the split injection can promotes the fuel evaporation process.

Figure 5.4 illustrates the definition of spray tip penetration of 2-D piston cavity impinging spray. The spray tip penetration of 2-D piston cavity impinging spray is calculated by adding the axial penetration and arc length along the cavity wall. The S_{Axial} is constant, equal to 30 mm.

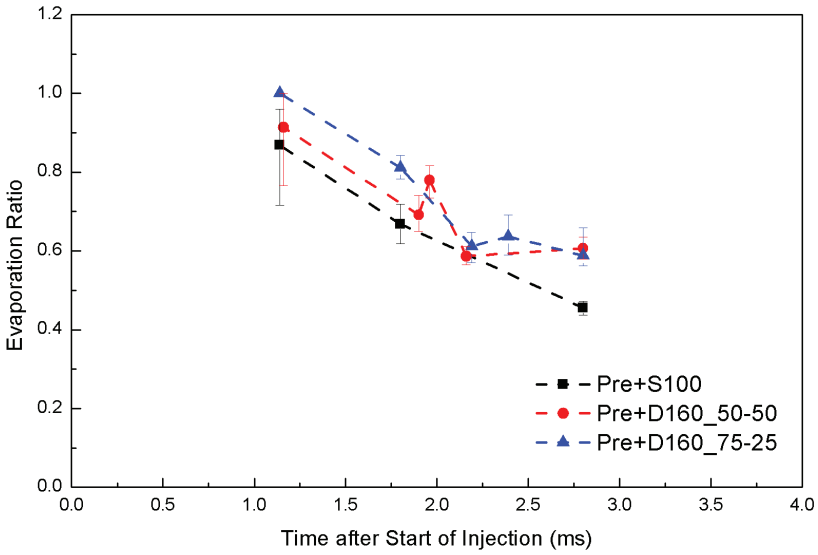

Figure 5.3 Evaporation ratio of impinging spray under three injection strategies

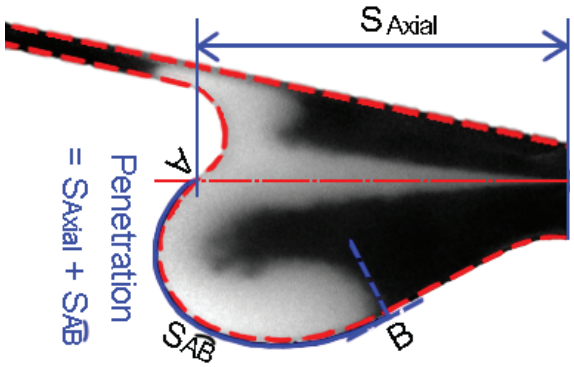

Figure 5.4 Definition of spray tip penetration of 2-D piston cavity impinging spray

Figure 5.5 presents the spray tip penetration of 2-D cavity spray versus time under the three injection strategies. As the injection pressure of Pre + D160_50-50 and Pre + D160_75-25 are higher than that of Pre + S100, the fuel in Pre + D160_50-50 and Pre + D160_75-25 attain a significantly higher momentum. Consequently, the spray tip penetration of Pre + D160_50-50 and Pre + D160_75-25 are longer than that of Pre + S100. The spray tip penetration of Pre + D160_75-25 during the first main injection is longer than that of Pre + D160_50-50 because of the bigger injected mass of Pre + D160_75-25. The second main injection catches up with the previous fuel gives the spray more momentum which makes the spray tip penetration of Pre + D160_50-50 and Pre + D160_75-25 are almost same after 2.0 ms ASOI. Moreover, the gradient from 1.9 ms

ASOI to 1.96 ms ASOI of Pre + D160_50-50 is larger than that of the other stages. The gradient from 2.19 ms ASOI to 2.39 ms ASOI of Pre + D160_75-25 is larger than that of the other stages. It implies that a split injection attains high momentum and induces the spray to penetrate faster.

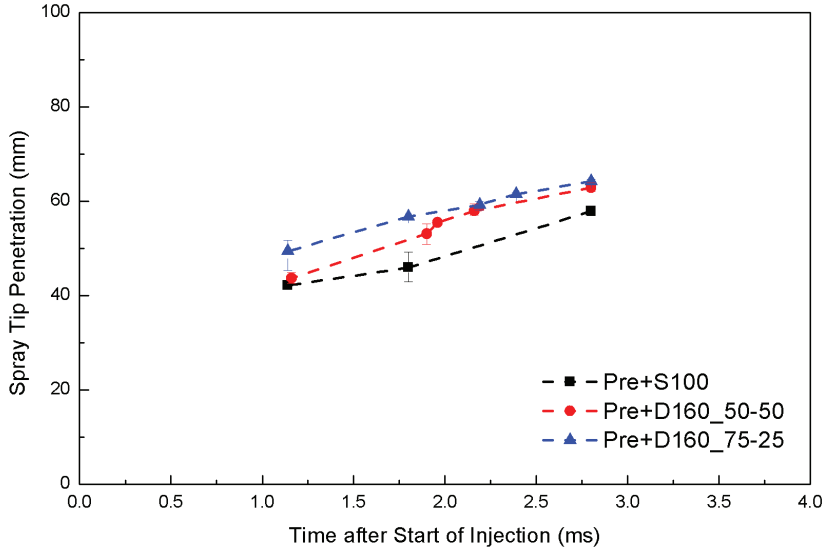

Figure 5.5 Spray tip penetration of impinging spray

5.5 COMBUSTION CHARACTERISTICS

Figure 5.6 shows the KL factor, temperature and OH* chemiluminescence spatial distribution of 2-D cavity impinging flames.

The area where OH* images exhibit strong signal display a small KL factor. High KL factor values are observed near the cavity wall region. However, high temperature does not have a fixed area. The pre-injection ignition timing (0.9 ms ASOI of Pre + S100, 0.8 ms ASOI of Pre + D160_50-50 and 0.8 ms ASOI of Pre + D160_75-25) of the 2-D piston cavity impinging flame is illustrated using OH* chemiluminescence images. It implies that a high injection pressure can promote the combustion. The first main injection ignition from OH* chemiluminescence can be detected at the time of 1.6 ms ASOI under the three injection strategies. The pre-injection combustion renders the

ambient more favorable for ignition, which results in almost equal first main injection ignition timing under the three injection strategies.

OH* chemiluminescence also appears prior to soot formation and temperature distribution, which is also consistent with the results wherein soot formation begins after ignition during the pre-mixed burn phase [65]. Moreover, that the KL factor and temperature at early timing are too weak to be observed is also a probable reason. The OH* chemiluminescence near the cavity wall is weak, which implies a low temperature around this area. This phenomenon can be proved from the temperature distribution images. The effect of wall heat loss causes this, which also establishes the results of Figure 5.4. From the KL and temperature distribution images of Pre + D160_50-50 and Pre + D160_75-25, the second main injection flame is evident at 2.8 ms ASOI (EOI). The local maximum OH* chemiluminescence of Pre + D160_50-50 and Pre + D160_75-25 are weaker than that of Pre + S100 at 2.8 ms ASOI. It implies the local mean temperature of Pre + D160_50-50 and Pre + D160_75-25 are lower than that of Pre + S100 at 2.8 ms ASOI; this can be also observed from the temperature distribution images. According to the shape of OH*, KL factor and temperature distribution, the projected areas of OH* chemiluminescence is larger than that of the KL factor and temperature distribution. In the near-cylinder head region of the flame, there is an apparent part which exhibits OH* chemiluminescence albeit no KL factor and no temperature. As time elapses and the fuel injection ends, the flame jet begins to move toward the cylinder head at the time of 4.0 ms ASOI of the three injection strategies. The OH* chemiluminescence stays strong at this moment, while the KL factor is highly marginal and the temperature is very low, which may indicate that the soot oxidation process involves the participation of OH and the high temperature reactions.

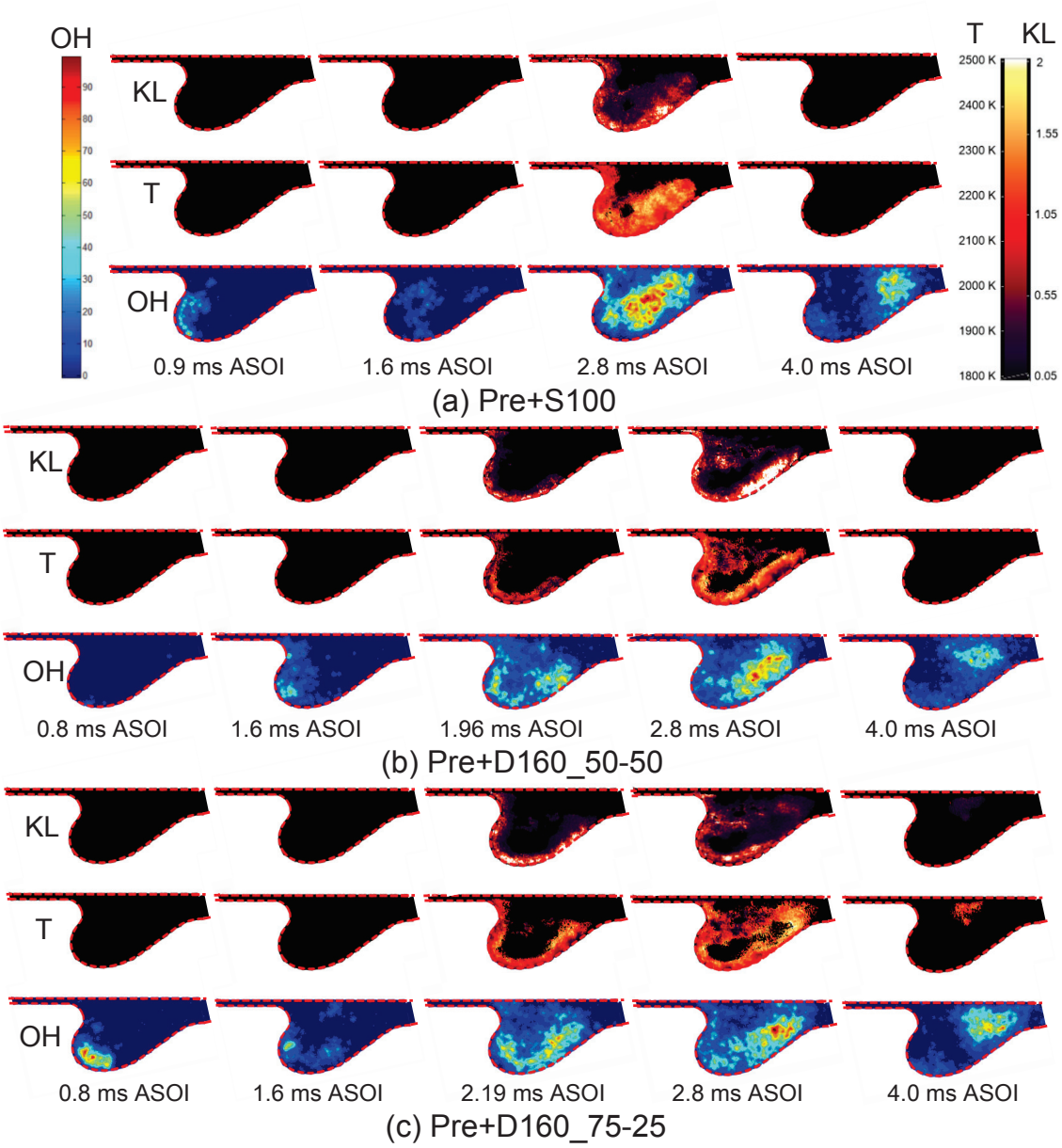

Figure 5.6 KL factor, temperature and OH* chemiluminescence of impinging spray under three injection strategies

Figure 5.7 presents the ignition delay of the pre-ignition and first main ignition under the three injection strategies. The ignition delay is defined as the time from the start of the injection to the ignition timing. The ignition timing is defined as the time the ignition happens through the OH* image. The higher injection pressure can decrease the ignition delay from the results of the pre-injection ignition delay. Pre-injection combustion can

significantly decrease the main injection ignition delay and then improve the main injection combustion. Pre-injection combustion makes the ambient environment more favorable for the main injection combustion. Compared with the previous paper's results [129], the OH* chemiluminescence enables a more precise observation of the ignition delay.

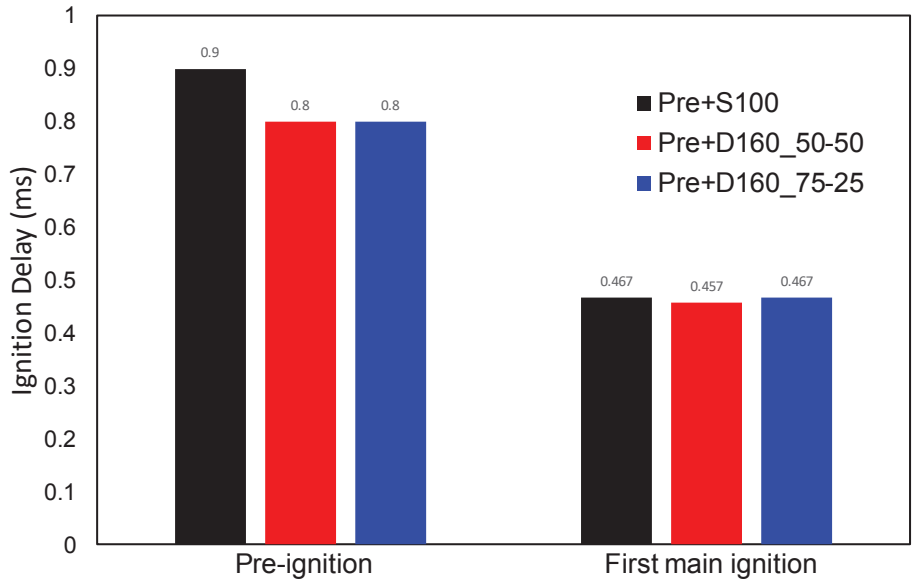

Figure 5.7 Ignition delay of pre and main ignition under three injection strategies

Figure 5.8 illustrates the integrated KL factor versus the integrated OH* intensity under the three injection strategies. The integrated OH* intensity is an indicator of heat release in the premixed combustion [133, 134], and the peak of the OH* chemiluminescence intensity corresponds significantly to the peaks of heat release and combustion pressure [135]. The first peak is at approximately 1.0 ms ASOI from the combustion of the pre-injection spray for Pre + S100, but 0.9 ms ASOI for Pre + D160_50-50 and Pre + D160_75-25. Moreover, the peak value of Pre + S100 is smaller than that of Pre + D160_50-50 and Pre + D160_75-25 during the pre-injection combustion. It implies that high injection pressure exhibits higher heat release and higher combustion pressure. The integrated OH* intensity tendency is same with the integrated KL factor, but time lag.

For Figure 5.8 (a), the maximum KL factor appears at 2.6 ms ASOI, but the main injection OH* intensity peak timing is 3.1 ms ASOI, 0.5 ms time lag. For Figure 5.8 (b),

the first main injection maximum KL factor appears at 2.3 ms ASOI and the second main injection maximum KL factor appears at 3.0 ms ASOI, but the first main injection OH* intensity peak timing is 2.7 ms ASOI and the second main injection OH* intensity peak timing is 3.4 ms ASOI. The time lag of the maximum KL factor and peak OH* intensity is 0.4 ms. For Figure 5.8 (c), the first main injection maximum KL factor appears at 2.3 ms ASOI and the second main injection maximum KL factor appears at 3.0 ms ASOI, but the first main injection OH* intensity peak timing is 2.7 ms ASOI and the second main injection OH* intensity peak timing is 3.1 ms ASOI. The time lag of the maximum KL factor and peak OH* intensity under two main injection is 0.4 ms. And 0.1 ms, respectively. The split injection decreases the time lag, and the split injection mass ratio also has the effect on the time lag.

The integrated KL factor of Pre + D160_50-50 and Pre + D160_75-25 are smaller than that of Pre + S100 from 1.8 ms ASOI to 2.4 ms ASOI. It implies that a high injection pressure decreases the soot formation at the initial combustion process. The integrated KL factor of Pre + D160_75-25 is also smaller than that of Pre + S100 from 2.4 ms ASOI to 2.8 ms ASOI. Moreover, the integrated KL factor decreases during this period. It implies that the interval of the split injection has a positive effect on the decrease of soot. The second main injection increases the integrated KL factor after 2.8 ms ASOI. The integrated KL factor of the second main injection combustion is smaller than that of the first main injection combustion, which is because the injection mass of the second main injection is smaller than that of the first main injection. However, the integrated KL factor of Pre + D160_50-50 is bigger than that of Pre + S100 after 2.8 ms ASOI. This is owing to the following two reasons: the second main injection combustion continues the effect on the soot formation after 2.8 ms ASOI; the fuel of the second main injection fuel catches up with the previous flame after 2.8 ms ASOI and deteriorates the combustion. If the interval is increased adequately, the second main injection fuel cannot catch up with the previous flame, which can decrease the soot. The split injection mass ratio has a significant effect on the soot evaluation. Moreover, the gradient of the integrated KL

factor of Pre + D160_50-50 and Pre + D160_75-25 are larger than that of Pre + S100 after 3.0 ms ASOI. It implies that the soot oxidation rate of the split injection is higher than that of the single injection.

Figure 5.9 indicates the spatial distributions of KL factor and temperature along the solid line at EOI. The line can be divided into two parts: the first part is the impinging spray flame (in the proximity of the wall region, around 0 to 4 mm) and the second part is the free spray flame (after 4 mm). As presented above, the sectional line selected is the region where the fuel of second main injection has already caught up with the previous flame in the case of Pre + D160_75-25 and has just caught up marginally with the previous flame in the case of Pre + D160_50-50. Consequently, the three injection strategies in the decreasing order of KL factor in the proximity of the wall region along this sectional line are Pre + D160_50-50, Pre + S100, and Pre + D160_75-25. It is evident that the fuel of second main injection infiltrates to the combustion region, which deteriorates the previous flame and generates more soot. However, the tendency of temperature (very near the wall region) among the three injection strategies is opposite to that the KL factor. From the enlarged images c, d and e, the three lines pass through a high soot region. Consequently, the KL factor has a peak value in the impinging spray flame region in each of the injection strategies. The KL factor of Pre + D160_50-50 is beyond the instrument's calibration, which resulted in the data being similar to that near the wall region. The tendency of KL factor of Pre + S100 and Pre + D160_75-25 is to decrease first, then increase and last decrease from 0 to 1.6 mm. The tendency of temperature for Pre + S100 and Pre + D160_75-25 is to increase from 0 to 1.6 mm. This is because high temperature soot gathers in this region (from 0 to 1.6 mm). The fluctuation of KL factor and temperature of Pre + S100 and Pre + D160_75-25 in the spray flame region is smaller than that of Pre + D160_50-50. This is because there is a single flame in the case of Pre + S100, and the split flame has already mixed in the case of Pre + D160_75-25; however, the split flame does not mix in the case of Pre + D160_50-50.

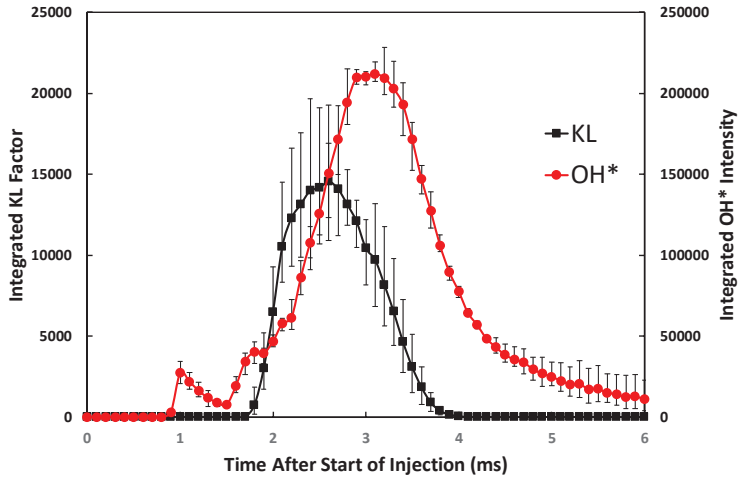

(a) Pre+S100

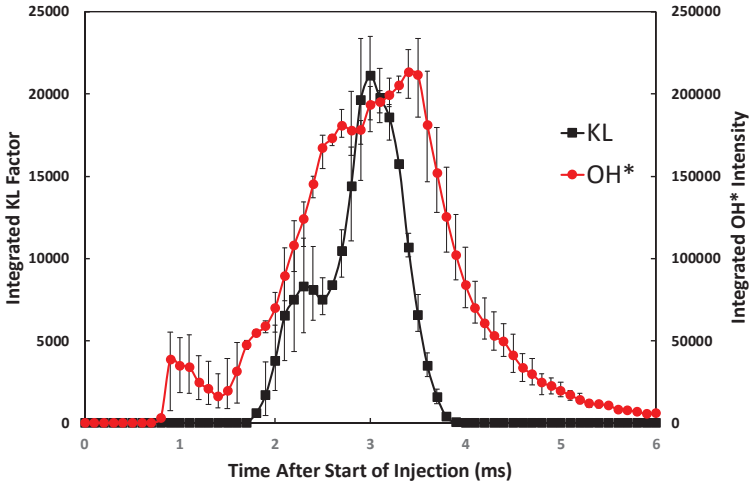

(b) Pre+D160_50-50

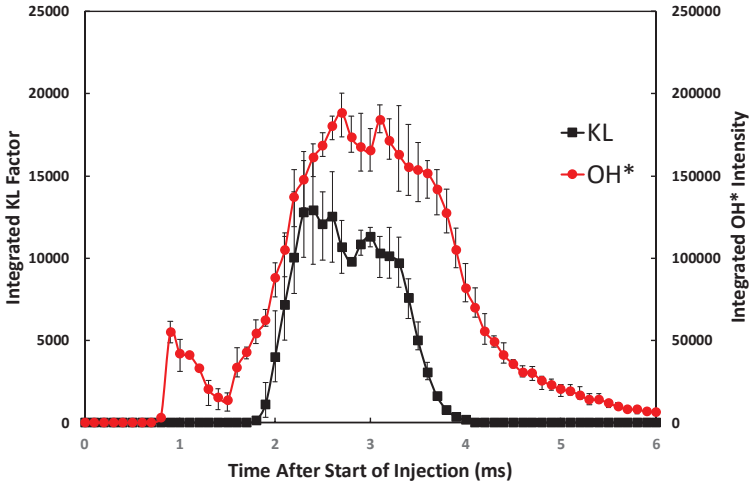

(c) Pre+D160_75-25

Figure 5.8 The integrated KL factor versus the integrated OH* intensity

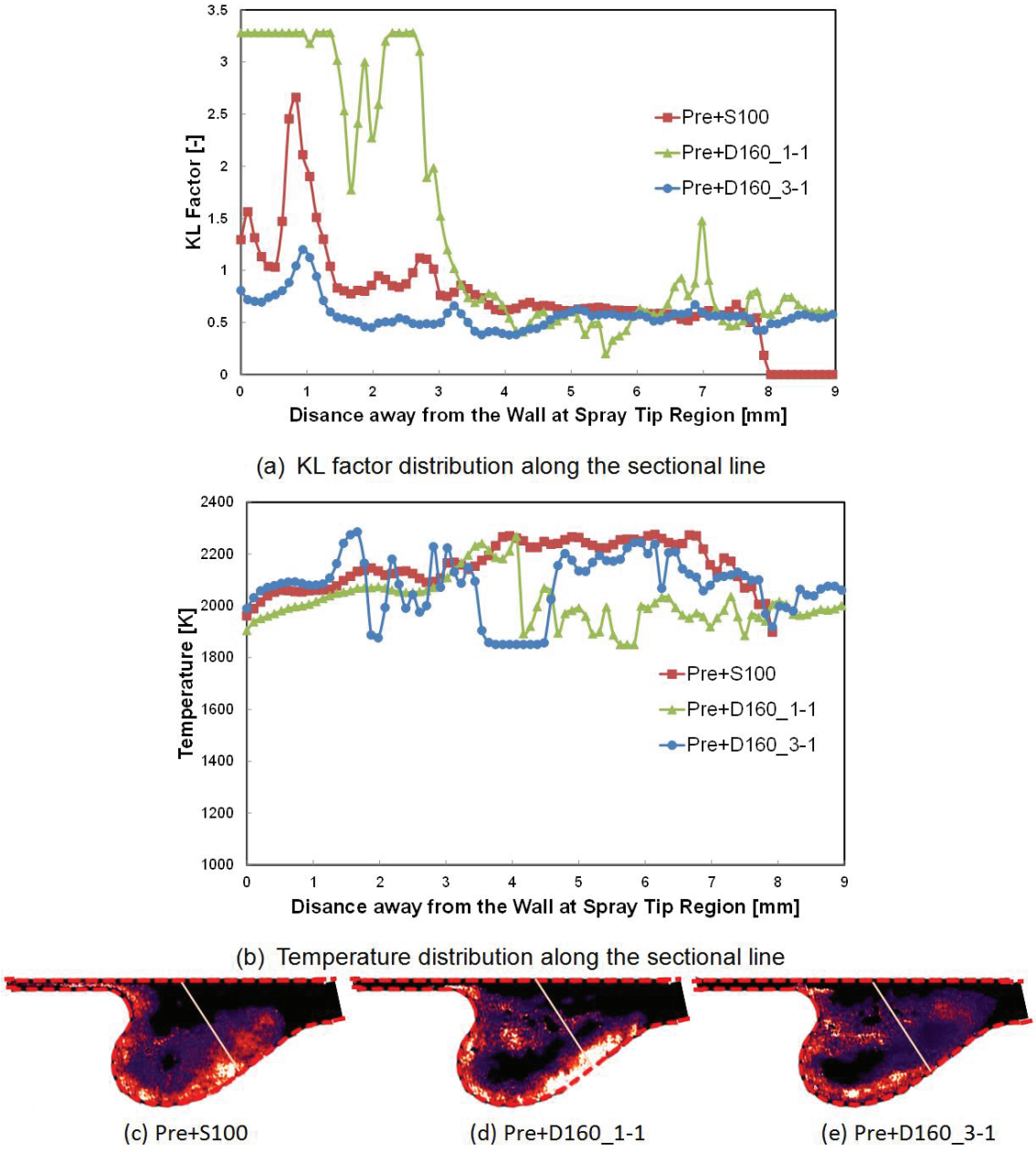

Figure 5.9 Spatial distributions of KL factor and temperature along the sectional line at EOI

In order to investigate the effect of the second main injection and previous flame, the spatial distributions of KL factor under Pre + D160_75-25 along the sectional line are illustrated in Figure 5.10. The KL factor in the impinging spray flame of 2.8 ms is higher than that of 2.6 ms, but smaller than that of 3.0 ms. This implies that the fuel of the second

main injection had already caught up with the previous flame in the flame tip region, causing the deterioration of the combustion and a KL factor at 3.0 ms, higher than at 2.8 ms. In the free spray flame region, the KL factor of the three strategies are approximately equal.

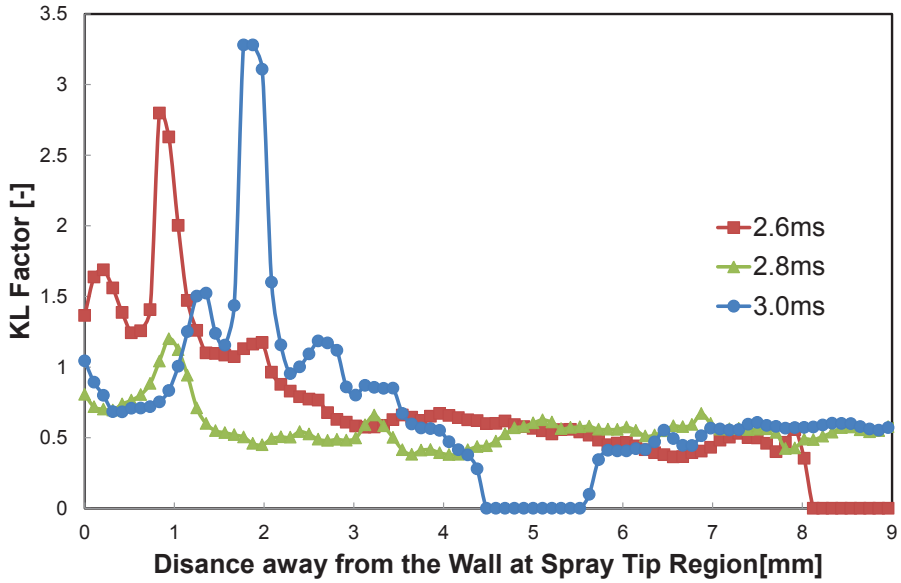

Figure 5.10 Spatial distribution of KL under Pre+D160_75-25 along the sectional line

According to the paper of Kamimoto [136], the KL factor equation can be obtained using the Rayleigh–Debye–Gans model.

$$KL = \frac{6\pi E(m) c_m}{\rho_p} L \tag{5.1}$$

E(m) is expressed as

$$E(m) = \mathrm{Im}\left(\frac{m^2-1}{m^2+2}\right) \tag{5.2}$$

where ρ_p (1.68 g/cm^3) is the density of the primary particles, L is the geometric thickness of the flame along the optical detection axis, c_m is the soot mass concentration, and m is the complex refractive index of the soot particles expressed by m = n – ik= (1.9 ±0.1) – i(0.55±0.10). Here we decided n=2.0 and k=0.55.

The soot mass (m_s) can be obtained by

$$m_s = \Delta a_{pix} \frac{\rho_p}{6\pi E(m)} \sum KL \tag{5.3}$$

where Δa_{pix} is the area of each pixel under the cross-section.

Figure 5.11 shows the ratio of the soot mass to the injected mass as time elapses. The ratio can be divided into two parts: one is from the SOI to the EOI as the injected mass is changing with time; the other is after EOI as the injected mass is constant. According to equation (3), the soot mass is related to the integrated KL factor. When the injected mass is similar, the ratio of the soot mass to the injected mass should have a shape identical to that of the integrated KL factor. This phenomenon can be compared with that of Figure 5.8. The timing of the maximum ratio for Pre + D160_75-25 is 2.3 ms ASOI, which is marginally earlier than that of the timing of the maximum integrated KL factor for Pre + D160_75-25 (2.4 ms ASOI) from Figure 5.8. The timing of the maximum ratio for Pre + S100 is 2.2 ms ASOI, which is apparently earlier than that of the timing of the maximum integrated KL factor for Pre + S100 (2.6 ms ASOI) from Figure 5.8. It implies that a lower injection pressure more straightforwardly produces a large soot mass. The timing of the maximum ratio for Pre + S100 and Pre + D160_75-25 are during the first part as we defined before. However, the timing of the maximum ratio for Pre + D160_50-50 is 3.0 ms ASOI (during the second part), which is same with that of maximum integrated KL factor. The split injection mass ratio has a significant effect on the maximum ratio timing. If the first main injection fuel mass is bigger than that of the second main injection, the maximum ratio timing is during the first part. If not, the maximum ratio timing is during the second part. Moreover, the gradient of the ratio for Pre + D160_50-50 from 2.2 ms ASOI to 2.5 ms ASOI and for Pre + D160_75-25 from 2.3 ms ASOI to 2.8 ms ASOI are larger than that of Pre + S100. It implies that the interval expedites the soot oxidation. The gradient of the ratio for Pre + D160_50-50 and Pre + D160_75-25 from 3.0 ms ASOI to 4.0 ms ASOI are larger than that of Pre + S100. It implies that the soot oxidation ratio of the split injection is higher than that of the single injection.

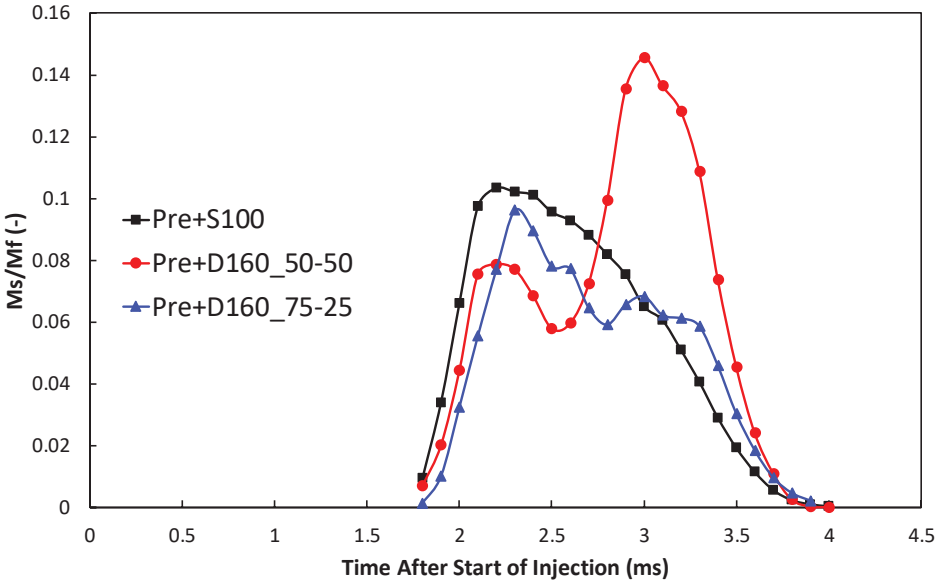

Figure 5.11 The ratio of soot mass to fuel mass

Figure 5.12 presents a soot index for combustion. The plots in the figure represent the soot mass gradient at this time. It is defined by the gradient of the two adjacent time points. The plots larger than zero imply "during the soot formation dominated process", while those smaller than zero imply "during the soot oxidation dominated process."

Pre + S100 is mainly divided into two parts: 1.8 ms ASOI to 2.6 ms ASOI and 2.6 ms ASOI to 4.0 ms ASOI; Pre + D160_50-50 is mainly divided into four parts: 1.8 ms to 2.3 ms ASOI, 2.3 ms to 2.5 ms ASOI, 2.5 ms to 3.0 ms ASOI and 3.0 ms to 4.0 ms ASOI; Pre + D160_75-25 is mainly divided into four parts: 1.8 ms to 2.4 ms ASOI, 2.4 ms ASOI to 2.8 ms ASOI, 2.8 ms ASOI to 3.0 ms ASOI, and 3.0 ms ASOI to 4.0 ms ASOI. Pre + S100 has soot formation and oxidation dominated processes. However, Pre + D160_50-50 and Pre + D160_75-25 exhibit soot formation, oxidation, formation and oxidation processes. The split injection combustion changes the soot evaluation. Due to the different split injection mass ratio, the soot evaluation period shows different duration. The ratio for Pre + S100 is larger than that for Pre + D160_50-50 and Pre + D160_75-25 during the initial period. A high injection pressure can decrease the soot formation process at the initial combustion. Moreover, the gradient of the ratio for Pre + S100 is smaller than that for Pre

+ D160_50-50 and Pre + D160_75-25 at the post combustion period which is same with the results of Figure 5.8. It implies that the split main injection accelerates the soot oxidation process at the post combustion period.

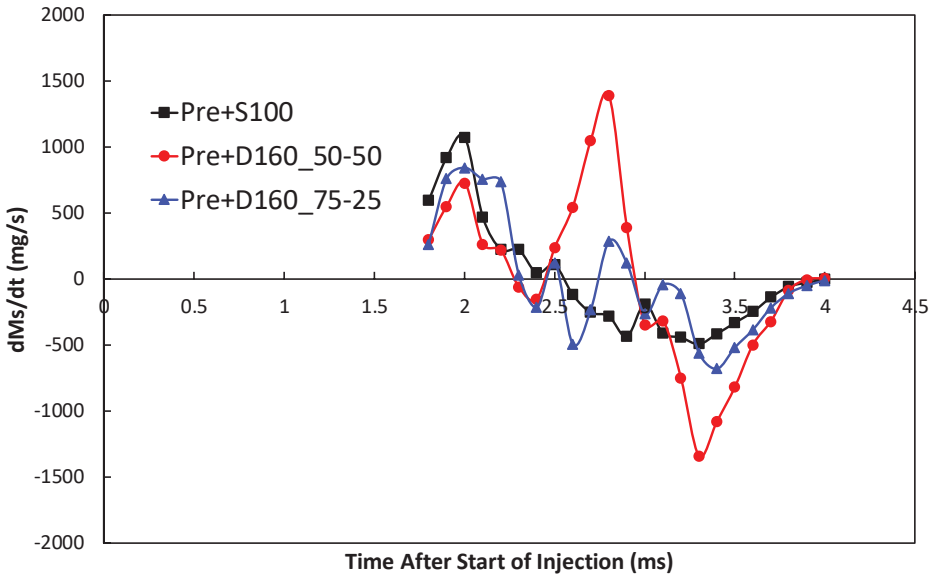

Figure 5.12 The soot index for combustion

5.6 SUMMARY

In this section, the comparison of the evaporation and combustion characteristics of 2-D cavity impinging spray were investigated. The evaporation processes were analyzed by the tracer LAS technique under the three injection strategies (Pre + S100, Pre + D160_50-50 and Pre + D160_75-25). The combustion processes were analyzed by the two-color pyrometry method and OH* chemiluminescence. The main conclusions are summarized as follows:

Evaporation Process - The vapor distribution of the split main injection is significantly more homogeneous than that of the single main injection at the EOI. It is observed that the fuel of the second main injection of the split main injection has already caught up with the previous fuel at the EOI in the case of Pre + D160_50-50. A higher injection pressure provides a larger momentum, which induces the spray to penetrate further. Because of the spray–wall interaction, the relative high droplet density is located

near the impingement point region and at the deep grove region of the cavity. A probable feature is that the air entrainment of the 2-D cavity is low, which deteriorates the evaporation process.

Combustion Process - The second main injection fuel of the split main injection almost catches up with the previous fuel, which causes the high KL factor distribution in the flame tip region in the case of Pre + D160_50-50. The higher injection pressure can decrease the ignition delay. The pre-injection combustion can significantly decrease the main injection ignition delay and then improve the main injection combustion. The split injection decreases the time lag, and the split injection mass ratio also has the effect on the time lag of the maximum integrated KL factor and the integrated peak OH* intensity. The soot oxidation rate of the split injection is higher than that of the single injection.

This study indicates that spray–wall interaction occurs in the 2-D cavity impinging spray, which causes shorter spray tip penetration and lower evaporation ratio. Pre-injection combustion has a positive effect on the main injection combustion. The split injection can reduce the soot formation and accelerate the soot oxidation process. Increases the split injection interval has a positive effective method to reduce the soot.

CHAPTER 6 COMPARISON OF FREE SPRAY AND 2-D CAVITY IMPINGING SPRAY EVAPORATION AND COMBUSTION CHARACTERISTICS

6.1 INTRODUCTION

Yeom et al. [137] indicates that in order to study the diesel spray behavior, it is needed to analyze the impinging spray and free spray, simultaneously as an injected spray development process consists of impinging and free spray in the diesel engine. Liu et al. [138] investigated the characteristics of diesel spray impingement based on droplet impact phenomenon and found that the spray height changes from spray contact with the wall. Mao et al. [139, 140] studied the characteristics of diesel spray wall collision by quantitative analysis. As we discussed above, not only the free spray evaporation and combustion characteristics need investigate, but also the 2-D cavity impinging spray evaporation and combustion characteristics need investigate. Thus, it is necessary to make a comparison of free spray and 2-D cavity impinging spray evaporation and combustion characteristics.

6.2 EXPERIMENTAL CONDITIONS

The experimental conditions are same with the above sections, expect the injection strategies. Two injection strategies are chosen, Pre + S100 and Pre + D160_75-25, to investigate the effect of pre-injection on the diesel free spray and 2-D cavity impingement evaporation and combustion characteristics. Figure 6.1 illustrates the result of the injection rate measurement with and without pre-injection. The Zuech type rate of injection meter was adopted to measure the injection rate.

It can be seen that the main injection part of two injection types is same. Considering Pre + S100 injection strategy as the base condition, the EOI of the high pressure split injection strategy (Pre + D160_75-25) was similar with that of the base one. The EOI

timing of with and without pre-injection were approximately 2.8 ms and 1.66 ms ASOI respectively. The end of pre-injection was approximately 0.5 ms ASOI. The total volume of tracer LAS fuel and diesel was identical.

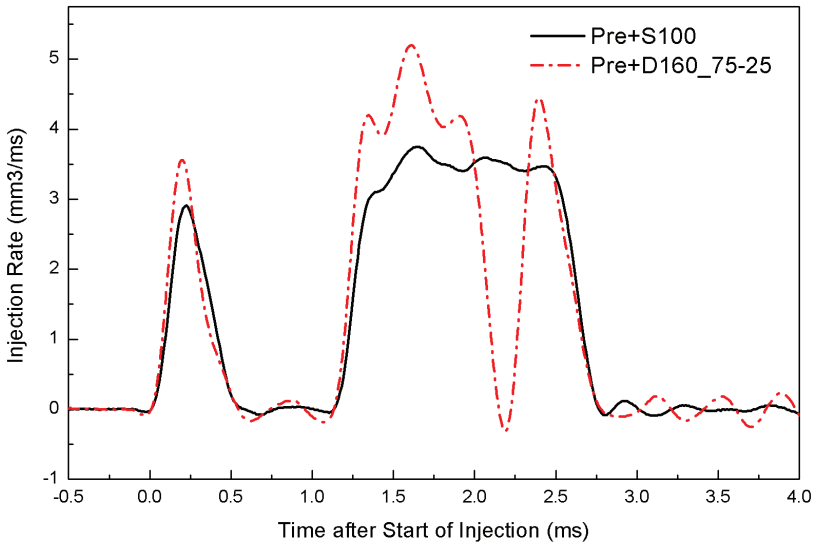

Figure 6.1 Injection rates of Pre + S100 and Pre + D160_75-25

6.3 COMPARISON OF EVAPORATION CHARACTERISTICS OF FREE SPRAY AND 2-D CAVITY IMPINGING SPRAY

The injection process with pre-injection, Pre + S100 and Pre + D160_75-25, was adopted to investigate the evaporation characteristics of free spray.

Figure 6.2 shows the spatial distributions of equivalence ratio of liquid and vapor phases (left and right column respectively). The timing chosen for Pre + S100 and Pre +D160_75-25 are the same, 1.14 ms ASOI (start of main injection), 1.8 ms ASOI (during the main injection) and 2.8 ms ASOI (end of injection) from left to right. The timing 2.19 ms ASOI of Pre + D160_75-25 indicates the start of second main injection.

The liquid phase equivalence ratio of Pre + D160_75-25 is leaner than that of Pre + S100 at 1.14, 1.8, and 2.8 ms ASOI. The vapor phase equivalence ratio of Pre + D160_75-25 is richer than that of Pre + S100 at 1.14 and 1.8 ms ASOI. It means a high injection

pressure accelerates the evaporation process. Moreover, the vapor distribution of Pre + D160_75-25 is much more homogeneous than that of Pre + S100 at 2.8 ms ASOI. Because of the split injection process, the fuel was injected in two steps, which makes the vapor distribution much more homogeneous, which is also a result of the high injection pressure.

It can be seen obviously that the second main injection fuel was injected from 2.19 ms ASOI and 2.39 ms ASOI under Pre + D160_75-25 condition. The spray tip penetration increases as the time elapses under the two injection strategies. The spray tip penetration of Pre + D160_75-25 is longer than that of Pre +S100 because of the high injection pressure.

The liquid phase optical thickness and the spatial distributions of the vapor mass per unit projected area of spray impingement on the 2-D piston cavity under the two injection strategies are presented in Figure 6.3. In order to compare with the results of free spray, the timings chosen here are the same.

The first column shows that the droplet of Pre + D160_75-25 is leaner than that of Pre + S100. The vapor mass distribution of Pre + D160_75-25 is richer than that of Pre + S100. The high injection pressure accelerates the fuel evaporation process. Higher injection pressure leads to greater fuel atomization, which would increase the rate of evaporation, and therefore, enhance the air–fuel mixing. This in turn, would help decrease the soot formation.

The second column shows the results during the main injection. It demonstrates that the droplet densities of Pre + S100 in the proximity of the impingement point region and at the deep groove region of cavity are smaller than that of Pre + D160_75-25. The fuel in the proximity of the impingement point is the fuel during the start of main injection, which implies that these injected fuel mass of Pre + S100 is smaller than that of Pre + D160_75-25. Moreover, the velocity of Pre + S100 is smaller than that of Pre + D160_75-25, which results in the weaker spray/wall interaction of Pre + S100. Moreover, the higher injection pressure accelerates the evaporation process. Accordingly, the effect of injection mass and spray/wall interaction on fuel evaporation is more significant than that of

injection pressure. The vapor mass distribution of Pre + D160_75-25 is significantly more homogeneous than that of Pre + S100 owing to the higher injection pressure.

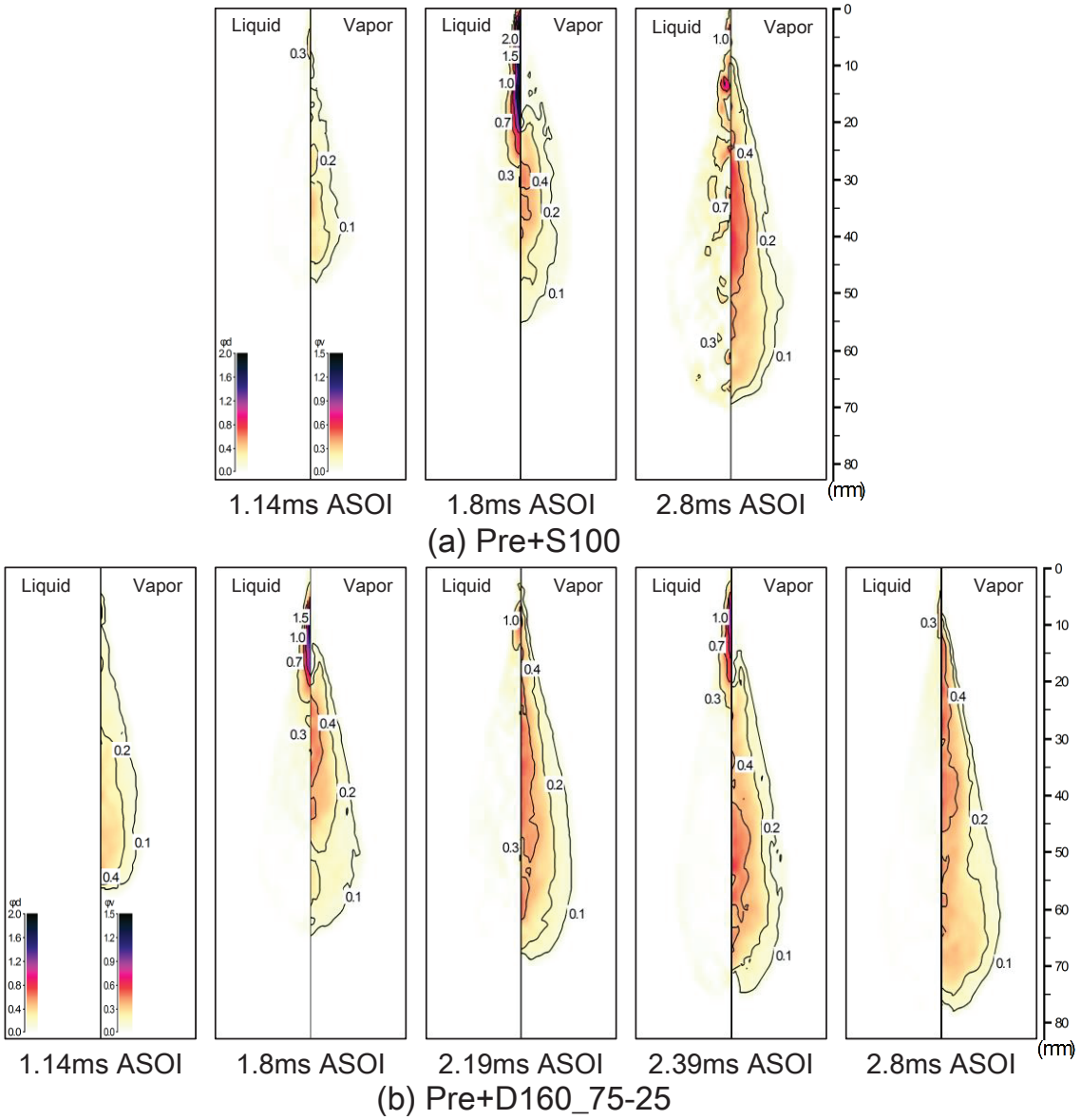

Figure 6.2 Spatial Distributions of equivalence ratio of liquid and vapor phases

The third and fourth columns of Pre + D160_75-25 are the images at the time of the start of second main injection and 0.2 ms after that. The second main injection is evident from the comparison of the third and fourth columns in the liquid images. The vapor fuel is mainly distributed at the impingement point and cavity wall.

The last column of the two injection strategies contains the images at EOI. It is

evident that the vapor mass distributions of Pre + D160_75-25 are richer than that of Pre + S100. For Pre + S100, the spray/wall interaction becomes strong at the EOI because of the big injection mass and low injection pressure, which results in high droplet density at the deep groove region of the cavity at the EOI. The vapor fuel is mainly distributed around the impingement point of the cavity wall.

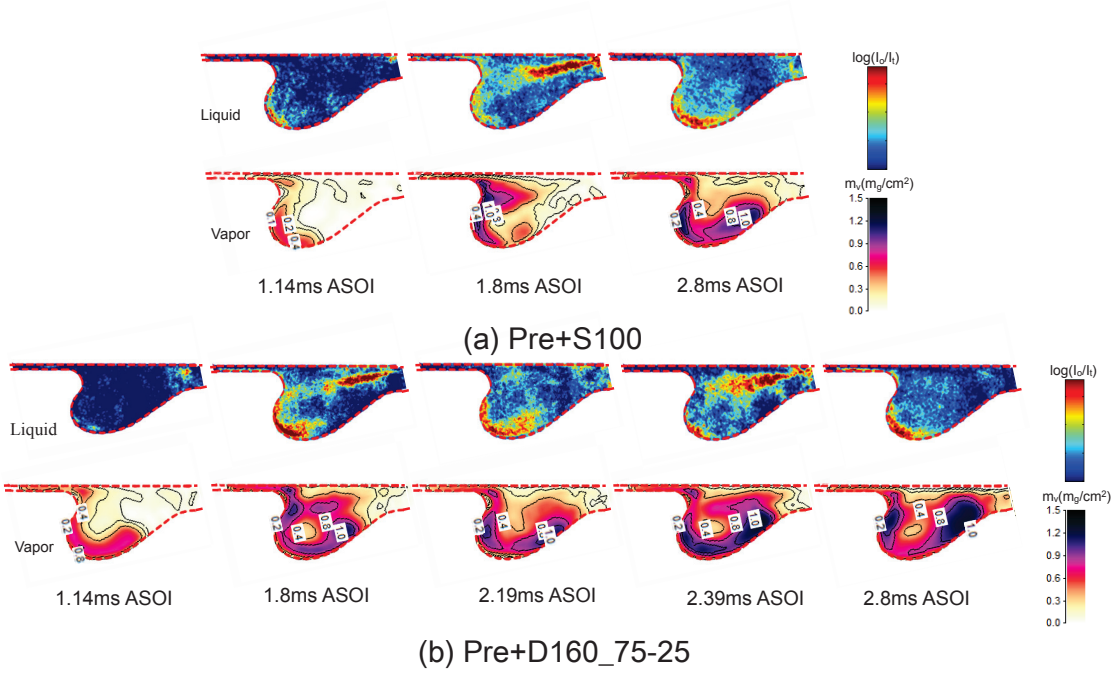

Figure 6.3 Spatial distributions of liquid phase optical thickness and vapor mass per unit projection area for 2-D cavity impinging sprays

Figure 6.4 presents the evaporation ratio of Pre + S100 under free spray and 2-D cavity impinging spray. The evaporation ratio signifies the ratio of fuel evaporation, which equals the vapor mass at a particular time divided by the injected fuel mass at that time. The evaporation ratio of Pre + S100 decreases from 1.14 ms to 1.8 ms ASOI, and then increases gently from 1.8 ms to 2.8 ms ASOI under free spray. However, the evaporation ratio decreases from 1.14 ms to 1.8 ms ASOI, and then decreases from 1.8 ms to 2.8 ms ASOI. The evaporation ratio of 2-D cavity impinging spray at 1.14 ms and 1.8 ms ASOI is slightly higher than that of free spray, but lower than that of free spray at 2.8 ms ASOI. This implies that the increase in the velocity of injected fuel mass is higher

than the evaporation rate when the injection amount is substantially large from 1.14 ms to 1.8 ms ASOI. And the entrainment gas of 2-D cavity is leaner than that of free spray, which causes the evaporation ratio decreases from 1.8 ms to 2.8 ASOI.

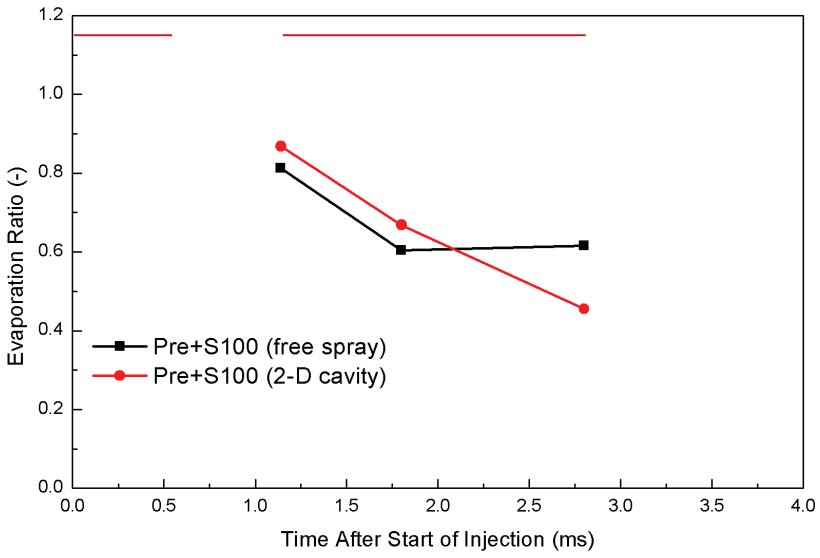

Figure 6.4 Evaporation ratio of Pre + S100

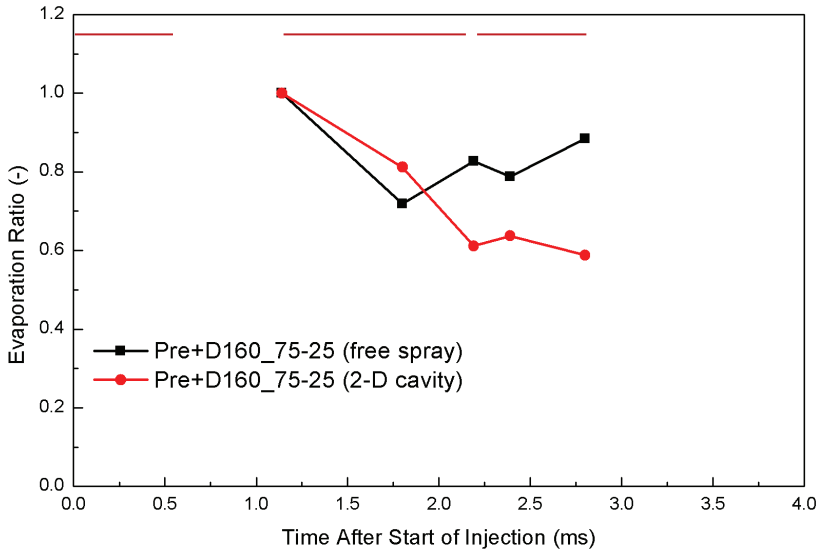

Figure 6.5 Evaporation ratio of Pre + D160_75-25

Figure 6.5 shows the evaporation ratio of Pre + D160_75-25 under free spray and 2-D cavity impinging spray. The whole tendency for Pre + D160_75-25 is same with that of Pre + S100 not only free spray but also 2-D cavity impinging spray. But during the

split interval, the evaporation ratio has a different tendency. For free spray, the evaporation ratio of 2.19 ms ASOI is higher than that of 1.8 ms and 2.39 ms ASOI. There is dense fuel at 2.39 ms ASOI because of the second main injection, which makes the evaporation ratio lower. The split injection interval improves the fuel evaporation process. However, the evaporation ratio of 2-D cavity at 2.39 ms ASOI is higher than that of 2.19 ms ASOI. The effect of split injection interval on the evaporation process has a delay compare with free spray. A probable reason for this is that the marginal injection amount of the second main injection results in an increase in the velocity of the injected fuel mass that is lower than the evaporation rate. Another probable reason is that the spray/wall interaction has a negative effect on the evaporation process. Compare Pre + S100 and Pre + D160_75-25, higher injection pressure and split injection improve the evaporation process.

6.4 COMPARISON OF COMBUSTION CHARACTERISTICS OF FREE SPRAY AND 2-D CAVITY IMPINGING SPRAY

Figure 6.6 presents the distributions for the KL factor and temperature obtained by analyzing the images captured from the high-speed video camera using the two-color pyrometry method. The temperature obtained here is for the soot temperature. Measurements for each injection strategy were performed three times. As the three sets of results for each injection strategy tend to be similar, a single set of results for each injection strategy are presented. The upper and bottom row of images for each injection strategy present the temperature and the KL factor respectively. Except the ignition timing of two injection strategies, other timings are the same with the timing of spray mixture formation process. The impinging spray flame exhibits a high KL factor and low temperature under two injection strategies.

The relative high KL factor locates in the flame tip region, while the relative high temperature does not have a fixed region. The KL factor and temperature at 1.6 ms ASOI

under two injection strategies are very small because of the ignition timing. The temperature of two injection strategies at 1.8 ms ASOI is almost the same. From the images for Pre + D160_75-25, the second main injection flame is evident at 2.8 ms ASOI (EOI). The high KL factors are observed around the flame tip region. The KL factors of Pre + S100 are significantly higher than that of Pre + D160_75-25. It means a high injection pressure can decrease the soot. The KL factor of single-injection strategies first increases and then decreases. However, for split injection strategies, the KL factor first increases from 1.6 ms ASOI to 2.19 ms ASOI. Thereafter, it decreases till the ignition of second main injection and 0.2 ms ASOI after that. It is evident that the split injection has effect on the soot formation.

Figure 6.7 presents the KL factor and OH* chemiluminescence distribution under two injection strategies. In the OH* images, background was represented by the blue color, and OH* chemiluminescence was shown in default jet colormap from Matlab.

The area where the KL factor is rich, while in the same area of OH* images, not much signal is observed. This agrees with the findings from Ref. [141]. The OH* chemiluminescence is observed at the time of 0.8 ms ASOI of Pre + D160_75-25 and 0.9 ms ASOI of Pre + S100, but no KL factor at this timing. The OH* chemiluminescence appears prior to soot formation in free spray flames soot formation begins after ignition during the pre-mixed burn phase [142]. The pre-injection combustion duration of Pre + S100 is from 0.9 ms ASOI to 1.6 ms ASOI, which is shorter than that of Pre + D160_75-25 from 0.8 ms ASOI to 1.8 ms ASOI. And the pre-ignition timing (0.8 ms ASOI) of Pre + D160_75-25 is a little advance than that of Pre + S100 (0.9 ms ASOI). It implies that high injection pressure can promote the combustion.

By the time of 1.5 ms ASOI, the OH* chemiluminescence appears prior to soot formation, which due to the KL factor is too small to detect. The OH* chemiluminescence of Pre + D160_75-25 is stronger than that of Pre + S100. By the time of 1.6 ms ASOI of Pre + S100 and 1.7 ms ASOI of Pre + D160_75-25, the KL factor can be detected.

It is interesting to notice that the KL factor appears a little farther downstream than

the OH* signal from 1.8 ms ASOI to 3.5 ms ASOI of Pre + S100, which may imply that the tip where form soot particle, while the high temperature reaction occurs at the mid-stream area at this moment [141]. And also the KL factor appears farther downstream than the OH* signal from 1.8 ms ASOI to 2.8 ms ASOI of Pre + D160_75-25. The first main injection combustion flame of Pre +D160_75-25 catches up with the pre-injection flame at 2.19 ms ASOI. And by the time of 2.19 ms ASOI, the second main injection of Pre + D160_75-25 has just injected. The second main injection flame can be detected by the time of 2.8 ms ASOI through the KL factor of Pre + D160_75-25. And by the time of 2.8 ms ASOI, the injection has just finished. It implies that there is no interaction between the second main injection fuel and the first main injection combustion.

As time continues and the fuel injection ends, the flame jet begins to move downstream at the time of 4.0 ms ASOI of two injection strategies. The OH* chemiluminescence stays strong at this moment, especially in the downstream, which may indicate that the soot oxidation process involves the participation of OH and the high temperature reactions. This agrees with the findings from Ref. [143].

Figure 6.8 shows the liquid length (LL) and lift off length (LOL) under two injection strategies versus time. Here the liquid length equals the length along the spray axis which starts from nozzle tip to the point where the liquid phase equivalence ratio equals 0.5. Lift-off length defined as the distance between the injector and the upstream most location of the 310 nm light in the images [13]. The LOL of main injection combustion will be stable during the injection. The LL of Pre + S100 at 1.8 ms ASOI and 2.8 ms ASOI is longer than that of LOL. For the split main injection, the LL of Pre + D160_75-25 is longer than that of LOL at 1.8 ms ASOI but shorter than that of LOL at 2.8ms ASOI. As we know, it will generate large soot when LL is longer than LOL, but small soot when LL is shorter than LOL. The gap between LL and LOL of Pre + D160_75-25 at 1.8 ms ASOI is shorter than that of Pre + S100, which means the soot of Pre + D160_75-25 is smaller than that of Pre + S100. The LL of Pre + D160_75-25 is shorter than that of LOL at 2.8ms ASOI, but the LL of Pre + S100 is longer than that of LOL at 2.8 ms ASOI, which leads to small

soot of Pre + D160_75-25.

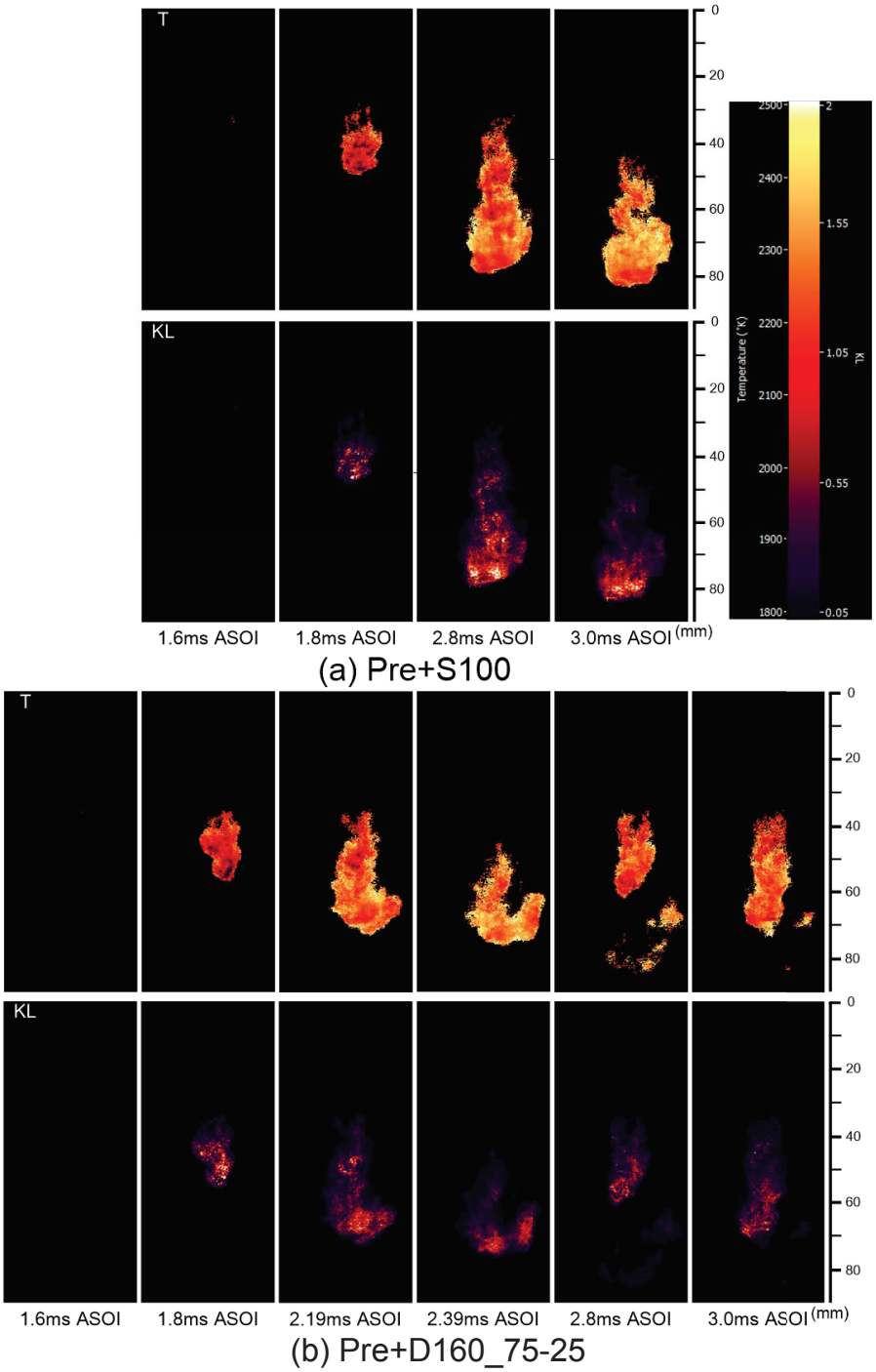

Figure 6.6 Mean temperature and KL factor distribution of free spray

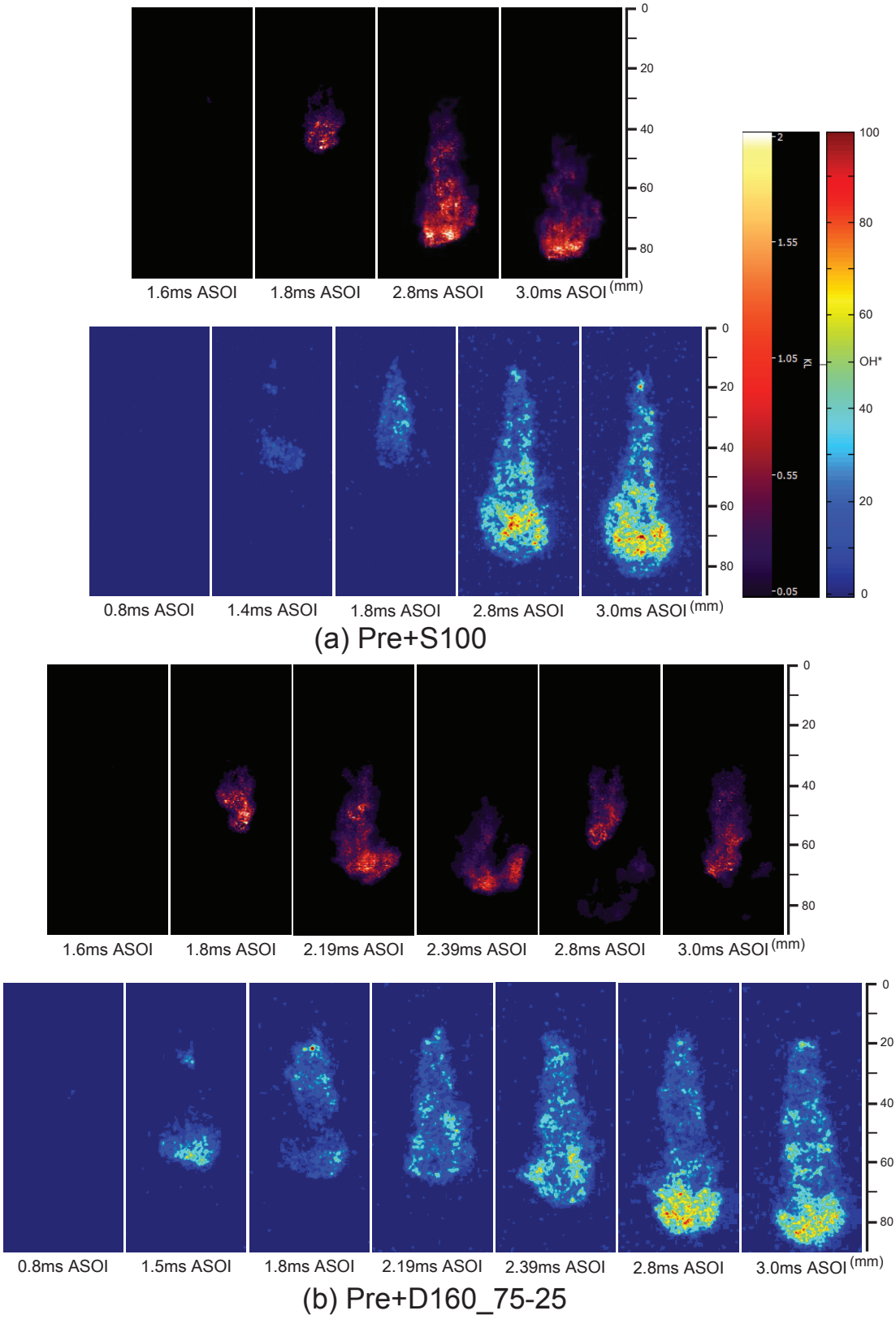

Figure 6.7 KL factor and OH* chemiluminescence distribution

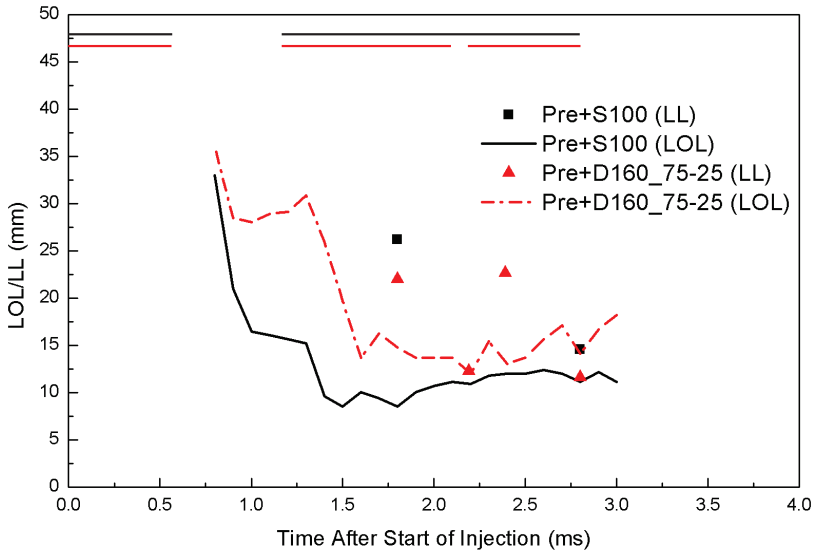

Figure 6.8 The liquid length (LL) and lift off length (LOL) of two injection strategies

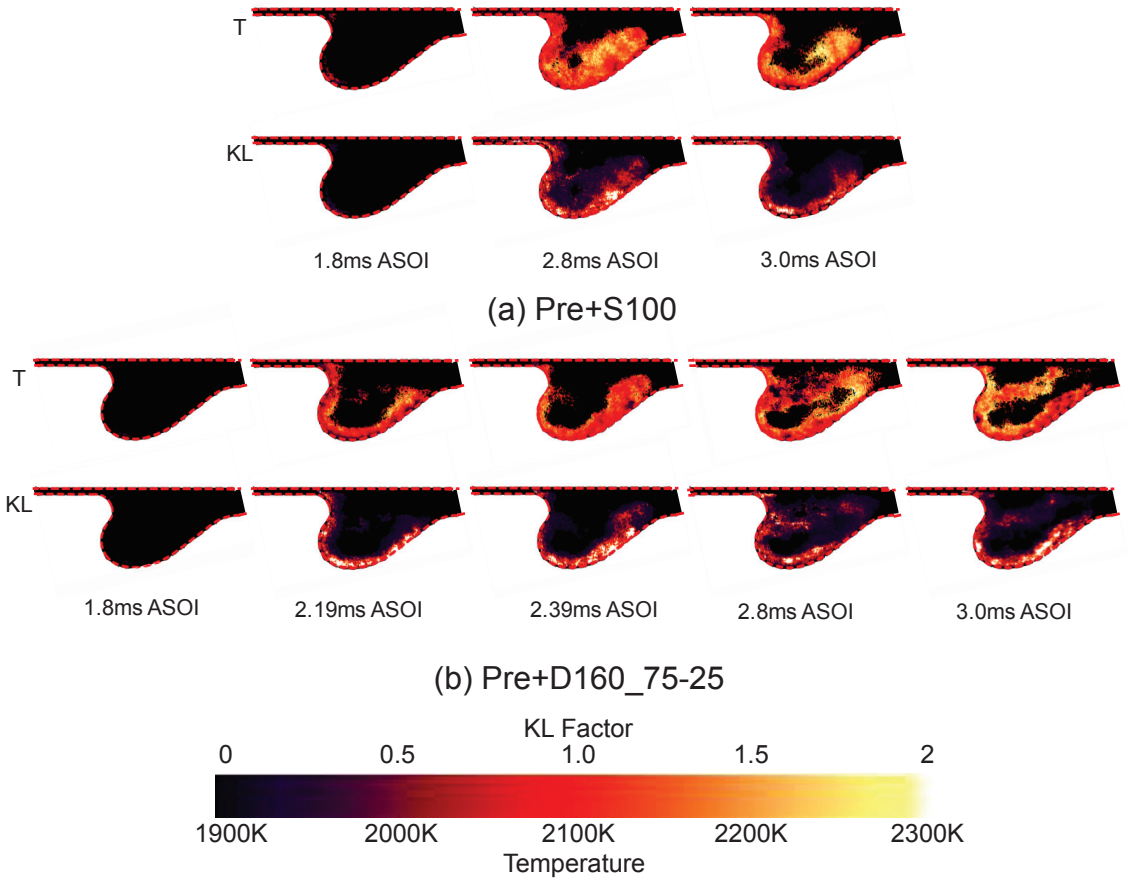

Figure 6.9 Mean temperature and KL factor distribution of impinging spray

Figure 6.9 presents the distributions for the KL factor and temperature obtained by

analyzing the images captured from the high-speed video camera using the two-color pyrometry method. The upper and lower row of images for each injection strategy present the temperature and the KL factor respectively. The timings chosen are the same with that of evaporation condition.

The KL factor for the flame tip region near the cavity wall first increases from 1.8 ms ASOI to EOI, and then decreases from EOI to 0.2 ms AEOI for Pre+S100. From the images of Pre+D160_75-25, the second main injection flame is evident at 2.8 ms ASOI (EOI). The KL factor in that region first increases from 1.8 ms ASOI to 2.39 ms ASOI, then decreases until EOI, and finally increases until 0.2 ms AEOI for Pre + D160_75-25.

In the case of Pre+D160_75-25, as time elapses until 0.2 ms AEOI (3.0 ms), the second main injection fuel almost catches up with the previous fuel, which causes the high KL factor distribution in the flame tip region.

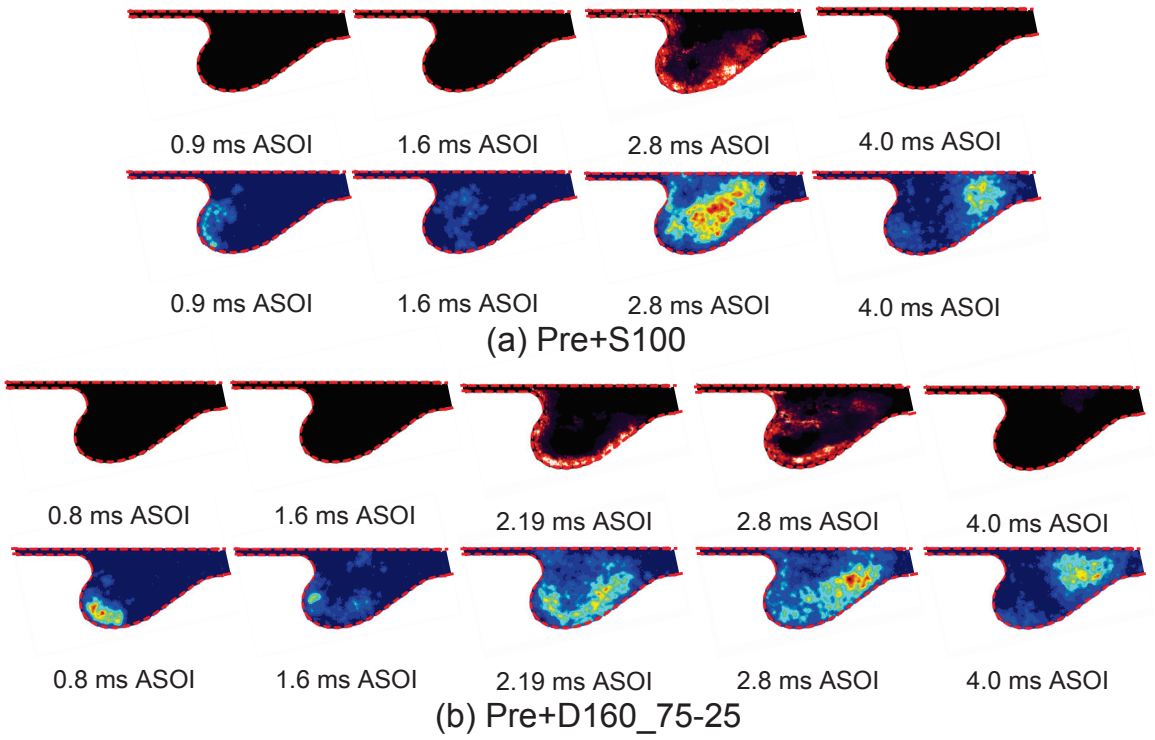

Figure 6.10 KL factor and OH* chemiluminescence distributions

The KL factor and OH* chemiluminescence spatial distribution of 2-D cavity impinging flames under two injection strategies are shown in Figure 6.10. In each figure, the KL factor images which are calculated by applying the two-color method are shown

in the top row; the OH* chemiluminescence images are shown at the bottom. The area where OH* images have strong signal has small KL factor. The high KL factor are observed near the cavity wall region, which means the soot formation happens near the cavity wall region.

The pre-injection ignition timing (0.9 ms ASOI of Pre + S100, 0.8 ms ASOI of Pre + D160_75-25) of 2-D piston cavity impinging flame from OH* chemiluminescence are same with that of free spray. Whereas, the first main injection ignition timing (1.6 ms ASOI of two injection strategies) is a little later than that of free spray (1.5 ms ASOI). The first main injection ignition from OH* chemiluminescence can be detected at the time of 1.6 ms ASOI under two injection strategies, but the first observed KL factor appears at 1.8 ms ASOI. It implies that high injection pressure can promote the combustion. And the pre-injection combustion makes the ambient more comfortable for ignition, which makes the first main injection ignition timing is same both in free spray and 2-D cavity impinging spray for two injection strategies.

The OH* chemiluminescence also appear prior to soot formation in 2-D piston cavity flames, which also agree with the results that soot formation begins after ignition during the pre-mixed burn phase [142]. The local maximum OH* chemiluminescence of Pre + D160_75-25 is weaker than that of Pre + S100 after 2.8 ms ASOI. And the OH* chemiluminescence near the cavity wall is weak, which means low temperature around this area. From the images of Pre + D160_75-25, the second main injection flame is evident at 2.8 ms ASOI (EOI). The KL factor of the flame tip region near the cavity wall first increases from 1.8 ms ASOI to EOI, and then decreases from EOI to 0.2 ms AEOI for Pre + S100. For Pre + D160_75-25, the KL factor in that region, first increases from 1.8 ms to 2.39 ms; then, it decreases as time elapses till EOI, and finally increases as time elapses till 0.2 ms AEOI. For Pre + D160_75-25, as time elapses until 0.2 ms AEOI (3.0 ms), the second main injection fuel almost catches up with the previous fuel, which causes the high KL factor distribution in the flame tip region. According to the shape of OH* and KL factor, the OH* chemiluminescence projected area is larger than that of the KL

factor. In the near TDC region of the flame, there is an obvious part which has OH* chemiluminescence but no KL factor. As time continues and the fuel injection ends, the flame jet begins to move TDC at the time of 4.0 ms ASOI of two injection strategies. The OH* chemiluminescence stays strong at this moment but very small KL factor, which may indicate that the soot oxidation process involves the participation of OH and the high temperature reactions.

Figure 6.11 shows the comparison of integrated KL factor of free and 2-D impinging sprays under Pre + S100. The integrated KL factor of impinging sprays is smaller than that of free spray before 3.1 ms ASOI. It means 2-D cavity has a positive effect to decrease the soot amount for single main injection during this phase. But the integrated KL factor of impinging sprays is higher than that of free after 3.1 ms ASOI. A probable reason is the entrained gas amount in the 2-D cavity is smaller than that of free spray, which makes the soot increases. The evaporation ratio of Pre + S100 under 2-D cavity condition at 2.8 ms ASOI is smaller than that of free spray should also be the reason.

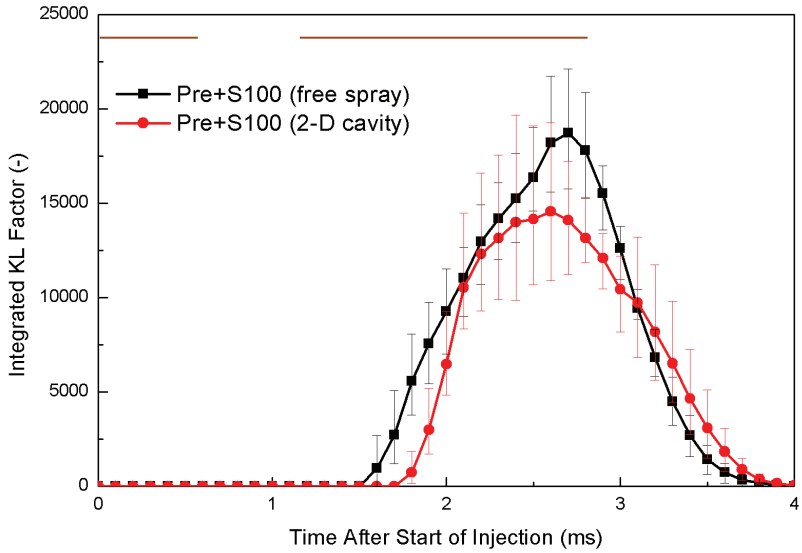

Figure 6.11 Integrated KL factor of Pre + S100 under two injection strategies

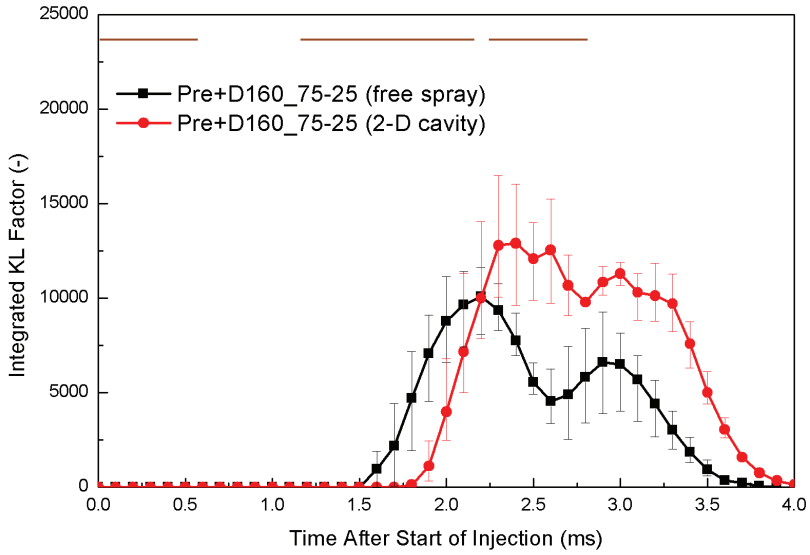

Figure 6.12 Integrated KL factor of Pre + D160_75-25 under two injection strategies

Figure 6.12 shows the comparison of integrated KL factor of free and 2-D impinging sprays under Pre + D160_75-25. The integrated KL factor of impinging sprays is smaller than that of free spray before 2.2ms ASOI. This is because the injected amount of Pre + D160_75-25 is smaller than that of Pre + S100 and the injection pressure of Pre + D160_75-25 is bigger than that of Pre + S100. But the integrated KL factor of Pre + D160_75-25 is bigger than that of Pre + S100 after 2.2 ms ASOI. Because of the spray/wall interaction, large momentum loss after impingement, which makes the second main injection fuel catches up with the previous flame and deteriorates the combustion.

6.5 SUMMARY

This chapter compared the free spray and 2-D cavity impinging spray evaporation and combustion characteristics. A high injection pressure accelerates the evaporation process, would help decrease the soot formation. The effect of injection mass and spray/wall interaction on fuel evaporation is more significant than that of injection pressure. The vapor fuel is mainly distributed at the impingement point and cavity wall. The spray/wall interaction has a negative effect on the evaporation process. KL factor

appears farther downstream than the OH* signal. There is no interaction between the second main injection fuel and the first main injection combustion under free spray.

The LOL of main injection combustion will be stable during the injection. The second main injection fuel almost catches up with the previous fuel, which causes the high KL factor distribution in the flame tip region. The area where OH* images have strong signal has small KL factor. The high KL factor are observed near the cavity wall region, which means the soot formation happens near the cavity wall region. The pre-injection ignition timing of 2-D piston cavity impinging flame from OH* chemiluminescence are same with that of free spray. Whereas, the first main injection ignition timing is a little later than that of free spray. The OH* chemiluminescence projected area is larger than that of the KL factor. In the near TDC region of the flame, there is an obvious part which has OH* chemiluminescence but no KL factor. The 2-D cavity has a positive effect to decrease the soot amount for single main injection, but negative effect to decrease the soot amount for split main injection.

CHAPTER 7 EFFECTS OF PRE-INJECTION AND LOW OXYGEN CONCENTRATION ON THE DIESEL EVAPORATION AND COMBUSTION CHARACTERISTICS

7.1 INTRODUCTION

Recently, owing to the consensus regarding improvement in the trade-offs between PM and NOx emissions, multiple injection strategies have been explored [144-147]. Cheng et al. [148] studied the effect of multiple injection strategies on the diesel fuel combustion process. With the advancement of pilot injection timing, NO_x and soot emissions have reduced. However, HC and CO emissions have increased. By retarding post injection timing, the NO_x emissions are reduced, whereas soot emission at first increases and then decreases. Nishida et al. [149] and Yang et al. [129] observed that the spray tip of the second injection pulse catches up and passes the first one when the fuel quantity injected by the second pulse is significantly high and the dwell between the two injection pulses is highly marginal. Seo et al. [150] determined that a split injection can increase the thermal efficiency and the rate of fuel consumption without optimization. However, it can result in poor combustion characteristics such as knocking, incomplete combustion, and soot emissions. In this section, the effect of pre-injection on the diesel evaporation and combustion characteristics will be discussed.

Jing et al. [151] investigated the effects of ambient temperature and oxygen concentration on diesel spray combustion and found that more mixing is required to achieve complete combustion for low ambient oxygen concentration conditions. Zhang et al. [152] have a research on the effect of the ambient temperature and oxygen concentration in droplet combustion. The results reveal that ambient temperature and oxygen concentration have a great influence on burning rates and ignition delay times.

Zhang et al. [153] studied the effects of ambient oxygen concentration on biodiesel and diesel spray combustion under simulated engine conditions. The 18% ambient O_2 condition works better for biodiesel than diesel in reducing soot luminosity. With 12% O_2, diesel combustion is significantly degraded. Azetsu et al. [154] investigated the effects of ambient O_2 concentration and pressure on the combustion characteristics of diesel spray. It is confirmed that O_2 concentration is the dominant factor affecting both the ignition delay and combustion period. The volumetric fraction of O_2 in ambient air has a significant effect on flame temperature and NO_x emission. Kuribayashi et al. [155] studied the effects of ambient oxygen concentration on soot processes in diesel spray flame. Comparing 21% and 15% ambient O_2 concentration, a consistent general trend showed that the soot is formed earlier in the upstream region and disappears earlier due to faster oxidation for higher O_2 concentration.

7.2 EXPERIMENTAL CONDITIONS

In this chapter, new injection strategies were adopted. The injection strategies of Pre + S100, S100, Pre + D160_75-25 and D160_75-25 were chosen to investigate the effect of pre-injection on the combustion characteristics. The 15% oxygen concentration was chosen to compare with that of 21% oxygen concentration.

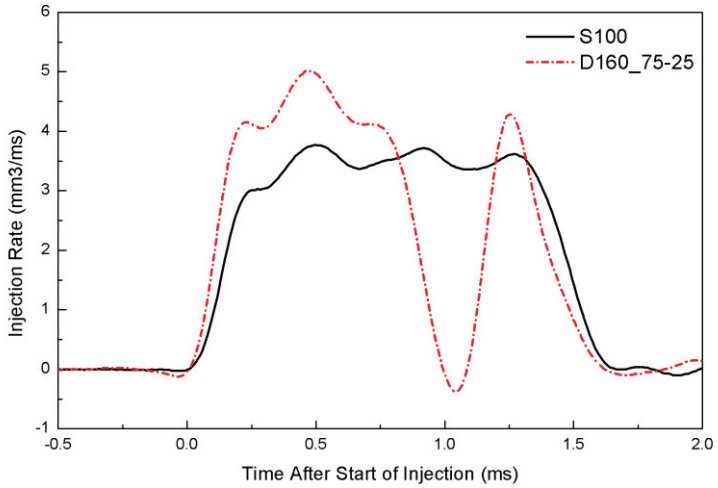

Figure 7.1 Injection rates of S100 and D160_75-25

Figure 7.1 shows the injection rate of S100 and D160_75-25. Considering S100 injection strategy as the base condition, the EOI of the high pressure split injection strategy (D160_75-25) was similar with that of the base one. The EOI timing of two injection strategies were approximately 1.62 ms ASOI. The total volume of main injection is same with that of Pre + S100 and Pre +D160_75-25.

7.3 COMBUSTION CHARACTERISTICS (21% O_2 WITHOUT PRE-INJECTION)

Figure 7.2 shows the mean temperature and KL factor distributions of impinging spray without pre-injection (S100 and D160_75-25). The O_2 concentration in the ambient gas is 21%. The timing chosen for S100 is 1.2 ms ASOI (ignition timing), 1.66 ms ASOI (EOI) and 1.86 ms ASOI (0.2 ms ASOI) from left to right. The timing chosen for D160_75-25 is 0.7 ms ASOI (ignition timing), 1.0 ms ASOI (start of second main injection), 1.2 ms ASOI (0.2 ms after start of second main injection), 1.66 ms ASOI (EOI) and 1.86 ms ASOI (0.2 ms ASOI) from left to right.

The relatively high KL factor and high temperature appear in the proximity of the impingement point region and at the deep groove region of the cavity rather than in the proximity of the spray tip region. This is because of the spray/wall interaction, the large momentum loss after impingement and droplet stagnation at those regions. Thereafter, high dense droplets generate high soot on those regions, which is in accordance with the results of with pre-injection strategies.

The ignition delay of D160_75-25 is shorter than that of S100. Comparing with the results of pre-injection strategies, the pre-injection can decrease the ignition delay, and weaken the effect of injection pressure. The KL factor of two injection strategies increases from ignition timing to 0.2 ms AEOI. It implies that the combustion process of main injection without pre-injection is longer than that with pre-injection.

Figure 7.3 illustrates the integrated KL factor ASOI of impinging spray under the

two injection strategies. The integrated KL factor of D160_75-25 is bigger than that of S100 before 1.5 ms ASOI. The D160_75-25 ignited advance than that of S100 which cause the integrated KL factor increases first. The KL factor of D160_75-25 decreases from 1.3 ms ASOI to 1.5 ms ASOI. This is because this period is the late combustion of first main injection. Then the integrated KL factor of D160_75-25 is smaller than that of S100 from 1.5 ms to 1.9 ms ASOI. This implies that the split injection interval can reduce the soot formation. Then the integrated KL factor of D160_75-25 is bigger than that of S100 after 1.9 ms ASOI. The second main injection flame causes more soot this period for the split injection. The late combustion of S100 and D160_75-25 is after 2.0 ms ASOI and 2.1 ms ASOI, respectively. The gradient of soot oxidation domain process of D160_75-25 is higher than that of S100. It implies that the split injection can accelerate the soot oxidation process.

The mean temperature ASOI of the two injection strategies is presented in Figure 7.4. The mean temperature of D160_75-25 is higher than that of Pre+S100 at first, and then becomes lower. The mean temperature of S100 increases first and then decreases. However, for D160_75-25, the mean temperature decreases during the combustion process, which is because of the late combustion of first main injection flame.

Figure 7.5 presents the integrated KL factor of S100 and Pre + S100 to investigate the effect of pre-injection on the single main injection. The ignition delay of main injection of S100 is 1.167 ms, but just 0.46 ms for Pre + S100. The pre-injection decreases the ignition delay. The pre-injection combustion increases the ambient temperature and pressure and makes the main combustion more easily. The integrated KL factor of S100 is bigger than that of Pre + S100 before 2.0 ms ASOI. The S100 ignited advance than that of Pre + S100 which cause the integrated KL factor increases first. Then the KL factor of Pre + S100 is higher than that of S100, which is because of the pre-injection combustion.

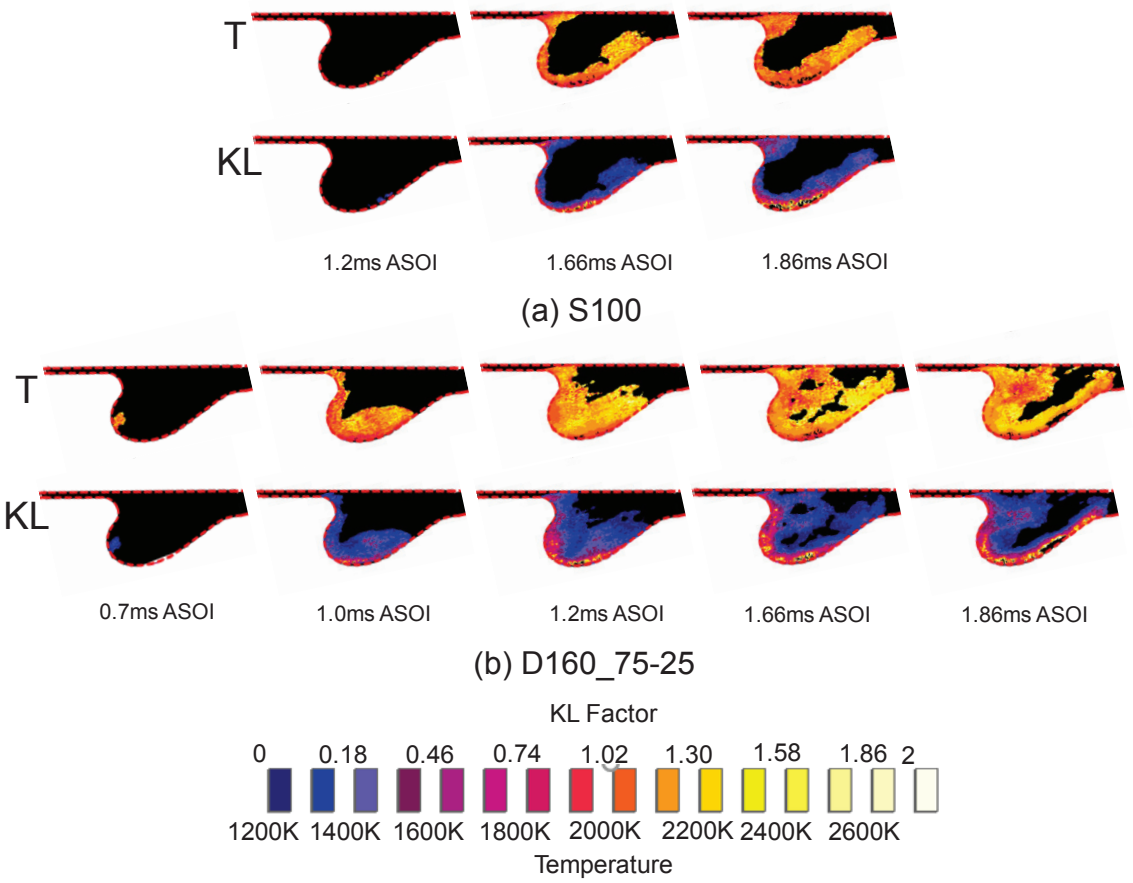

Figure 7.2 Mean temperature and KL factor distributions under two injection strategies

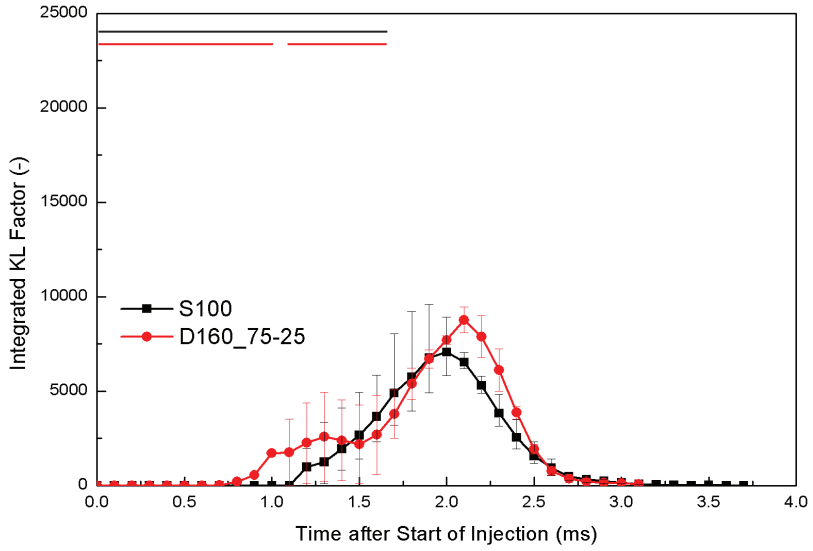

Figure 7.3 Integrated KL factor under without pre-injection condition

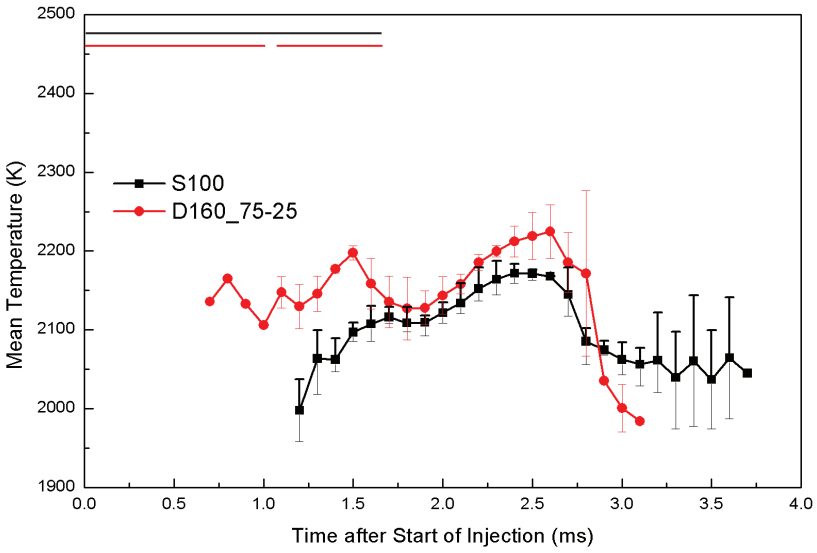

Figure 7.4 Mean temperature under without pre-injection condition

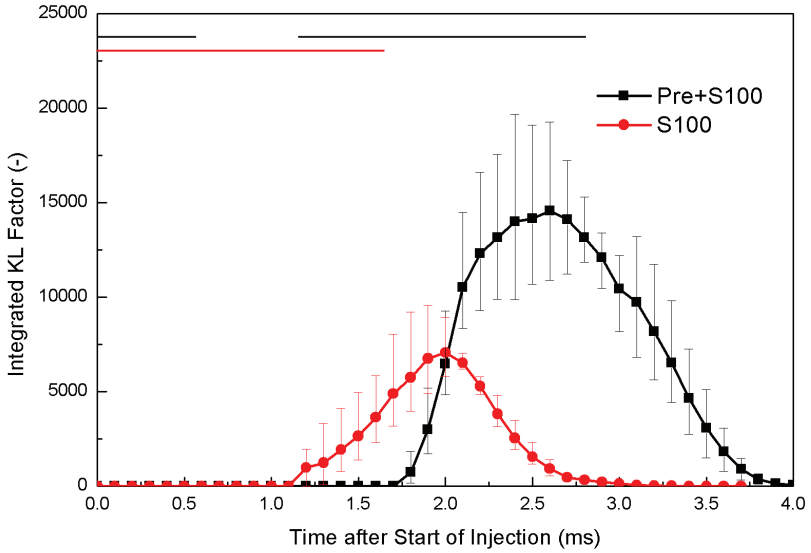

Figure 7.5 Comparison of S100 and Pre + S100 on the integrated KL factor

Figure 7.6 presents the integrated KL factor of D160_75-25 and Pre + D160_75-25 to investigate the effect of pre-injection on the split main injection. It shows the tendency that the pre-injection decreases the ignition delay of the main injection combustion. The integrated KL factor of D160_75-25 is bigger than that of Pre + D160_75-25 before 2.2 ms ASOI. The timing when the integrated KL factor of S100 becomes smaller than that of Pre + S100 and the timing when the integrated KL factor of D160_75-25 becomes

smaller than that of Pre + D160_75-25 are the maximum integrated KL factor timing. And the split injection interval also has an effect on the integrated KL factor from 1.3 ms to 1.5 ms ASOI under D160_75-25. However, the effect degree on the D160_75-25 is not huge than that of Pre + D160_75-25.

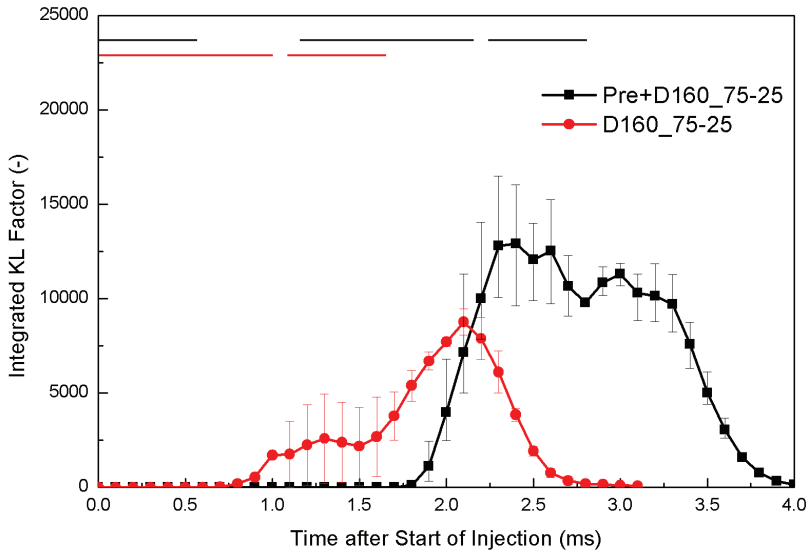

Figure 7.6 Comparison of D160_75-25 and Pre + D160_75-25 on the integrated KL factor

7.4 COMBUSTION CHARACTERISTICS (15% O_2 WITH PRE-INJECTION)

This part will show the effect of low oxygen concentration on the combustion characteristics. Figure 7.7 shows the mean temperature and KL factor distributions of impinging spray (Pre + S100 and Pre + D160_75-25) conditions. The O_2 concentration in the ambient gas is 15%. The timing chosen for Pre + S100 is 1.9 ms ASOI (ignition timing), 2.8 ms ASOI (EOI), 3.0 ms ASOI (0.2 ms AEOI) and 4.0 ms ASOI (1.2 ms AEOI) from left to right. For D160_75-25, the ignition timing is also 1.9 ms ASOI, 2.19 ms ASOI (around the start of second main injection) and the rest are the same.

For Pre + D160_75-25, the relatively high KL factor and high temperature appear at

the deep groove region of the cavity rather than in the proximity of the spray tip region. However, for Pre + S100, the relatively high KL factor appears not only at the deep groove region of the cavity but also at the spray tip region. The ignition delay for both two injection strategies are 1.9 ms ASOI. The pre-injection combustion has a positive effect on the main injection ignition.

The KL factor distribution of Pre + D160_75-25 is leaner than that of Pre + S100 at EOI and 0.2 ms AEOI. But the KL factor distribution of Pre + D160_75-25 is richer than that of Pre + S100 at 4.0 ms ASOI. The soot evaluation process of Pre + D160_75-25 is longer than that of Pre + S100. Low oxygen concentration has a complex effect on the soot evaluation of single main injection and split main injection.

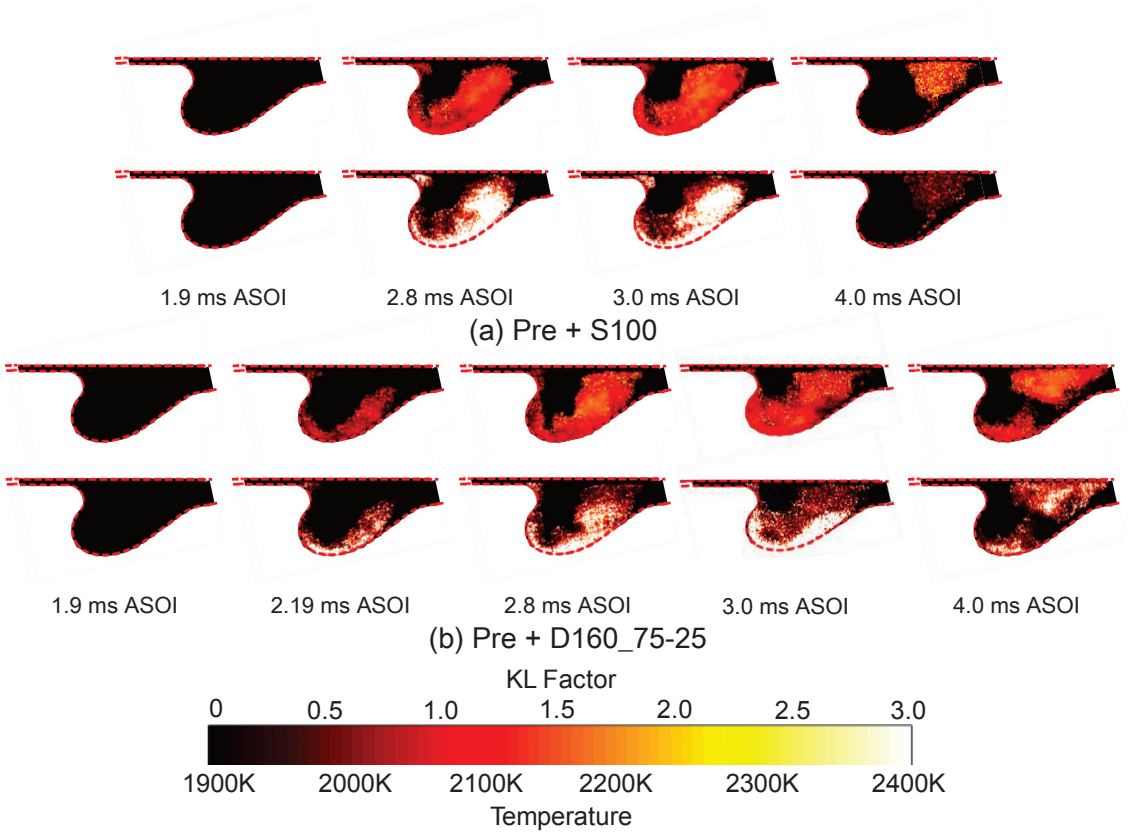

Figure 7.7 Mean temperature and KL factor distributions under two injection strategies

Figure 7.8 illustrates the integrated KL factor ASOI of impinging spray under the two injection strategies. The integrated KL factor of Pre + D160_75-25 is almost bigger than that of Pre + S100 during the soot evaluation process. Low oxygen concentration has

a negative effect on the soot. As the oxygen concentration is low, there is no enough air entrainment for the split injection. But the split injection also can decrease the soot formation during the split injection interval. Figure 7.9 shows the mean temperature of impinging spray under two injection strategies. It can be seen that the mean temperature of two injection strategies are almost same. Expect the mean temperature of Pre + D160_75-25 is lower than that of Pre + S100 as the split injection interval influence.

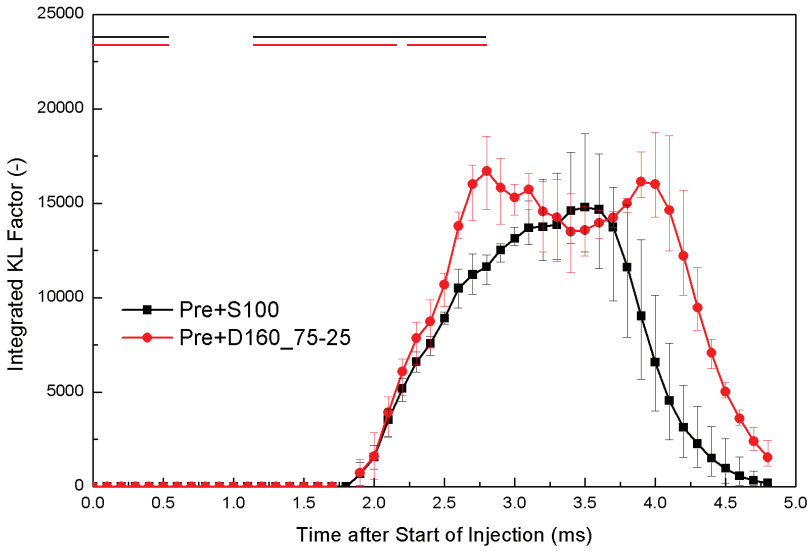

Figure 7.8 Integrated KL under two injection strategies

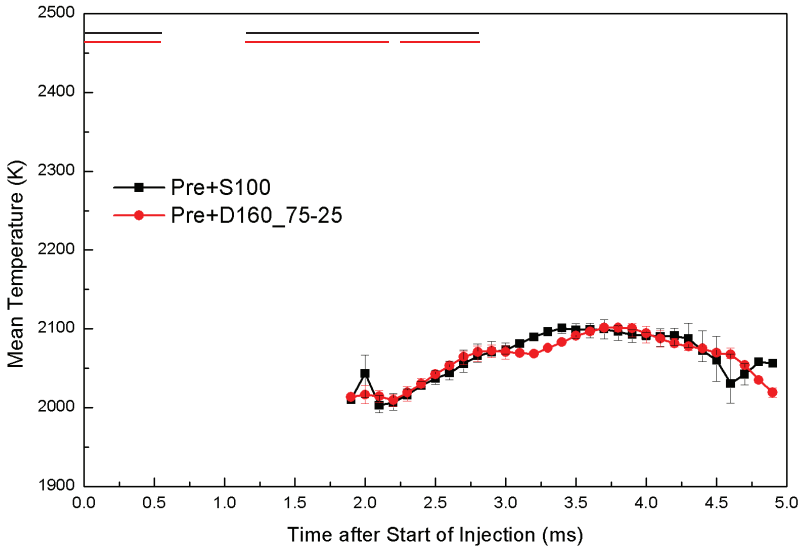

Figure 7.9 Mean temperature under two injection strategies

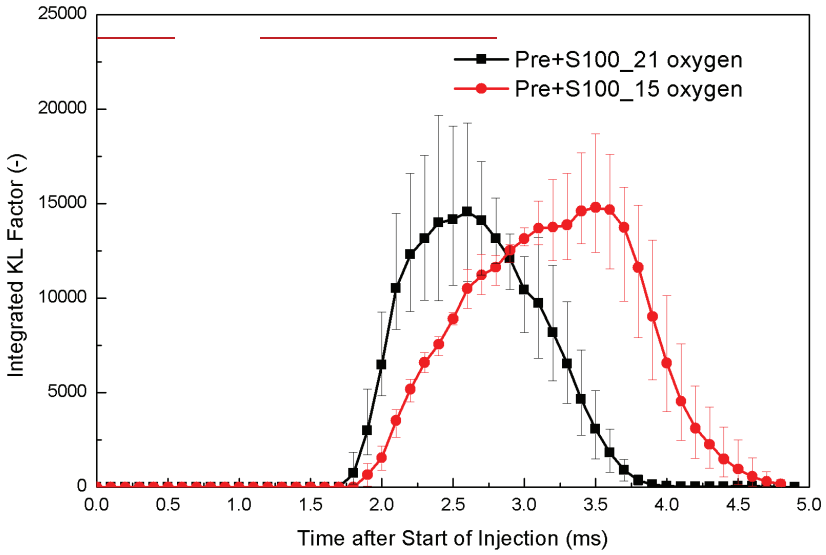

Figure 7.10 Comparison of S100 and Pre + S100 on the integrated KL factor

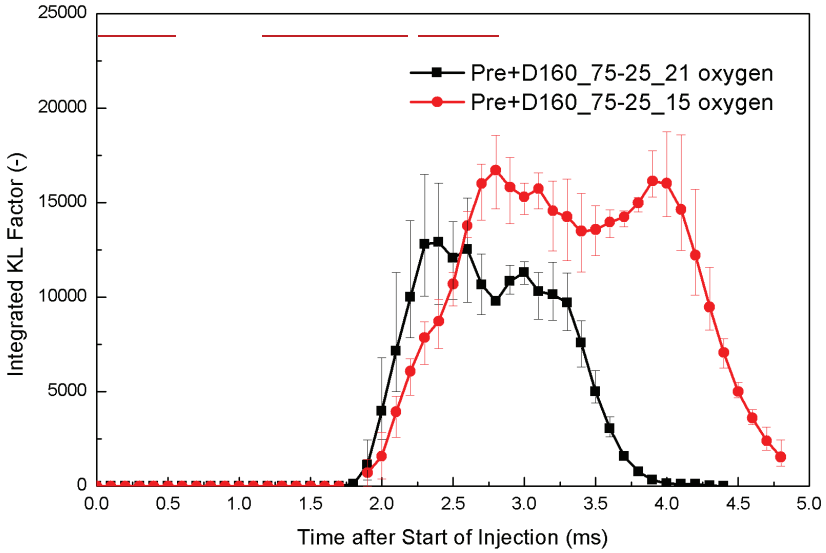

Figure 7.11 Comparison of D160_75-25 and Pre + D160_75-25 on the integrated KL factor

Figure 7.10 presents the integrated KL factor of Pre + S100 under 21% O_2 and 15% O_2 two oxygen concentrations to investigate the effect of low oxygen concentration on the single main injection. The low oxygen concentration delays the ignition delay. And the low oxygen concentration will delay the whole combustion process. But the integrated KL factor is almost at the same level.

Figure 7.11 presents the integrated KL factor of Pre + D160_75-25 under 21% O_2 and 15% O_2 two oxygen concentrations to investigate the effect of low oxygen concentration on the split main injection. The low oxygen concentration delays the ignition delay. And the low oxygen concentration will delay the whole combustion process. But the integrated KL factor of 15% O_2 is bigger than that of 21% O_2 after 2.6 ms ASOI. The low oxygen concentration worsens the combustion process.

7.5 COMBUSTION CHARACTERISTICS (15% O_2 WITHOUT PRE-INJECTION)

Figure 7.12 shows the mean temperature and KL factor distributions of impinging spray without pre-injection (S100 and D160_75-25) conditions. The O_2 concentration in the ambient gas is 15%. The timing chosen for S100 is 1.2 ms ASOI (ignition timing), 1.66 ms ASOI (EOI) and 1.86 ms ASOI (0.2 ms AEOI) from left to right. For D160_75-25, the ignition timing is 1.3 ms ASOI, while the rest are the same.

The ignition delays of S100 are the same under two O_2 concentration conditions. However, for D160_75-25, it is longer for low O_2 concentration. The air entrainment space of D160_75-25 is smaller than that of S100, and the O_2 concentration decreases, which makes the ignition delay longer.

Moreover, the KL factor and temperature also become bigger and higher from the ignition timing to the 0.2 ms ASOI, which is same with the results of Figure 7.2. It can be seen that the KL factor of D160_75-25 is obviously smaller than that of S100 during this period. Furthermore, the mean temperature of D160_75-25 is lower than that of S100 during this period.

Figure 7.13 illustrates the integrated KL factor ASOI of impinging spray under the two injection strategies. The KL factor of D160_75-25 is smaller than that of S100 before 2.4 ms ASOI. Thereafter, the second main injection fuel catches up with the first main injection flame and deteriorates the combustion. The timing that the second main injection

fuel deteriorates the combustion of 15% O_2 is late than that of 21% O_2. The combustion duration of 15% O_2 is longer than that of 21% O_2 because of the low O_2 concentration. The KL factor of 15% O_2 is bigger than that of 21% O_2. It implies that the low O_2 concentration worsen the combustion.

Figure 7.14 illustrates the mean temperature of impinging spray flame under two injection strategies. The tendency of S100 and D160_75-25 increases first and then decreases, which is similar to the results of 21% O_2. The timing for the late combustion of first main injection is 1.7 ms ASOI, which is almost the same with that of 21% O_2 (1.6 ms ASOI). Even the ignition delay of 21% O_2 is shorter than that of 15% O_2, but it does not have significant effect on the late combustion timing of first main injection. Comparing the results, there is a 100 K drop in the mean temperature due to lower oxygen concentration.

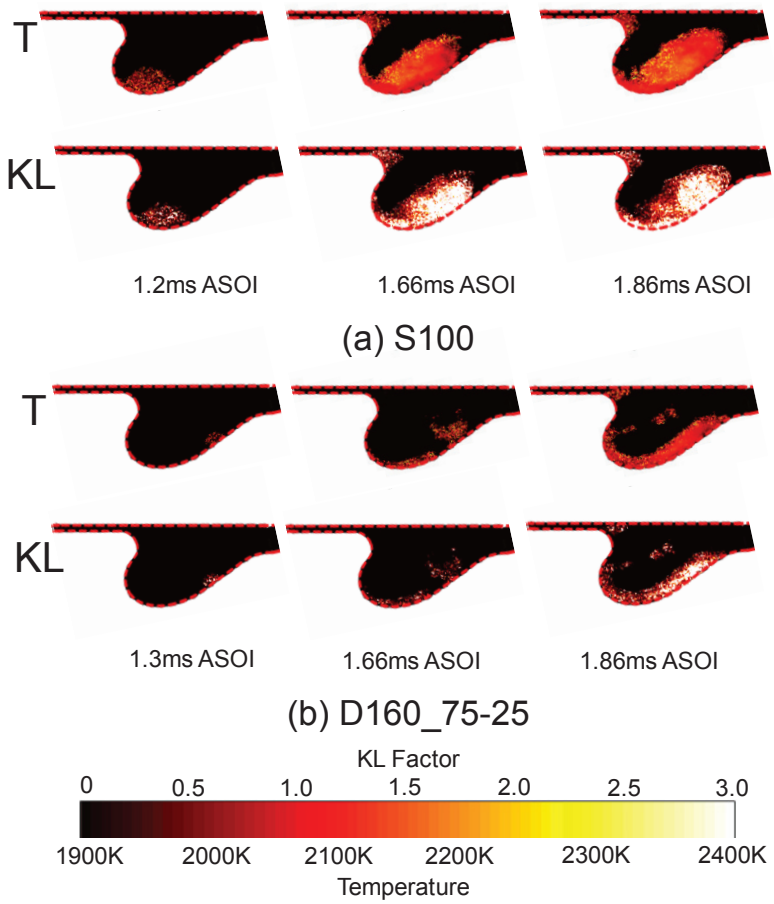

Figure 7.12 Mean temperature and KL factor distributions of impinging spray

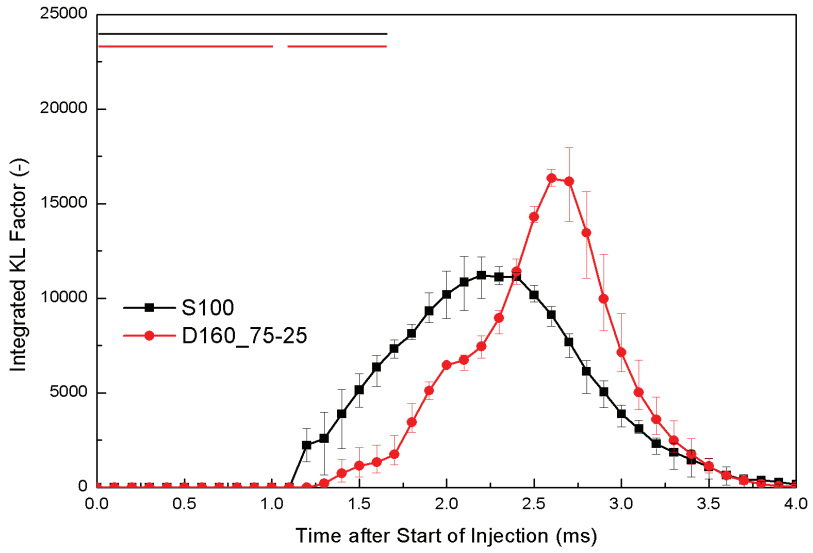

Figure 7.13 Integrated KL factor of impinging spray flame under two injection strategies

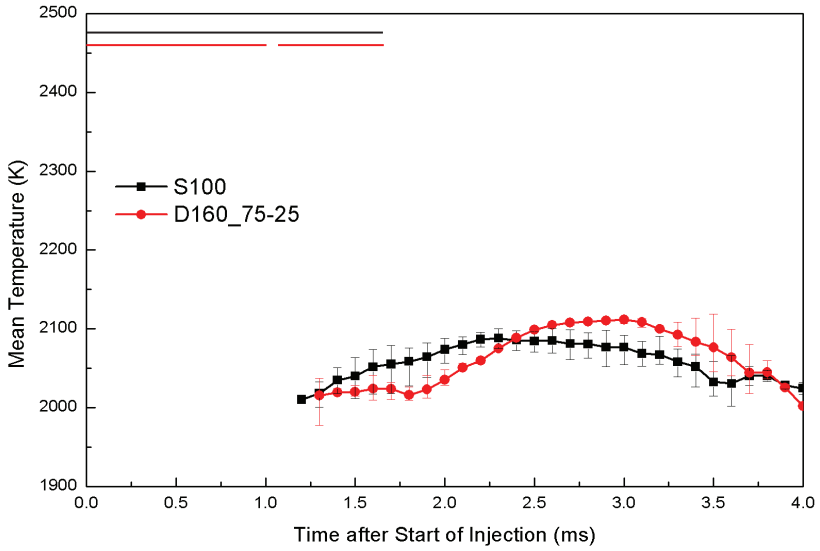

Figure 7.14 Mean temperature of impinging spray flame under two injection strategies

Figure 7.15 presents the integrated KL factor of S100 and Pre + S100 to investigate the effect of pre-injection on the single main injection. The ignition delay of main injection of S100 is 1.2 ms, but just 0.67 ms for Pre + S100. The pre-injection decreases the ignition delay. The pre-injection combustion increases the ambient temperature and pressure and makes the main combustion more easily. The integrated KL factor of S100

is bigger than that of Pre + S100 before 2.5 ms ASOI. The S100 ignited advance than that of Pre + S100 which cause the integrated KL factor increases first. Then the KL factor of Pre + S100 is higher than that of S100, which is because of the pre-injection.

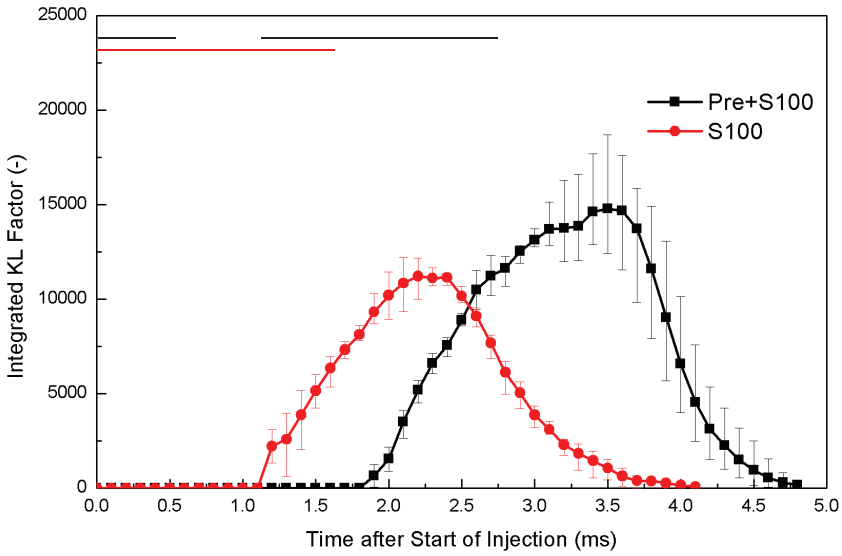

Figure 7.15 Comparison of S100 and Pre + S100 on the integrated KL factor

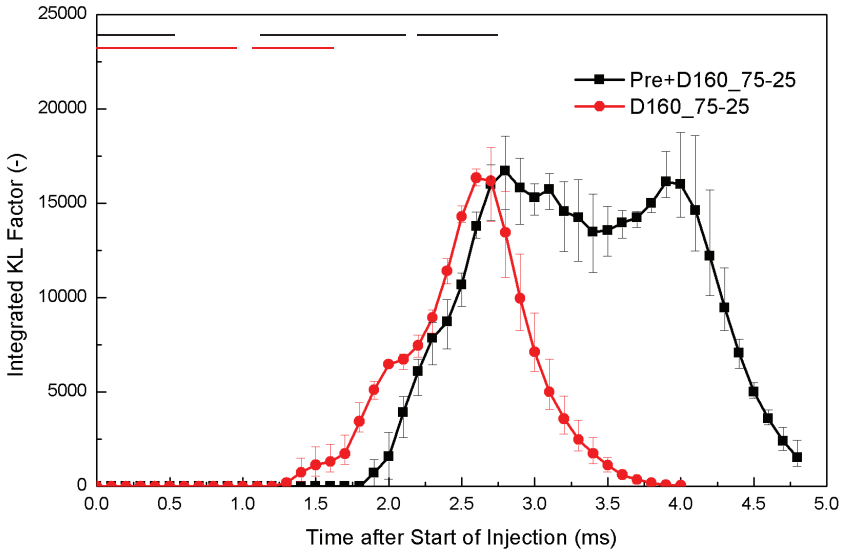

Figure 7.16 Comparison of D160_75-25 and Pre + D160_75-25 on the integrated KL factor

Figure 7.16 presents the integrated KL factor of D160_75-25 and Pre + D160_75-25 to investigate the effect of pre-injection on the split main injection. It shows same

tendency with Figure 7.15 that the pre-injection decreases the ignition delay of the main injection combustion. The integrated KL factor of D160_75-25 is bigger than that of Pre + D160_75-25 before 2.7 ms ASOI. The timing when the integrated KL factor of S100 becomes smaller than that of Pre + S100 and the timing when the integrated KL factor of D160_75-25 becomes smaller than that of Pre + D160_75-25 are 0.1 ms after the maximum integrated KL factor timing. The low oxygen concentration delays this timing. The split injection interval has a significant effect to decrease the integrated KL factor from 3.1 ms to 3.4 ms ASOI under Pre + D160_75-25. However, there is no effect to decrease the integrated KL factor under Pre + D160_75-25.

7.6 IGNITION DELAY

Figure 7.17 shows the ignition delay of all the conditions. The red and green columns indicate the main injection of S100 and D160_75-25 respectively. The ignition delay defined in this part is the timing when KL factor can be observed.

Comparing the results of free spray and 2-D cavity impinging spray, it can be seen that the ignition delay becomes longer in the 2-D cavity due to the lean air in it. Moreover, the pre-injection can decrease the ignition delay of main injection. Because the pre-injection combustion increases the air temperature, thereby making it easier to be ignited for the main injection. For ignition delay of without pre-injection conditions, low O_2 concentration has a significant effect on the D160_75-25, which is owing to two factors: (1) the ambient air mass in the 2-D cavity is small; (2) the ambient air entrainment space of D160_75-25 is narrow than that of S100 through the KL factor images. The pre-injection also has a significant effect on the ignition delay not only for the single main injection but also split main injection under low oxygen concentration.

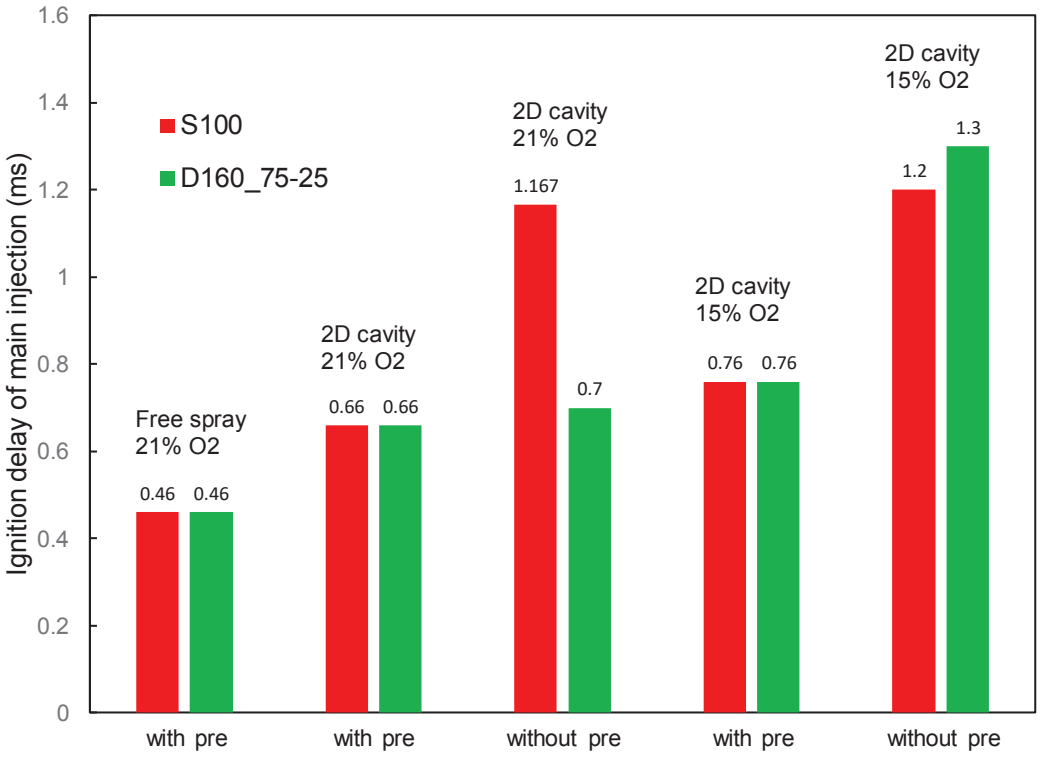

Figure 7.17 Ignition delay of all the conditions

7.7 SUMMARY

This chapter investigated the effect of pre-injection and low oxygen concentration on the combustion characteristics. The combustion process of main injection without pre-injection is longer than that with pre-injection. The split injection can accelerate the soot oxidation process. The pre-injection combustion increases the ambient temperature and pressure and makes the main combustion more easily. The pre-injection combustion has a positive effect on the main injection ignition. The pre-injection combustion increases the ambient temperature and pressure and makes the main combustion more easily.

Low oxygen concentration has a complex effect on the soot evaluation of single main injection and split main injection. Low oxygen concentration has a negative effect on the combustion. But the split injection also can decrease the soot formation during the split injection interval. The low oxygen concentration delays the ignition delay. And the low

oxygen concentration will delay the whole combustion process. The timing that the second main injection fuel deteriorates the combustion of 15% O_2 is late than that of 21% O_2. The combustion duration of 15% O_2 is longer than that of 21% O_2 because of the low O_2 concentration. There is a 100 K drop in the mean temperature due to lower oxygen concentration. For ignition delay of without pre-injection conditions, low O_2 concentration has a significant effect on the D160_75-25. The pre-injection also has a significant effect on the ignition delay not only for the single main injection but also split main injection under low oxygen concentration.

CHAPTER 8 CONCLUSIONS

This dissertation work is aimed at the clarifying the effects of impingement and multiple injection on mixture formation process, combustion and soot emission characteristics of D.I. Diesel spray. The spray mixture formation process was investigated using the Mie scattering technique and LAS technique to acquire the qualitative and quantitative information on the characteristics of free spray and 2-D cavity impinging spray. The combustion behaviors were investigated by applying the two-color method and the OH* chemiluminescence recording system. In this investigation, firstly three kinds of injection amounts (0.27, 0.89 and 2.97 mg) and three kinds of injection pressures (100, 150 and 170 MPa) were selected to investigate the effect of small injection amount on the evaporation and combustion characteristics of free spray; secondly three kinds of split injection strategies (Pre + S100, Pre + D160_50-50 and Pre + D160_75-25) were adopted to check the effect of split injection on the evaporation and combustion characteristics of free spray and 2-D cavity impinging spray; thirdly the effect of pre-injection (S100, D160_50-50 and D160_75-25) and low oxygen (15% O_2) on the combustion characteristics of 2-D cavity impinging spray were also investigated. The general conclusions will be introduced gradually in this chapter.

8.1 MAIN FINDINGS OF THIS STUDY

In Chapter 1, the significance of this search subject was firstly introduced and a review on characterization of diesel spray flame evolution under free and 2-D impinging condition, multiple injection spray and its combustion in diesel engines, and optical diagnostics for measurements of spray characteristics and flame behaviors was made.

In Chapter 2, the experimental apparatus such as Mie scattering, LAS technique, two color method and OH* chemiluminescence system. And the Specification of 2-D cavity and the Egg-shaped Mazda Skyactiv-D cavity were introduced briefly. The principle of

LAS technique and the calibration of two color method were introduced.

The tracer LAS technique for diesel spray was different with the traditional one, in this study, it is modified. The blend fuel with 2.5 volumetric percentage of α-MN and 97.5 volumetric percentage of n-tridecane was adopted.

In Chapter 3, the evaporation and combustion characteristics of small injection amount were investigated. The evaporation characteristics were investigated by the tracer LAS technique and the combustion characteristics were analyzed by the two-color method. The investigation was aimed to clarify the effect of small injection amount (0.27 mg) on the fuel evaporation and combustion processes. It has been found that, firstly, the smaller injection amount gives the shorter time to achieve stoichiometric vapor phase, the leaner air-fuel mixture and the shorter spray tip penetration under same injection pressure and same ambient conditions. The effect of injection pressure shows that the spray tip penetration becomes longer when the injection pressure decreases at the small injection amount (0.27 mg). The volume of the flame and the KL factor intensity increase when the injection amount increases. It's a significant way to reduce soot formation with increasing the injection amount. The time from ignition to combustion peak is shorter under the smaller injection amount condition. And the mean flame temperature also decreases as the injection amount decreases. Consequently, it's an efficient way to reduce the soot formation by adopting small injection amount. It implies that it is an efficient way to reduce the soot formation by adopting the multiple injection strategy.

In Chapter 4, the free spray experiments were carried out to observe the fuel non-evaporation, evaporation, and combustion characteristics. The non-evaporation processes applied the Mie scattering method under three injection strategies (Pre + S100, Pre + S160, and Pre + D160_75-25). The results reveal that the split injection provides much more ambient gas amount, which improves the spray breakup and atomization process under the non-evaporation condition. Split injection gives the fuel more momentum to penetrate quickly. Split injection can make the vapor phase more homogeneous and make the soot distribution more homogeneous. Split injection can enhance the combustion and decrease

the soot emissions. Split injection has a positive effect on the degree of homogeneity of KL versus temperature in the whole flame region. The soot evaluation process finishes at the same time when the injection strategies have the same SOI and EOI.

In Chapter 5, the comparison of the evaporation and combustion characteristics of 2-D cavity impinging spray were investigated under three injection strategies (Pre + S100, Pre + D160_50-50 and Pre + D160_75-25). For evaporation process, the vapor distribution of the split main injection is significantly more homogeneous than that of the single main injection at the EOI. It is observed that the fuel of the second main injection of the split main injection has already caught up with the previous fuel at the EOI in the case of Pre + D160_50-50. The spray–wall interaction has a significant effect on the high density droplet location. For combustion process, the second main injection fuel of the split main injection almost catches up with the previous fuel, which causes the high KL factor distribution in the flame tip region in the case of Pre + D160_50-50. The pre-injection combustion can significantly decrease the main injection ignition delay and then improve the main injection combustion. The split injection can reduce the soot formation and accelerate the soot oxidation process. Increases the split injection interval has a positive effective method to reduce the soot.

In Chapter 6, the free spray and 2-D cavity impinging spray evaporation and combustion characteristics under two injection strategies (Pre + S100, Pre + D160_75-25) were compared. There is no interaction between the second main injection fuel and the first main injection combustion under free spray. The LOL of main injection combustion will be stable during the injection. The second main injection fuel almost catches up with the previous fuel, which causes the high KL factor distribution in the flame tip region under 2-D cavity impinging spray. The pre-injection ignition timing of 2-D piston cavity impinging flame from OH* chemiluminescence are same with that of free spray. In the near TDC region of the flame, there is an obvious part which has OH* chemiluminescence but no KL factor. The 2-D cavity has a positive effect to decrease the soot amount for single main injection, but negative effect to decrease the soot amount for

split main injection.

In Chapter 7, the effect of pre-injection and low oxygen concentration on the combustion characteristics were investigated. The injection strategies adopted here are S100, D160_75-25, Pre + S100 and Pre + D160_75-25. The combustion process of main injection without pre-injection is longer than that with pre-injection. The split injection can accelerate the soot oxidation process. The pre-injection combustion has a positive effect on the main injection ignition. Low oxygen concentration has a complex effect on the soot evaluation of single main injection and split main injection. Low oxygen concentration has a negative effect on the combustion. But the split injection also can decrease the soot formation during the split injection interval. The low oxygen concentration delays the ignition delay. And the low oxygen concentration will delay the whole combustion process. There is a 100 K drop in the mean temperature due to lower oxygen concentration. For ignition delay of without pre-injection conditions, low O_2 concentration has a significant effect on the D160_75-25.

8.2 RECOMMENDATIONS FOR FUTURE WORKS

Several recommendations can be made for future work in this field.

The detail mechanism of the effect of liquid/wall interaction on spray evolution and combustion need to be further investigated. Until now, the LAS technique cannot deal with the liquid film on the wall surface, to resolve, the precision of LAS technique on the liquid phase should be improved. Other injection strategies such as different split main injection mass ratio, different split main injection interval should be further investigated to find a better injection strategy which can avoid the second main injection catching up with first injection flame. Different oxygen concentrations should also be investigated to find an ideal oxygen concentration which can decrease the soot emissions significantly. Besides, the computational fluid dynamics should be applied to simulate the spray evolution and to further investigate the liquid film behaviors.

Current results reveal that the split injection has a positive effect to reduce the soot emissions. Pre-injection combustion can improve the main injection combustion. Increases the split injection interval should have a positive effect to decrease the soot emissions under 2-D cavity impinging spray. Therefore, more fundamental experiments with different injection strategies under 2-D cavity are recommended.

The ultimate purpose of this research is to improve the performance in a real engine. Although the physical ambient conditions in a real engine are similar with this work, the turbulent flow may play a role in mixture formation and combustion process. Therefore, it is recommended to investigate the mixture and combustion characteristics in an optical engine by applying different chamber shapes, injection pressures, injection amount and multiple injection strategies.

REFERENCE

1. **Khalid, A., and Manshoor, B.** (2012) Effect of High Injection Pressure on Mixture Formation, Burning Process and Combustion Characteristics in Diesel Combustion. Approaches to Solve Problems of the Premixed Lean Diesel Combustion. *International Journal of Mechanical and Mechatronics Engineering,* 6(11).
2. **BP Energy Outlook.** (2018) https://www.bp.com/en/global/corporate/energy-economics/energy-outlook/energy-outlook-downloads.html.
3. **Dallmann, T., and Menon, A.** (2016) Technology Pathways for Diesel Engines Used in Non-Road Vehicles and Equipment. *The international council on clean transportation*.
4. **Alperstein, M., Swim, W.B., and Schweitzer, P.H.** (1958). Fumigation Kills Smoke - Improves Diesel Performance. *SAE Technical Paper* 580058.
5. *Wisconsin Engine Research Consultants*. https://www.w-erc.com/services/rcci/.
6. **Kalghatgi, G., Hildingsson, L., and Johansson, B.** (2009). Low NOx and Low Smoke Operation of a Diesel Engine Using Gasoline-Like Fuels. *ASME ICES.*
7. **Musu, E., Gentili, R., and Reitz, R.D.** (2009). Homogeneous Charge Progressive Combustion (HCPC): CFD Study of an Innovative Diesel HCCI Concept. *SAE Technical Paper* 2009-01-1344.
8. **Sandia National Laboratories.** http://crf.sandia.gov/how-low-temperature-combustion-enables-cleaner-more-efficient-engines/.
9. **Li, J., Yang, W.M., An, H., Zhou, D.Z., and Kraft, M.** (2016). Application of Dynamic ϕ–T Map: Analysis on a Natural Gas/Diesel Fueled RCCI Engine. *Journal of Engineering for Gas Turbines and Power,* 138.
10. **Dec, J.E.** (2009) Advanced Compression-Ignition Engines-Understanding the In-Cylinder Processes. *Proc. Combust. Inst.,* 32(2):2727-2742.
11. **Splitter, D., Kokjohn, S., Rein, K., Hanson, R., Sanders, S., and Reitz, R.** (2010) An Optical Investigation of Ignition Processes in Fuel Reactivity Controlled PCCI

Combustion. *SAE Int. J. Engine,* 3(1):142-162.

12. **Yang, K., Yasaki, S., Nishida, K., and Ogata, Y.** (2018) Injection Strategy to Enhance Mixture Formation and Combustion of Fuel Spray in Diesel Engine. *SAE Technical Paper* 2018-01-0241.
13. **Jaat, M., Khalid, A., Manshoor, B., and Ramsy, H.** (2013) Review of the Investigation of Mixture Formation and Combustion Process Using Rapid Compression Machine and Direct Visualization System. *2nd International Conference on Mechanical Engineering Research*.
14. **Varde, K.S., and Watanabe, T.** (2000) Characteristics of High Pressure Spray and Exhaust Emissions in A Single Cylinder DI Diesel Engine. *SAE Technical Paper* 2000-05-0333.
15. **Shehata, M.S., and Abdel-Razek, S.M.** (2009) Effect of Nozzle Hole and Pump Plunger Diameters on Performance and Emissions of Diesel Engine. *ASCEE,* 4:140-154.
16. **Bergstrand, P., and Denbratt, I.** (2001) Diesel Combustion with Reduced Nozzle Orifice Diameter. *SAE Technical Paper* 2001-01-2010.
17. **Zurlo, J., and Chigier, N.** (1991) Impinging Diesel Spray Dynamics. *Atomization sprays*, 1:303-318.
18. **Senda, J., Tanabe, Y., Fujimoto, H., et al.** (1992) Vizualization of Evaporative Diesel Spray Impinging Upon Wall Surface by Exciplex Fluorescence Method. *SAE Technical Paper* 920578.
19. **Cossall, G., Coghe, A., and Brunello, G.** (1993) Effect of Spray-Wall Interaction on Air Entrainment in a Transient Diesel Spray. *SAE Technical Paper* 930920.
20. **Tomonaga, T., Mural, K., Takano, T., and Sami, H.** (1996) A study on Combustion Behaviors of a Diesel Fuel Spray Impinging on a Wall. *SAE Technical Paper* 960028.
21. **Wang, X.G.** (2011) Effects of Ultra-High Injection Pressure and Micro-Hole on Flame Structure and Soot Formation of Impinging Diesel Spray. *Appl Energ*, 88:1620-1628.

22. **Dec, J. and Tree, D.** (2001) Diffusion-Flame/Wall Interactions in a Heavy-Duty DI Diesel Engine. *SAE Technical Paper* 2001-01-1295.
23. **Jakob, M., Hulser, T., Janssen, A., et al.** (2012) Simultaneous High-Speed Visualization of Soot Luminosity and OH* Chemiluminescence of Alternative-Fuel Combustion in a HSDI Diesel Engine under Realistic Operating Conditions. *Combust Flame,* 159:2516-2529.
24. **Li, K., Nishida, K., Ogata, Y., and Shi. B.** (2015) Effect of Flat-Wall Impingement on Diesel Spray Combustion. *Proc IMechE Part D: J Automobile Engineering*, 229(5) :535-549.
25. **Ricaud, J.C., and Lavoisier, F.** (2004) Optimizing the Multiple Injection Settings on an HSDI Diesel Engine. *Thermo-and Fluid Dynamic Processes in Diesel Engine,* 199-234.
26. **Shimo, D., Kataoka, M. and Fujimoto, H.** (2004) Effect of Cooling of Burned Gas by Vertical Vortex on NOx Reduction in Small DI Diesel Engines. *SAE technical paper* 2004-01-0125.
27. **Terazawa, Y., Nakai, E., Kataoka, M., et al.** (2011) The New Mazda Four-Cylinder Diesel Engine. *Motortechnische Zeitschrift Worldwide,* 72(9):26-32.
28. **Hiroyasu, H., and Kadota, T.** (1974) Fuel Droplet Size Distribution in Diesel Combustion Chamber. *SAE technical paper* 74071.
29. **Hiroyasu, H., Shimizu, M., and Arai, M.** (1982) The Breakup of a High Speed Jet in a High Pressure Gaseous Atmosphere. *2nd International Conference on Liquid Atomization and Spray Systems (ICLASS)*.
30. **Hiroyasu, H.** (1985) Diesel Engine Combustion and Its Modeling. *COMODIA-85*.
31. **Hiroyasu, H., and Arai, M.** (1990) Structures of Fuel Sprays in Diesel Engines. *SAE technical paper* 900475.
32. **Hiroyasu, H., Arai, M., and Shimuzu, M.** (1991) Break-up Length of a Liquid Jet and Internal Flow in a Nozzle. *ICLASS 1991, Gaithersburg, USA,* 275-282.
33. **Arai, M., Tabata, M., Hiroyasu, H., and Shimizu, H.** (1984) Disintegrating Process

and Spray Characterization of Fuel Jet Injected by a Diesel Nozzle. *SAE technical paper* 840275.

34. **Tabata, M., Arai, M., and Hiroyasu, H.** (1986) Atomization of High Viscosity Liquid by a Diesel Nozzle. *Bulletin of JSME,* 29(252):1795-1986.
35. **Raeie, N., Emami, S., and Sadaghiyani O.K.** (2014) Effects of Injection Timing, Before and After Top Dead Center on the Propulsion and Power in a Diesel Engine. *Propulsion and Power Research,* 3(2):59-67.
36. **Sayin, C., and Canakci, M.** (2009) Effects of Injection Timing on the Engine Performance and Exhaust Emissions of a Dual-Fuel Diesel Engine. *Energy Conversion and Management,* 50(1):203-213.
37. **Borz, M., Kim, Y., and O'Connor, J.** (2016) The Effects of Injection Timing and Duration on Jet Penetration and Mixing in Multiple-Injection Schedules. *SAE technical paper* 2016-01-0856.
38. **Diwakar, R., Fansler, T.D., French D.T., et al.** (1992) Liquid and Vapor Fuel Distributions from an Air-Assist Injector – An Experimental and Computational Study. *SAE technical paper* 920422.
39. **Suzuki, M., Nishida, K., and Hiroyasu, H.** (1993) Simultaneous Concentration Measurement of Vapor and Liquid in an Evaporating Diesel Spray. *SAE technical paper* 930863.
40. **Dec, J. E.** (1997) A Conceptual Model of DI Diesel Combustion Based on Laser-Sheet Imaging. *SAE technical paper* 970873.
41. **Flynn, P.F., Durrett, R.P., Hunter, G.L., et al.** (1999) Diesel Combustion: An Integrated View Combining Laser Diagnostics, Chemical Kinetics, And Empirical Validation. *SAE technical paper* 1999-01-0509.
42. **Zeldovich, Y.B.** (1946) The Oxidation of Nitrogen in Combustion and Explosions. *Acta Physicochim,* 21:577-628.
43. **Baumgarten, C.** (2006) Mixture Formation in Internal Combustion Engine. *Berlin Heidelberg, Springer- Verlag*.

44. **Janssens, M.L.** (1991) Measuring Rate of Heat Release by Oxygen Consumption. *Fire Technology,* 27(3):234-249.
45. **Garcia, M.T., Aguilar, F.J.J.E., and Lencero T.S.** (2009) Combustion Characteristics, Emissions and Heat Release Rate Analysis of a Homogeneous Charge Compression Ignition Engine with Exhaust Gas Recirculation Fuelled with Diesel. *Energy Fuels,* 23(5):2396-2404.
46. **Bruneaux, G.** (2005) Mixing Process in High Pressure Diesel Jets by Normalized Laser Induced Exciplex Fluorescence Part 2: Wall Impinging Versus Free Jet. *SAE technical paper* 2005-01-2097.
47. **Zhang, W., Nishida, K., and Gao. J.** (2008) An Experimental Study on Mixture Formation Process of Flat Wall Impinging Spray Injected by Micro-Hole Nozzle under Ultra-High Injection Pressures. *SAE technical paper* 2008-01-1601.
48. **Bruneaux G, Causse M, Omrane A.** (2011) Air Entrainment in Diesel-Like Gas Jet by Simultaneous Flow Velocity and Fuel Concentration Measurements, Comparison of Free and Wall Impinging Jet Configurations. *SAE technical paper* 2011-01-1828.
49. **Mohammadi, A., Kidoguchi, Y., and Miwa, K.** (2002) Effect of Injection Parameters and Wall-Impingement on Atomization and Gas Entrainment Processes in Diesel Sprays. *SAE technical paper* 2002-01-0497.
50. **Li, K., Dong, P., Matsuo, et al.** (2014) Characteristics of Diesel Spray Flame under Flat Wall Impinging Condition-LAS, OH* Chemiluminescence and Two Color Pyrometry Results. *SAE technical paper* 2014-01-2636.
51. **Lopez, J., and Pickett, L.** (2004) Jet/Wall Interaction Effects on Soot Formation in a Diesel Fuel Jet. *The international symposium on diagnostics and modeling of combustion in internal combustion engines*.
52. **Pickett, L., and Lopez, J.** (2005) Jet-Wall Interaction Effects on Diesel Combustion and Soot Formation. *SAE technical paper* 2005-01-0921.
53. **Wang, X., Huang, Z., Zhang, W., Kuti, O.A., and Nishida, K.** (2011) Effects of Ultra-High Injection Pressure and Micro-Hole Nozzle on Flame Structure and Soot

Formation of Impinging Diesel Spray. *Applied Energy*, 88(5):1620-1628.

54. **Dec, J., and Tree, D.** (2001) Diffusion-Flame Interactions in a Heavy-Duty DI Diesel Engine. *SAE technical paper* 2001-01-1295.
55. **Ricaud, J.C., and Lavoisier, F.** (2004) Optimizing the Multiple Injection Settings on an HSDI Diesel Engine. *Thermo-and Fluid Dynamic Processes in Diesel Engine, Springer*.
56. **Cheng, X., Chen, L., Yan, F., et al.** (2013) Investigations of Split Injection Strategies for the Improvement of Combustion and Soot Emissions Characteristics Based on the Two-Color Method in a Heavy-Duty Diesel Engine. *SAE technical paper* 2013-01-2523.
57. **Tao, F., Reitz, R.D., Foster, D.E., and Liu, Y.** (2009) Nine-Step Phenomenological Diesel Soot Model Validated Over a Wide Range of Engine Conditions. *Int J Therm Sci,* 48(6):1223-1234.
58. **Farrell, P.V., Chang, C.T., and Su, T.F.** (1996) High Pressure Multiple Injection Spray Characteristics. *SAE technical paper* 960860.
59. **Magdi, K.K., and Hannu, J.** (2013) Diesel fuel injection. *DieselNet*.
60. **Bianchi, G., Pelloni, P., Corcione, F., and Luppino, F.** (2001) Numerical Analysis of Passenger Car HSDI Diesel Engines with the 2nd Generation of Common Rail Injection Systems: The Effect of Multiple Injections on Emissions. *SAE technical paper* 2001-01-1068.
61. **Heechang, O., and Choongsik, B.** (2014) Effects of a Split Injection in a Spray-Guided Direct-Injection Spark Ignition Engine under Lean Stratified Operation. *Proceedings of the Institution of Mechanical Engineers, Part D: Journal of Automobile Engineering*, 228(10):1232-1244.
62. **Skeen, S., Manin, J., and Pickett, L.** (2015) Visualization of Ignition Processes in High-Pressure Sprays with Multiple Injections of n-Dodecane. *SAE technical paper* 2015-01-0799.
63. **Blomberg, C.K., Zeugin, L., Pandurangi, S.S., et al.** (2016) Modeling Split

Injections of ECN “Spray A” Using a Conditional Moment Closure Combustion Model with RANS and LES. *SAE technical paper* 2016-01-2237.

64. **Cha, J., Yang, S.Y., Naser, N., et al.** (2015) High Pressure and Split Injection Strategies for Fuel Efficiency and Emissions in DI Diesel Engine. *SAE technical paper* 2015-01-1823.
65. **Nehmer, D.A., and Reitz, R.D.** (1994) Measurement of the Effect of Injection Rate and Split Injections on Diesel Engine Soot and NOx Emissions. *SAE technical paper* 940668.
66. **Tow, T., Pierpont, A., and Reitz, R.D.** (1994) Reducing Particulate and NOx Emissions by Using Multiple Injections in a Heavy Duty D.I. Diesel Engine. *SAE technical paper* 940897.
67. **Nishida, K., Imanishi, H., Sato, T., et al.** (1999) Wall Impingement Behavior of the Diesel Spray with Split Injection. *JSAE Transaction,* 30(3):17-23.
68. **Seo, J., Lee, J.S., Choi, K.H., Kim, H.Y., and Yoon, S.S.** (2013) Numerical Investigation of the Combustion Characteristics and Wall Impingement with Dependence on Split-Injection Strategies from a Gasoline Direct-Injection Spark Ignition Engine. *Proceedings of the Institution of Mechanical Engineers, Part D: Journal of Automobile Engineering*, 227(11):1518-1535.
69. **Nishioka, Y., Tomoda, H., Nishida, K., and Ogata, Y.** (2015) Combustion Characteristics of Diesel Spray with Temporally-Splitting High-Pressure Injection. *JSAE Paper* 20159825/*SAE Paper* 2015-32-0825.
70. **Zhao, H., and Ladammatos, N.** (2001) Engine Combustion Instrumentation and Diagnostics. *Warrendale, SAE*.
71. **Siebers, D.L.** (1998) Liquid-Phase Fuel Penetration in Diesel Sprays. *SAE technical paper* 980809.
72. **Gulder, O.L., Smallwood, G.J., and Snelling, D.R.** (1992) Diesel Spray Structure Investigation by Laser Diffraction and Sheet Illumination. *SAE technical paper* 920577.

73. **David, W.H.** (2009) Light Scattering Theory. University of Florida.

74. **Panigrahi, P. K., and Muralidhar, K.** (2012) Schlieren and Shadowgraph Methods in Heat and Mass Transfer. *SpringerBriefs in Thermal Engineering and Applied Science*.

75. **Nishida, K., Murakami, N., and Hiroyasu, H.** (1987) Holographic Measurement of Evaporating Diesel Sprays at High Pressure and Temperature. *JSME international journal,* 30(259):107-115.

76. **Schnars, U., Falldorf, C., Watson, J., and Jüptner, W.** (2015) Digital Holography and Wavefront Sensing. *Springer-Verlag Berlin Heidelberg*.

77. **Crolla, D.** (2015) Encyclopedia of Automotive Engineering. *Online © 2014 John Wiley & Sons, Ltd*.

78. **Andresen, P., Meijer, G., Schluter, H., Voges, H., Koch, A., Hentschel, W., Oppermann, W., and Rothe, E.** (1990) Fluorescence Imaging inside an Internal Combustion Engine using Tuable Excimer Lasers. *Applied optics,* 26:2392-2404.

79. **Talley, D.G., Verdieck, J.F., Lee, S.W., McDonell, V.G., and Samuelsen, G.S.** (1996) Accounting for laser sheet extinction in applying PLLIF to sprays. *AIAA,* 96-0469.

80. **Yeh, C.-N., Kamimoto, T., Kobori, S., and Kosaka, H.** (1994) Quantitative Measurement of 2-D Fuel Vapor Concentration in a Transient Spray via Laser-Induced Fluorescence Technique. *SAE technical paper* 941953.

81. **Seitzman, J.M., and Hanson, R.K.** (1993) Planar Fluorescence Imaging in Gases. *Instrumentation for Flows with Combustion*, 405-466.

82. **Melton, L.A., and Verdieck, J.F.** (1984) Vapor/Liquid Visualization for Fuel Sprays. *20th Symposium (International) on Combustion,* 217-222.

83. **Melton, L.A.** (1983) Spectrally Separated Fluorescence Emissions for Diesel Fuel Droplets and Vapor. *Applied Optics,* 22(14): 2224-2226.

84. **Melton, L.A., and Verdieck, J.F.** (1985) Vapor/Liquid Visualization in Fuel Sprays. *20th Symposium (International) on Combustion,* 1283-1290.

85. **Leidenberger, U., Hüttl, C., Haugg, S., and Brüggemann, D.** (2010) Application of Laser-Induced Exciplex Fluorescence with Alternative Diesel Fuels. *23rd Annual Conference on Liquid Atomization and Spray Systems*.
86. **Senda, J., Kanda, T., Kobayashi, M., and Fujimoto, H.** (1997) Quantitative Analysis of Fuel Vapor Concentration in Diesel Spray by Exciplex Fluorescence Method. *SAE technical paper* 970796.
87. **Senda, J., Kobayashi, M., Iwashita, S., and Fujimoto, H.** (1994) Modeling of Diesel Spray Impingement on a Flat Wall. *SAE technical paper* 941894.
88. **Senda, J., Tanabe, Y., Fujimoto, H., and Fukami, Y.** (1992) Vizualization of Evaporative Diesel Spray Impinging Upon Wall Surface by Exciplex Fluorescence Method. *SAE technical paper* 920578.
89. **Bruneaux, G.** (2001) Liquid and Vapor Spray Structure in High-Pressure Common Rail Diesel Injection. *Atomization and Sprays,* 11: 533-556.
90. **Bruneaux, G.** (2005) Mixing Process in High Pressure Diesel Jets by Normalized Laser Induced Exciplex Fluorescence Part I: Free Jet. *SAE technical paper* 2005-01-2100.
91. **Bruneaux, G.** (2008) Combustion Structure of Free and Wall-Impingement Diesel Jets by Simultaneous Laser-Induced Fluorescence of Formaldehyde, Poly-Aromatic Hydrocarbons, and Hydroxides. *International Journal of Engine Research,* 9:249-265.
92. **Andersson, M., Yamaguchi, A., and Wang, H.** (2017) Imaging of Gasoline-like Sprays with Planar Laser-induced Exciplex Fluorescence using a Stereoscopic Imaging System. *28th Conference on Liquid Atomization and Spray Systems,* 546.
93. **Espey, C., Dec, J.E., Litzinger, T.A., and Santavicca, D.A.** (1997) Planar Laser Rayleigh Scattering for Quantitative Vapor-Fuel Imaging in a Diesel Jet. *Combustion and Flame,* 109: 65-78.
94. **Johnston, S.,** (1979) Precombustion Fuel/Air Distribution in a Stratified Charge Engine Using Laser Raman Spectroscopy. *SAE technical paper* 790433.
95. **Sawersyn, J.P., Sochet, L., Desenne, D., Crunelle-Cras, M., Grase, F., and**

Bridoux, M. (1986) A Study of Spatial Distribution of Molecular Species in an Engine by Pulsed Multichannel Raman Spectroscopy. *Proc. 21st Symposium (International) on Combustion,* 491-496.

96. **Miles, P., and Hinze, P.** (1998) Characterization of the Mixing of Fresh Charge with Combustion Residuals Using Laser Raman Scattering with Broadband Detection. *SAE technical paper* 981428.
97. **Reising, H.H.** (2017) Application of Spontaneous Raman Scattering for Measurements of Thermal Non-Equilibrium in High-Speed Mixing and Combustion. *Dissertation, The University of Texas*.
98. **Chraplyvy, A.R.** (1981) Nonintrusive Measurements of Vapor Concentrations inside Sprays. *Appl. Opt,* 20:2620-2624.
99. **Suzuki, M., Nishida, K., and Hiroyasu, H.** (1993) Simultaneous Concentration Measurement of Vapor and Liquid in an Evaporating Diesel Spray. *SAE technical paper* 930863.
100. **Zhang, Y.Y.,** (2001) A Study on Mixture Formation in Diesel Spray with Split Injection Strategy. *Dissertation, University of Hiroshima*.
101. **Gao, J., Matsumoto, Y., Namba, M., and Nishida, K.** (2007) Group-Hole Nozzle Effects on Mixture Formation and In-cylinder Combustion Processes in Direct-Injection Diesel Engines. *SAE technical paper* 2007-01-4050.
102. **Matsuo, T., Li, K.C, Itamochi, M., Nishida, K., Ogata, Y., Shi, B., Shimo, D., Namba, M., Kim, S. and Kanzaki, J.** (2014) Tracer LAS Technique for Quantitative Mixture Concentration Measurement of Evaporating Diesel Spray. *17th Annual Conference on Liquid Atomization and Spray Systems - Asia*.
103. **Itamochi, M., Matsuo, T., Li, K.C, Nishida, K., Ogata, Y., Shimo, D., Namba, M., Kim, S. and Kanzaki, J.** (2015) Laser Absorption Scattering Technique Using Tracer-Doped Fuel (Tracer LAS) for Quantitative Measurement of Mixture Concentration Distribution in Diesel Spray, *13th Triennial International Conference on Liquid Atomization and Spray Systems*.

104. **Corcione, F.E., and Valentino, G.** (1990) Turbulence Length Scale Measurements by Two-Probe-Volume LDA Technique in a Diesel Engine. *SAE technical paper* 902080.

105. **Baby, X., and Floch, A.** (1997) Investigation of the In-Cylinder Tumble Motion In a Multi-Valve Engine: Effect of the Piston Shape. *SAE technical paper* 971643

106. *In Process Particle-Size Population,* https://www.sequip-particle-technology.de/english/inline-image-analysis/.

107. **Lockwood, D.J.** (2015) Rayleigh and Mie Scattering. *In: Luo R. (eds) Encyclopedia of Color Science and Technology*.

108. **Suzuki, M., Nishida, K., and Hiroyasu, H.** (1993) Simultaneous Concentration Measurement of Vapor and Liquid in an Evaporating Diesel Spray, *SAE technical paper* 930863.

109. **Zhang, Y.Y, Nishida, K., and Yoshizaki, T.** (2001) Quantitative Measurement of Droplets and Vapor Concentration Distributions in Diesel Sprays by Processing UV and Visible Images. *SAE technical paper* 2001-01-1294.

110. **Zhang, Y.Y., and Nishida, K.** (2004) Imaging of Vapor/Liquid Distributions of Split-Injected Diesel Sprays in a Two-Dimensional Model Combustion Chamber. *Combustion Science and Technology,* 176:1465-1491.

111. **Mancaruso, E., and Vaglieco, B.** (2011) Spectroscopic Measurements of Premixed Combustion in Diesel Engine. *Fuel,* 90(2):511-520.

112. **Gaydon, A, G.** (1974) The Spectroscopy of Flames. *Chapman and Hall Ltd., London*.

113. **Hitomi, M., Nakai, E., Terazawa, Y., Takamatsu, H., and Shimo, D.** (2014) Development of a New Generation Clean Diesel Engine (2.2L) which Achieves both Driving Pleasure and Environmental Performance -Realization of a Concept for Ultra-Low Compression Ratio of 14.0.

114. **Morawski, P., Coutinho, J. A. P., and Domanska, U.** (2005) High Pressure (Solid + Liquid) Equilibria of n-alkane Mixtures Experimental Results, Correlation

and Prediction. *Fluid Phase Equilibria*, 230:72-80.

115. **Milhet, M., Pauly, J., Coutinho, J. A. P., Dirand, M., and Daridon, J.L.** (2005) Liquid Solid Equilibria under High Pressure of Tetradecane + Pentadecane and Tetradecane + Hexadecane Binary Systems. *Fluid Phase Equilibria,* 235:173-181.

116. **Zhang, Y., and Nishida, K.** (2007) Vapor Distribution Measurement of Higher and Lower Volatile Components in an evaporating Fuel Spray via Laser Absorption Scattering (LAS) Technique. *Combustion Science and Technology*, 179(5).

117. **Hottel, H., and Broughton, F.** (1932) Determiantion of True Temperature and Total Radiation from Luminous Gas Flames. *Ind and Eng. Chem.*, 4(2):166-174.

118. **Svensson, K.I., Mackrory, A,J., Richards, M.J., and Tree, D.R.** (2005) Calibration of an RGB, CCD Camera and Interpretation of its Two-Color Images for KL and Temperature. *SAE technical paper* 2005-01-0648.

119. **Mancaruso, E., and Vaglieco, B.** (2011) Spectroscopic Measurements of Premixed Combustion in Diesel Engine. *Fuel,* 90(2):511-520.

120. **Dec, J.E, and Espey, C.** (1998) Chemiluminescence Imaging of Autoignition in a DI Diesel Engines. *SAE technical paper* 982685.

121. **Laget, O., Pacaud, P., and Perrin, H.** (2009) Cold Start on Low Compression Ratio Diesel Engine: Experimental and 3D RANS Computation Investigations. *Oil & Gas Science and Technology*, 64:407-429.

122. **MacMillan, D., La Rocca, A., Shayler, P., Morris, T. et al.** (2009) Investigating the Effects of Multiple Pilot Injections on Stability at Cold Idle for a Dl Diesel Engine. *SAE Int. J. Engines,* 2(1):370-380.

123. **Hiroyasu, H., and Kadota, T.** (1974) Fuel Droplet Size Distribution in Diesel Combustion Chamber Exxon Mobil. *SAE Technical Paper* 740715.

124. **Hiroyasu, H.** (1985) Diesel Engine Combustion and Its Modeling. *COMODIA*.

125. **Hiroyasu, H., and Arai, M.** (1990) Structures of Fuel Sprays in Diesel Engines, *SAE Technical Paper* 900475.

126. **Xu, M., Nishida, K., and Hiroyasu, H.** (1992) A Practical Calculation Method

for Injection Pressure and Spray Penetration in Diesel Engines. *SAE Technical Paper* 920624.

127. **Imanishi, H., Yoshizaki, T., and Hiroyasu, H.** (1996) Simulation Study of Effects of Injection Rate Profile and Air Entrainment Characteristics on D.I. Diesel Combustion. *SAE Technical Paper* 962059.

128. **Tabata, M., Fujii, H., Arai, M., and Hiroyasu, H.** (1988) Mean Drop Diameter of a Diesel Spray in a Vaporizing Process. *JSME International Journal Series,* 34(3).

129. **Yang, K., Yamakawa, H., Nishida, K., Ogata, Y., and Nishioka, Y.** (2018) Effect of Split Injection on Mixture Formation and Combustion Processes of Diesel Spray Injected Into Two-Dimensional Piston Cavity. *Proceedings of the institution of Mechanical Engineers, Part D: Journal of Automobile Engineering,* 232(8).

130. **Kosaka, H., Aizawa, T., and Kamimoto, T.** (2005) Two-Dimensional Imaging of Ignition and Soot Formation Process in a Diesel Flame. *International Journal of Engine Research,* 6(1):21-42.

131. **Nishioka, Y., Tomoda, H., Nishida, K., and Ogata, Y.** (2015) Combustion Characteristics of Diesel Spray with Temporally-Splitting High-Pressure Injection. *JSAE Paper* 20159825.

132. **Nehmer, D.A., and Reitz, R.D.** (1994) Measurement of the Effect of Injection Rate and Injections on Diesel Engine Soot and NOx Emissions. *SAE Technical Paper* 940668.

133. **Panoutsos, C.S., Hardalupas, Y., and Taylor, AMKP.** (2009) Numerical Evaluation of Equivalence Ratio Measurement using OH* and CH* Chemiluminescence in Premixed and Non-Premixed Methane-Air Flame. *Combust Flame*, 156:273-291.

134. **Tinaut, F.V., Reyes, M., Gimenez, B., and Pastor, JV.** (2011) Measurements of OH* and CH* Chemiluminescence in Premixed Flames in a Constant Volume Combustion Bomb under Auto-Ignition Conditions. *Energy Fuel,* 25:119-129.

135. **Pickett, L.M., and Siebers, D.L.** (2004) Soot in Diesel Fuel Jets: Effects of

Ambient Temperature, Ambient Density, and Injection Pressure. *Combust Flame,* 138:114-135.

136. **Takeyuki, K., Noboru, U., Tetsuya, A., Katsufumi, K., and Tatsuya, K.** (2017) Diesel Flame Imaging and Quantitative Analysis of In-cylinder Soot Oxidation. *International Journal of Engine Research*, 18(5-6).

137. **Yeom, J., Park, J., and Chung, S.** (2005) An Analysis on Structure of Impinging and Free Diesel Spray with Exciplex Fluorescence Method in High Temperature and Pressure Field. *Journal of Mechanical Science and Technology,* 19(2).

138. **Liu, Y.F., Xiang, Q., Li, Z.J., Yao, S.Z., Liang, X.Y., and Wang, F.** (2018) Experiment and Simulation Investigation on the Characteristics of Diesel Spray Impingement Based on Droplet Impact Phenomenon. *Appl. Sci.,* 8(384).

139. **Mao, L.W., Su, W.H., and Pei, Y.Q.** (2016) Study on Fuel Distribution of Diesel Spray Flat Wall Impingements. *Neiranji Gongcheng/Chin. Intern. Combust. Eng. Eng.,* 37:98-104.

140. **Mao, L., Su, W., and Pei, Y.** (2015) Quantitative Study of Impingement Characteristics of Diesel Spray. *J. Combust. Sci. Technol.,*21:521-529

141. **Steven, E.** (2001) Piston Wetting in an Optical DISI Engine: Fuel Films, Pool Fires, and Soot Generation. *SAE Technical Paper* 2001-01-1203.

142. **Pickett, L.M., and Siebers, D.L.** (2004) Soot in Diesel Fuel Jets: Effects of Ambient Temperature, Ambient Density, and Injection Pressure. *Combust Flame,* 138:114-135.

143. **Senda, J., Kukami, Y., Tanabe Y., and Fujinoto, H.** (1992) Visualization of Evaporative Diesel Spray Impinging upon Wall Surface by Exciplex Fluorescence Method. *SAE Technical Paper* 920578.

144. **Carlucci, A.P., FIcarella, A., and Laforgia, D.** (2005) Effects on Combustion and Emissions of Early and Pilot Fuel Injections in Diesel Engines. *International Journal of Engine Research,* 6(1):43-60.

145. **Sperl, A.** (2011) The Influence of Post-Injection Strategies on the Emissions of Soot and Particulate Matter in Heavy Duty Euro V Diesel Engine. *SAE Technical Paper* 2011-36-0350.

146. **Fang, Q., Fang, J., Zhuang, J., and Huang, Z.** (2012) Influences of Pilot Injection and Exhaust Gas Recirculation (EGR) on Combustion and Emissions in a HCCI-DI Combustion Engine. *Applied Thermal Engineering,* 48:97-104.

147. **Zhuang, J., Qiao, X., Bai, J., and Hu, Z.** (2014) Effect of Injection-Strategy on Combustion, Performance and Emission Characteristics in a DI-diesel Engine Fueled with Diesel from Direct Coal Liquefaction. *Fuel,* 121:141-148.

148. **Cheng, X., Chen, L., Yan, F., et al.** (2013) Investigations of Split Injection Strategies for the Improvement of Combustion and Soot Emissions Characteristics Based on the Two-Color Method in a Heavy-Duty Diesel Engine. *SAE Technical Paper* 2013-01-2523.

149. **Nishida, K., Imanishi, H., Sato, T., et al.** (1999) Wall Impingement Behavior of the Diesel Spray with Split Injection. *JSAE Transaction,* 30(3):17-23.

150. **Seo, J. et al.** (2013) Numerical Investigation of the Combustion Characteristics and Wall Impingement with Dependence on Split-Injection Strategies from a Gasoline Direct-Injection Spark Ignition Engine. *Proceedings of the Institution of Mechanical Engineers, Part D: Journal of Automobile Engineering*, 227(11):1518-1535.

151. **Jing, W., L.Roberts, W., and Fang, T.G.** (2013) Effects of Ambient Temperature and Oxygen Concentration on Diesel Spray Combustion Using a Single-Nozzle Injector in a Constant Volume Combustion Chamber. *Combustion Science and Technology,* 185(9).

152. **Zhang, Y.B., Fan, W.J., Zhang, R.C., Xu, H.Q., and Lei, H.W.** (2017) Effect of the Ambient Temperature and Oxygen Concentration in Droplet Combustion under Natural Convection Conditions. *EEMS,* 94.

153. **Zhang, J., Jing, W., L.Roberts, W., and Fang, T.G.** (2013) Effects of Ambient Oxygen Concentration on Biodiesel and Diesel Spray Combustion under Simulated

Engine conditions. *Fuel,* 57:722-732.

154. **Azetsu, A., et al.** (2015) Effects of Ambient O2 Concentration and Pressure on Combustion Characteristics of Diesel Spray. *SAE Technical Paper* 2015-01-1831.

155. **Kuribayashi, M., Mizutani, Y., Ishizuka, Y., Taki, N. et al.** (2014) Effects of Ambient Oxygen Concentration on Soot Processes in Diesel Spray Flame-Qualitative Comparison between TEM Analysis and LII/Scattering Laser Measurements. *SAE Technical Paper* 2014-01-2642.

ACKNOWLEDGEMENTS

This thesis was accomplished at the Fluid Engineering Laboratory, Faculty of Engineering, University of Hiroshima. I would like to express my gratitude to all those who helped me during the working of this dissertation.

My deepest gratitude goes first and foremost to Professor. Keiya Nishida, my academic advisor, for his constant encouragement, earnest guidance, constructive criticism and invaluable discussions throughout the three years.

Gratefulness is also given to Prof. Yoichi Ogata, for his extremely valuable comments and helpful suggestions in directing me to fulfill this thesis. Also, my sincere appreciation goes to the thesis committee members: Prof. Shinnichi Naber and Prof. Akira Miyoshi.

Thanks are also given to Dr. Shimo (Mazda Co), Dr. Dong, Mr. Itamochi, Mr. Yasaki, for their assistance in the experiment.

Thanks are also given to Prof. Maozhao Xie (Dalian University of Technology) for his moral support and encouragement during this 3-year research and in the previous studies.

I would like to appreciate the CSC (China Scholarship Council), China, for sponsoring my studies by providing scholarship and tuitions fees.

Last but not least, my deepest gratitude goes to my family, especially to my fiancee, Rui Guo, for her consistent love, encouragement, and support.